

NATIONAL LIBRARY
OTTAWA



BIBLIOTHÈQUE NATIONALE
OTTAWA

8474

NAME OF AUTHOR...Jenkins, Robert.W.....
TITLE OF THESIS..Primary cosmic ray measurements near sunspot
.....minimum with a cerenkov-scintillation system.
.....
UNIVERSITY.....U of A (Calgary).....
DEGREE FOR WHICH THESIS WAS PRESENTED...Ph.D.....
YEAR THIS DEGREE GRANTED...1965 (1966).....

Permission is hereby granted to THE NATIONAL LIBRARY
OF CANADA to microfilm this thesis and to lend or sell copies
of the film.

The author reserves other publication rights, and
neither the thesis nor extensive extracts from it may be
printed or otherwise reproduced without the author's
written permission.

(Signed).....*Robert Jenkins*.....

PERMANENT ADDRESS:

.....% 959. TUDOR AVE.,.....
.....NORTH VANCOUVER...B.C.,
.....

DATED...MARCH 31, 1971...~~18~~

NL-91 (10-68)

UNIVERSITY OF ALBERTA AT CALGARY

'PRIMARY COSMIC RAY MEASUREMENTS NEAR SUNSPOT MINIMUM
WITH A CERENKOV-SCINTILLATION SYSTEM'

by

ROBERT W. JENKINS

A THESIS

SUBMITTED TO THE FACULTY OF GRADUATE STUDIES
IN PARTIAL FULFILMENT OF THE REQUIREMENTS FOR THE DEGREE
OF DOCTOR OF PHILOSOPHY

DEPARTMENT OF PHYSICS


CALGARY, ALBERTA

OCTOBER 1965


UNIVERSITY OF ALBERTA AT CALGARY

FACULTY OF GRADUATE STUDIES


The undersigned certify that they have read, and recommend to the Faculty of Graduate Studies for acceptance, a thesis entitled 'Primary Cosmic Ray Measurements Near Sunspot Minimum with a Cerenkov-Scintillation System' submitted by Robert W. Jenkins in partial fulfilment of the requirements for the degree of Doctor of Philosophy.



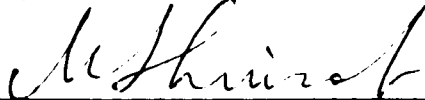
Supervisor B. G. Wilson




J. R. Prescott



W. R. Webber



M. Shimrat



C. D. Anger

Date October 26, 1965

ABSTRACT

A balloon borne Cerenkov-scintillation counter system for the monitoring of the primary cosmic radiation was designed and built. This detection system combined low cost and light balloon package weight with a fairly high counting rate (approximately 5 counts/second at altitude). Four flights were made with this system, at times spanning the recent eleven year maximum in cosmic ray intensity as determined by ground level monitors.

The presence of a large number of background counts of uncertain origin limited the usefulness of the data, but several conclusions could still be made. The proton differential rigidity spectra were seen to be similar to that measured near the previous solar minimum by Webber and McDonald (1964), and earlier in the present minimum by Balasubrahmanyam and McDonald (1964). An upper limit to the 'rollover point' in the alpha particle rigidity spectra of 2.5 GV was obtained for all flights. An absorption length for alpha particles in air of $51 \pm 3 \text{ g/cm}^2$ was determined. The mean alpha flux for the flights was seen to be in agreement with that measured near the previous solar minimum, for rigidities greater than 4.5 GV (Waddington, 1963). Measurements of the ratio of protons to alpha particles were made. The data was not sufficiently accurate or did not extend over a wide enough range of energies to discriminate between a velocity dependent or rigidity dependent common form for the

primary proton and alpha particle spectra. For each of the two flights made from the Calgary vicinity, a geomagnetic cut-off in the neighbourhood of 1.0 GV was inferred. One of the two Churchill flights showed an unusual decrease of low rigidity protons which was not apparent on ground level monitor records. The origin of this decrease is thought to be in the primary radiation, although instrumental effects cannot be completely disregarded as a possible cause.

ACKNOWLEDGEMENTS

The author would like to express his gratitude to:
Dr B. G. Wilson, who supervised the experiment and provided much of the coordination necessary for its success,
Drs C. D. Anger and T. A. Clark, whose efforts made the balloon program possible, and who offered much helpful advice concerning the specialized equipment necessary for the balloon flights,
Dr J. R. Prescott, for his very useful advice concerning the detectors,
Mr C. Hansen, Mr D. Pitt, and Mr D. Will, for their invaluable advice and assistance concerning the electronics, and for their aid in operating the ground station, various members of the U.A.C. Computing Center, for their help in writing computer programs necessary for analysis of the data,
Mr W. Jones and the rest of the Physics Workshop staff, who constructed the detector telescope assemblies, and various pieces of the ground-based recording station,
Miss J. Nicholson, who typed this manuscript, and the many other people, too numerous to mention here, who aided in the balloon launchings, provided discussion, and gave encouragement.

Thanks are also due to the University of Alberta at Calgary and the National Research Council of Canada for financial aid in the form of a Teaching Assistantship (U.A.C.), a Studentship (N.R.C.), and a Dissertation Fellowship (U.A.C.) during the course of this research.

TABLE OF CONTENTS

| | Page Number |
|--|----------------|
| ABSTRACT | i |
| ACKNOWLEDGEMENTS | iii |
| TABLE OF CONTENTS | iv |
| LIST OF FIGURES | vii |
| LIST OF TABLES | ix |
| CHAPTER ONE: INTRODUCTION | 1 |
| CHAPTER TWO: SOLAR MODULATION OF COSMIC RADIATION | 4 |
| 2.1 Techniques of Observation | 4 |
| 2.1.1 Ground-Based Equipment: The Neutron Monitor | 4 |
| 2.1.2 Balloon, Rocket, and Satellite-Borne Equipment | 6 |
| 2.1.2.1 Photographic Emulsions | 6 |
| 2.1.2.2 Electronic Ionization Detection Devices | 7 |
| 2.1.2.3 Cerenkov Detection Devices | 8 |
| 2.1.2.4 Cerenkov-Scintillation Devices | 9 |
| 2.1.2.5 dE/dx by E Detectors | 10 |
| 2.2 Slowly Varying Modulation: The Eleven Year Cycle | 11 |
| 2.3 Transient Solar Attenuation Phenomena | 17 |
| 2.3.1 The Forbush Decrease | 17 |
| 2.3.2 The Twenty-Seven Day Variation | 18 |
| 2.4 Transient Solar Injection Phenomena | 19 |
| 2.4.1 Ground-Level Increases | 19 |
| 2.4.2 Polar Cap Absorption Events | 20 |
| 2.5 Daily Variation | 22 |
| 2.6 Summary: State of Knowledge of the Solar Modulation and Purpose of the Experiment | 23 |
| CHAPTER THREE: THEORY OF THE CERENKOV-SCINTILLATION PARTICLE DETECTION SYSTEM | 25 |
| CHAPTER FOUR: EXPERIMENTAL APPARATUS | 29 |
| 4.1 General Description of the System | 29 |
| 4.2 Detection Apparatus | 31 |
| 4.3 Balloon-Flown Detector Electronics | 33 |

| | Page Number |
|---|----------------|
| 4.4 Decoding Electronics, Display System, and Punch Tape Recorder | 37 |
| 4.5 System Appraisal | 44 |
| CHAPTER FIVE: PREFLIGHT ADJUSTMENT AND CALIBRATIONS OF THE APPARATUS | 54 |
| CHAPTER SIX: BALLOON FLIGHT HISTORIES | 56 |
| CHAPTER SEVEN: ANALYSIS OF THE DATA | 62 |
| 7.1 Organization of the Data into an Easily Analyzable Representation | 63 |
| 7.2 Calibration of the Scintillation Detector System | 65 |
| 7.3 Preliminary Examination of the Cerenkov Distributions | 67 |
| 7.4 Initial Correction of the Data | 69 |
| 7.4.1 Background Correction in Alpha Region | 69 |
| 7.4.2 Background Correction in Proton Region | 73 |
| 7.4.3 Detector Correction | 74 |
| 7.4.4 Recording Correction | 77 |
| 7.5 Atmospheric Correction of the Data | 78 |
| 7.5.1 Ionization Loss in the Atmosphere | 78 |
| 7.5.2 Alpha Particle Absorption | 78 |
| 7.5.3 Production of Alpha Particles by Fragmentation of Heavier Nuclei | 79 |
| 7.5.4 Secondary Effects Involving Singly Charged Particles | 81 |
| 7.6 Determination of the Alpha Particle Mean Free Path in Air | 83 |
| CHAPTER EIGHT: EXPERIMENTAL RESULTS | 84 |
| 8.1 Scintillation Output Calibration and Particle Energy Intervals | 84 |
| 8.2 Background and Detector Correction; Particle Counts at the Detector | 90 |
| 8.3 Atmospheric Corrections | 95 |
| 8.3.1 Proton Correction | 95 |
| 8.3.2 Alpha Correction | 95 |

| | Page Number |
|--|----------------|
| 8.4 Proton and Alpha Particle Integral Rigidity Spectra | 100 |
| 8.4.1 Proton Integral Rigidity Spectra | 100 |
| 8.4.2 Alpha Integral Rigidity Spectra | 103 |
| 8.4.3 Determination of $\Gamma_{p\alpha}(R)$ | 104 |
| 8.5 Differential Rigidity Spectra | 106 |
| 8.5.1 Protons | 106 |
| 8.5.1.1 Churchill Flights | 106 |
| 8.5.1.2 Calgary Flights | 108 |
| 8.5.1.3 Variation over a Single Flight | 109 |
| 8.5.2 Alpha Particles | 109 |
| 8.6 Proton and Alpha Fluxes as Functions of Energy per Nucleon | 112 |
| 8.7 Associated Solar and Ground Level Cosmic Ray Detector | 114 |
| CHAPTER NINE: CONCLUSIONS | 116 |
| APPENDIX I: DETAILS OF BALLOON-FLOWN ELECTRONICS | 119 |
| APPENDIX II: DETAILS OF GROUND-BASED ELECTRONICS | 125 |
| REFERENCES | 137 |

| Figure | LIST OF FIGURES | Facing Page |
|--------|--|----------------|
| 1 | Differential Proton and Alpha Particle Rigidity Spectra at Different Times of the Solar Activity Cycle: 1956-9 | 12 |
| 2 | Differential Proton and Alpha Particle Rigidity Spectra: 1963-4 | 14 |
| 3a | Cerenkov and Ionization Losses of Singly Charged Particles as a Function of Velocity Cerenkov vs Ionization Loss and Doubly Charged Particles | 26 |
| 3b | | |
| 4a | Balloon Package (photograph) Decoding Electronics and Tape Punch System (photograph) | 29 |
| 4b | | |
| 5 | Block Diagram of Apparatus | 30 |
| 6 | Detector Arrangement | 31 |
| 7 | Detailed Block Diagram of Balloon-Borne Electronics | 33 |
| 8 | Decoding Electronics | 37 |
| 9 | Balloon Package Train Assembly | 56 |
| 10 | Pressure-Time Curves for Balloon Flights | 57 |
| 11 | Balloon Flight Paths | 58 |
| 12 | Cerenkov-Scintillation Diagram for Flight 1 | 63 |
| 13 | Scintillation Output Distributions for Various Cerenkov Outputs for Flight 1 | 65 |
| 14 | | |
| 15 | Cerenkov Output Distributions for Various Scintillation Outputs Defined in Terms of Particle Energy for Flight 1 | 67 |
| 16 | Cerenkov Distributions Found by McDonald (1956) over Alpha Ionization Intervals | 71 |
| 17 | Cerenkov Distributions in Scintillation Regions Containing Mostly Background Counts, for Flight 1 | 72 |
| 17 | Cerenkov Distributions for Alpha Scintillation Intervals, for Flight 1 | 72 |

| Figure | | Facing Page |
|--------|--|----------------|
| 18 | Background Correction over Proton Region for Flight 4 | 74 |
| 19 | Ground Level Muon Scintillation Distribution for Flight 1 Compared with Theoretical Curve | 77 |
| 20 | Counting Rates during Ascent for Flight 1 Proton Scintillation Output Region | 82 |
| 21 | Counting Rate in Fast Alpha Region during Ascent for Flight 1 | 83 |
| 22 | Proton Integral Rigidity Spectra for All Balloon Flights | 100 |
| 23 | Proton Integral Rigidity Spectra for All Flights, with Flight 1 Normalized to Other Flights at High Rigidity End | 101 |
| 24 | Alpha Particle Integral Rigidity Spectra, for All Flights | 103 |
| 25 | Proton Differential Rigidity Spectra, for Churchill Flights | 106 |
| 26 | Proton Differential Rigidity Spectra, for Calgary Flights | 108 |
| 27 | Proton Differential Rigidity Spectra, for Different Times During Flight 4 | 109 |
| 28 | Alpha Particle Differential Rigidity Spectra, for All Flights | 110 |
| 29 | Proton and Alpha Particles Integral Energy Spectra, for All Flights | 112 |
| 30 | Solar and Cosmic Ray Parameters for 1964-65 Solar Minimum Period | 114 |
| 31 | Sulphur Mountain Neutron Monitor Rates over Period of Balloon Flights | 115 |

LIST OF TABLES

| Table | | Page Number |
|-------|---|----------------|
| 1 | Supplement to Figure 11. Times of Radar Readings Shown in Figure | 58 |
| 2 | Particle Energy Intervals, Defined in Terms of Most Probable Scintillation Output | 86 to 89 |
| 3 | Counts per Interval: Total, Background, Particle, and Particle after Correction for Statistical Spreads in Output | 91 to 94 |
| 4a | Change in Proton Rate from 20 to 10 mb Pressure | 97 |
| 4b | Proton Atmospheric Correction Factors | |
| 5a | Observed Alpha Particle Absorption Lengths | 98 |
| 5b | Alpha Atmospheric Correction Factors | |
| 6 | Balloon Flight Parameters | 99 |

CHAPTER ONE



INTRODUCTION

The study of cosmic radiation is revealing, not only of the nature of the radiation itself, but also of the interactions it suffers before reaching the observer. These interactions fall into two broad classes, macroscopic electromagnetic interactions and microscopic particle-particle interactions. Their regions of application may be conveniently divided into the extrasolar and solar vicinities, the magnetosphere, and the terrestrial atmosphere.

The extrasolar region refers to the portion of the universe that the cosmic radiation passes through before reaching the solar system. Both electromagnetic fields and particles are thought to exist in this region, in such intensities as to exert a noticeable influence on the cosmic radiation. The region in which the cosmic radiation is affected by solar-associated phenomena extends out from the sun to a point well past the earth. Solar plasma and the associated magnetic fields play a large part in the cosmic ray modulation in this region. Here the interactions are expected to be mainly of a macroscopic electromagnetic nature. Cosmic ray particles approaching the earth come under the influence of the geomagnetic field, as soon as the magnetosphere is reached. Microscopic interactions in this region are negligible. The atmospheric region changes the nature of the cosmic radiation drastically. Particle-particle interactions give rise to many secondary types of particles not evident in the original primary radiation, and cause absorption of the primary component. On the ground, all that is detected is the secondary radiation.

A theory dealing with the cosmic radiation can investigate any one of these modulation regions separately. However, because of their inclusive nature as far as the point of observation is concerned, present experimental techniques can only examine the radiation after it has passed through the extrasolar and solar regions. In order to examine many of the parameters of the primary cosmic radiation, it is necessary that the detecting apparatus be placed above most of the earth's atmosphere, so as to reduce the atmospheric effects to an easily correctable level. Satellite experiments, for which the effects of the atmosphere are entirely removed, are costly and should therefore be considered only for purposes for which they are essential. High altitude balloons are feasible for most such studies, but are limited by a small residual amount of atmosphere (usually less than 10 g/cm^2) and the short-lived nature of most balloon flights (10 or so hours). The geomagnetic modulation of the primary radiation is easily corrected for. The radiation above a certain rigidity (momentum/charge) is unaffected in intensity, for a given direction, while below this rigidity for the same direction, it is removed completely. This 'cut-off rigidity' depends on the geomagnetic latitude of the apparatus, being much less for high latitudes than low ones. Above 65°N magnetic, the low rigidity limit of particle detection for measuring devices is defined by the instrument and the atmosphere above it rather than the geomagnetic field, for most balloon experiments. Thus, by the use of balloon flights at high latitudes, one can remove most

of the effects of the atmosphere and geomagnetic field on the cosmic radiation.

Studies of the solar modulation effects on the primary cosmic radiation are of interest to the present investigation, both as an indicator of the physical processes that occur in the solar system and in order to be able to correct for the modulation, deriving extrasolar cosmic ray fluxes from fluxes measured in the vicinity of the earth. These solar modulation effects fall into several different classifications, which will be described in the next chapter.

CHAPTER TWO

SOLAR MODULATION OF COSMIC RADIATION

2.1 Techniques of Observation

The solar modulation of the cosmic radiation is a composite of several different effects, quite varied in their characteristics. All the solar modulation phenomena, however, are distinguishable from the galactic modulation by their time dependences, on the assumption that the characteristic time constants of the galactic modulation are much greater. In the examination of these modulations, various experimental techniques are useful, each technique being better suited for some particular area of investigation than the others.

2.1.1 Ground-based Equipment: The Neutron Monitor

In ground-based detectors, the secondary products of the primary cosmic radiation are observed, and thus the primary radiation is indirectly monitored. Any change in the primary cosmic radiation should be reflected in the observations of a detector sensitive to the products of that radiation.

Ground-based detectors have the advantage of high counting rates and ease of information recovery, unlike the detectors which directly monitor the primary radiation in balloons, rockets, or satellites and space probes. Their reliability is higher and, as they are capable of observing the radiation for a much longer period of time than the remotely operated equipment, they lend themselves to secular studies of the solar modulation.

However, ground-based detectors are sensitive to changes in the atmosphere as well as in the primary flux, and must be corrected for these atmospheric changes. Pressure and temperature

effects are observed for most equipment. A correction for pressure is easily made, but continuous atmospheric temperature measurements are not feasible and therefore complete temperature corrections cannot be made for most studies.

The neutron monitor is a device intended to monitor the nucleonic component of the secondary cosmic radiation. The principles of its operation were first demonstrated by Tongiorgi (1949). The advantages of the nucleon component of the secondary radiation as an indicator of primary changes were pointed out by Simpson (1951), and the neutron monitor was developed for the detection of this radiation by Simpson, Fonger, and Treiman (1953). As the nucleonic component consists of nearly stable or stable particles, and the atmospheric temperature effect arises from the instability of certain other particles, neutron monitors do not need to be corrected for atmospheric temperature. As well, the neutron monitor's sensitivity is biased towards a lower energy portion of the cosmic ray spectrum than is that of other types of ground-level detectors, such as ionization detectors and meson telescopes. As the solar modulation effects are most strongly felt in the lower energy particles, the neutron monitor is relatively sensitive to these effects. The good statistics and high accuracy of atmospheric correction available with such a detector makes it a good instrument with which to observe small amplitude changes in primary cosmic ray intensity.

A single neutron monitor cannot provide an accurate study of the spectral characteristics of a solar-associated variation, but several monitors located at either different latitudes or altitudes and therefore having different primary energy sensitivities can.

2.1.2 Balloon, Rocket, and Satellite-Borne Equipment

Certain features of the primary radiation, such as charge spectra, cannot be examined with ground-based equipment. For investigations of these features, more direct observations must be used. It is necessary to locate the observing equipment above or near the top of the atmosphere for this. This constraint has led to the development of specialized observing equipment for this purpose. The advantages and disadvantages of several different techniques will now be discussed.

2.1.2.1 Photographic Emulsions

The photographic emulsion was one of the first apparatus to come into widespread use for the detection of primary cosmic radiation. The techniques involved and many of the early results found with emulsions are described in a review article by Peters (1951). Emulsion work is best suited for balloons, but has also been carried out with rockets and even satellites. Recovery of the emulsion after the flight is essential, making the use of this technique in satellites difficult.

The photographic emulsion is basically an integrating device, recording every particle that interacts with the emulsion. The data obtained cannot be divided into that taken at altitude

and that taken while ascending or descending. This disadvantage can be corrected for by flying a second identical set of emulsion plates which are released as soon as the balloon reaches altitude. The data from this set of plates is then subtracted from that of the first set, to obtain a picture of the data obtained at altitude only.

Both the charge and the energy of the primary cosmic ray particles can be determined quite accurately over a wide range of values with this apparatus. Studies of time variations have been made, using several balloon flights. Detailed studies of interactions are possible. Emulsions do not, in general, lend themselves to studies of short-time variations in the primary radiation. The statistical accuracy obtainable with emulsions is limited by the number of particles any one stack can detect and the time needed for manual analysis of each particle 'track'.

Emulsions are still a valuable tool for studies of the primary radiation.

2.1.2.2 Electronic Ionization Detection Devices

These devices observe the charged primary radiation by its ionization loss in some form of electronic detector, such as an ionization chamber, geiger counter, or scintillation detector. They have the advantage of a high counting rate, and therefore good statistical accuracy, which facilitates study of the temporal variations in the primary radiation. Recovery is not necessary with electronic devices, as the information can be transmitted

to the ground. As these detectors utilize the ionization process, it is possible to obtain information on particle charge and velocity with them. The complexity of electronic ionization detection systems varies considerably, depending on the amount of information being conveyed. These instruments have had very widespread use, in balloons, rockets, and satellites and space probes.

2.1.2.3 Cerenkov Detection Devices

These detectors utilize the small amount of light radiated by a charged particle when it passes through a medium with a speed greater than the speed of light in that medium. The light is normally picked up by a photomultiplier tube and converted into an electronic signal.

As the light emitted depends upon the charge and velocity of the particle, Cerenkov devices are capable of conveying this information. Unlike ionization detectors, they are insensitive to low velocity particles. They do not experience the similarity between outputs of low velocity singly charged particles and high velocity doubly charged particles that ionization detectors do. Cerenkov detectors have proved useful in examination of the charge spectrum of the primary radiation (Webber and McDonald, 1955; Webber, 1956) and the rigidity spectrum of the high Z primary radiation (Durney et al., 1964). The directional property of the Cerenkov radiation has been utilized to determine the flux of fast upwards moving cosmic ray albedo in balloon regions

(Winckler and Anderson, 1954; Anderson, 1957). Uncertainty does arise due to the equal outputs of intermediate velocity doubly charged particles and fast singly charged particles.

2.1.2.4 Cerenkov-Scintillation Devices

These devices are a combination of the two types of detectors mentioned in 2.1.2.2 and 2.1.2.3. By combining these two detectors, the uncertainties between particle charge and velocity mentioned above are removed. The theory involved is presented in Chapter 3.

The first such detector was built by McDonald (1956), who demonstrated its usefulness in studying the energy spectra of the primary alpha particles in a series of balloon flights. The proton data from the same series of flights was later presented by McDonald and Webber (1959). This type of detection device has also been proven capable of examining the primary charge spectrum for particles with charge up to $Z = 8$ (McDonald and Webber, 1962; Balasubrahmanyam and McDonald, 1964).

The Cerenkov-scintillation detection system has the advantage of the retrieval of a comparatively large amount of information concerning the particles passing through it, for an electronic system, as well as the potential attainment of a high statistical accuracy. Since it is an 'electronic' type of detector, the information can theoretically be transmitted, thereby eliminating the necessity of package recovery. However, up until now most recording has been done on moving film or magnetic tape, in the balloon package. Cerenkov-scintillation apparatus appears well-suited for a study of the rapid temporal variations in the

primary radiation, both of charge and energy. The complexity of this system, however, is an undesirable feature.

2.1.2.5 dE/dx by E Detectors

These detectors combine measurements of the ionization energy loss (dE/dx) of particles with those of total energy (E). They are therefore capable of determining the charge, velocity and, from the energy, the mass of the cosmic ray particles, and are thus useful in isotopic studies of the primary radiation. Such detectors have been used to examine low energy portions of the primary cosmic ray spectrum, in the ranges 15 to 75 MeV (McDonald and Ludwig, 1964) and 80-350 MeV (Vogt, 1962; Meyer and Vogt, 1963), extending the primary spectra inferred from measurements by other devices to quite low energies.

2.2 Slowly Varying Solar Modulation: The Eleven Year Cycle

An eleven year variation in cosmic ray intensity occurs which is negatively correlated with solar activity. The existence of this variation was first demonstrated by Forbush (1954), using ground level ionization detectors. It was shown to be a persistent feature of the cosmic radiation, not merely arising from the contribution of transient decreases in intensity which occurred more frequently at solar active times.

The decrease in cosmic ray intensity, following the eleven year maximum, sometimes lags behind the increase in solar activity following solar minimum. This delay was found to occur and be of the order of a year for ground level ionization detectors for the 1954 minimum (Forbush, 1958), but was not apparent in the neutron monitor data at Ottawa (Fenton et al, 1958) or the high latitude balloon-flown ionization chamber measurements of Neher and Anderson (1958). As the two latter types of measurement detect lower energy primaries, an energy dependence of the 'lag time' is suggested.

The eleven year variation in cosmic ray intensity is energy dependent, having an amplitude of approximately 4 per cent for the ground level ionization detectors of Forbush (1954), and 20 per cent for the Ottawa neutron monitor, which is biased toward lower energies. This energy dependence is also reflected in the shifting of the cosmic ray 'knee' in the geomagnetic latitude versus ground level nucleon intensity curve northward, as solar

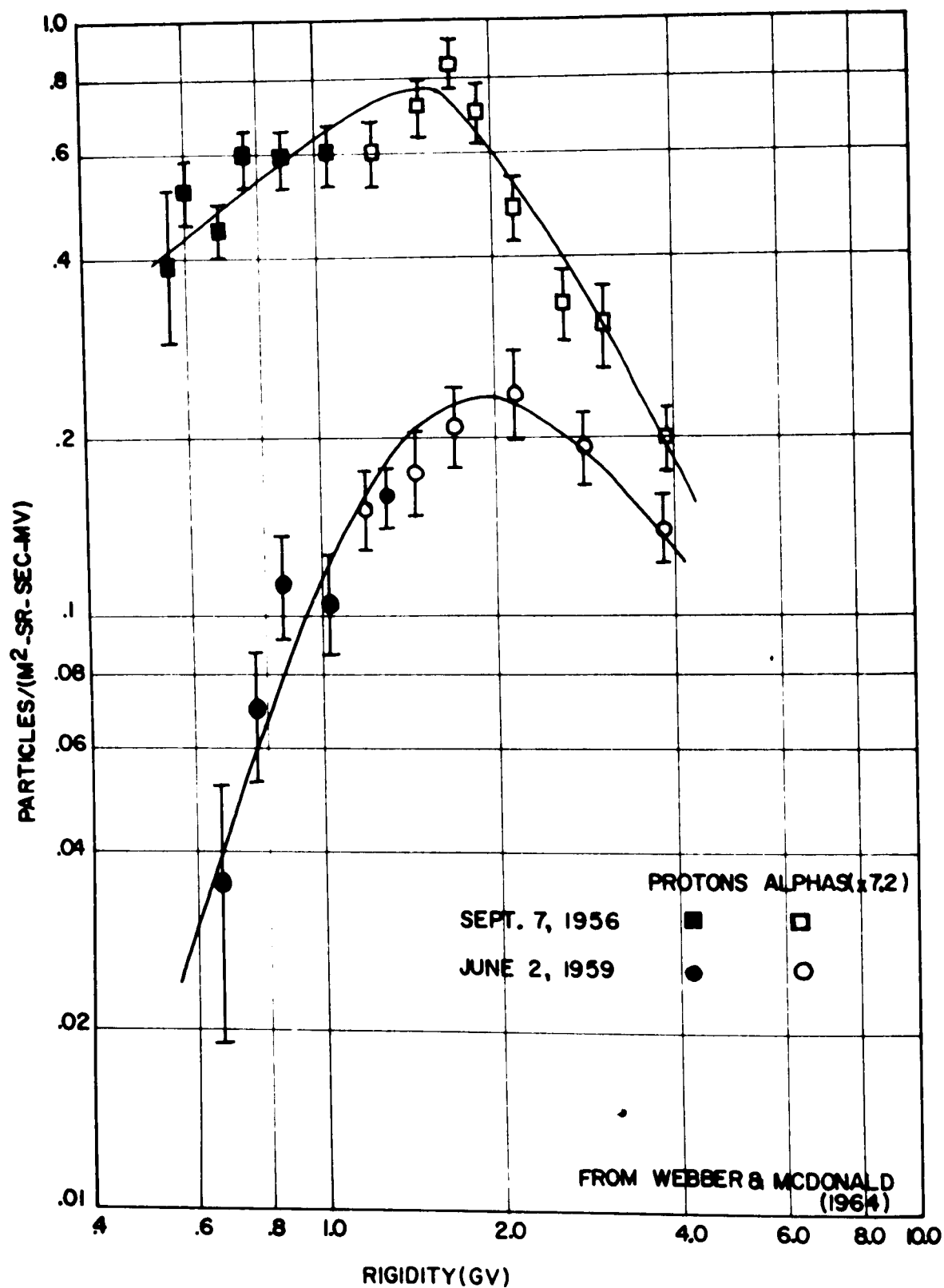


Figure 1 Differential Proton and Alpha Particle Rigidity Spectra at Different Times of the Solar Activity Cycle: 1956-9.

minimum is approached (Meyer and Simpson, 1955). The shift suggest the presence of a proportionately higher amount of low rigidity primaries at solar minimum than at other times.

A comparison of the data obtained with balloon-borne Cerenkov-scintillation detectors between 1956 and 1959 (Webber and McDonald, 1964) provides a picture of the changes that took place with respect to the parameter of particle rigidity between these times. Figure 1 illustrates their results. The alpha particle data have been multiplied by a factor of 7.2, in order to use it along with the proton data. From this figure, the flux at 1.0 GV rigidity changed by a factor of 5.5 between the two times, while that at 3.5 GV rigidity changed by a factor of 1.6. The corresponding factor for the Ottawa neutron monitor is 1.13. These results, therefore, illustrate a strong rigidity dependence of the eleven year modulation mechanism.

Determinations of two different geomagnetic cut-off rigidities at solar maximum and comparison with the values measured near minimum (McDonald, 1959; McDonald and Webber, 1959) revealed that they did not change appreciably. Therefore the eleven year modulation cannot be due to a change in geomagnetic cut-off. A later paper (Webber and McDonald, 1964) confirmed the idea of a 'sharp' geomagnetic cut-off, as is expected from the Störmer theory. (For a treatment of this theory, see Vallarta (1961).)

The rigidity spectra for primary protons and alpha particles observed by Cerenkov-scintillation techniques, were found to

be of the same shape during 1955-6, soon after solar minimum (McDonald and Webber, 1959). Although the rigidity spectra changed as solar maximum approached, further Cerenkov-scintillation counter balloon flights during 1958 revealed that the rigidity spectra for protons and alpha particles remained similar, down to rigidities of 1.0 GV. A study during the same period of the heavier nuclei, Be, B, C, N, and O, having rigidities greater than 2 GV, showed that these particles also displayed the same relative rigidity spectrum as the protons and alpha particles throughout this phase of the solar cycle (McDonald and Webber, 1962). This similarity is suggested by Figure 1.

More recent measurements taken in June, 1963 as the present minimum in solar activity was being approached, by Balasubrahmanyam and McDonald (1964) with a balloon-borne Cerenkov detector, and simultaneously by Fichtel et al (1964) with emulsions, indicated that the proton rigidity spectrum was similar to that measured in 1956 by Webber and McDonald (1964). However, the alpha particle rigidity spectrum showed a proportionately lower fraction of low rigidity particles than the proton spectrum. At the high rigidity end, the alpha spectrum agreed with the measurements taken in 1956. dE/dx by E studies aboard the IMP-1 satellite from December, 1963 to May, 1964, by McDonald and Ludwig (1964), in which particles in the energy range 15 to 75 MeV/nucleon were examined, extended the flux measurements of protons and alpha particles to lower rigidities, and added further weight to the observed split in the alpha and proton rigidity spectra. These

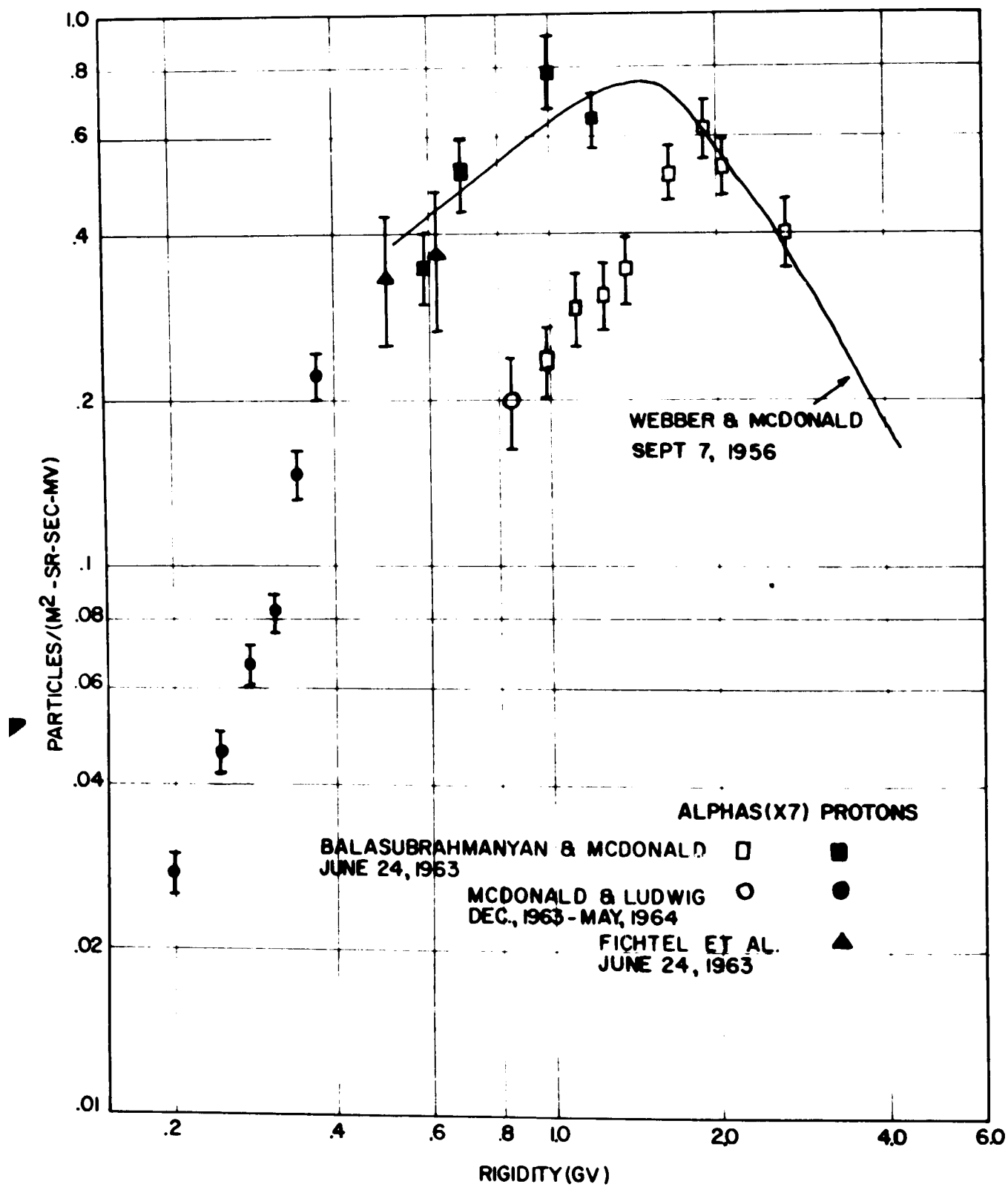


Figure 2 Differential Proton and Alpha Particle Rigidity Spectra: 1963-4.

results are summarized in Figure 2. As in Figure 1, the alpha data have been multiplied by a factor of 7.

Spatial, rather than temporal, investigations of the eleven year solar modulation of cosmic rays have been carried out near solar maximum using the space probe Pioneer V. The smallness of the cosmic ray gradient measured over 0.1 A.U. between the earth and sun suggested that the solar modulation was heliocentric, and occurred mainly well outside the earth's orbit (Fan et al, 1960; Simpson et al, 1961).

During the last solar maximum an unexpectedly high flux of protons of energy less than 500 MeV was observed for Aug. - Sept., 1960, which had not been seen previously (Vogt, 1962). Comparison with measurements of July - Aug., 1961 showed it to decrease with a decreasing level of solar activity, as the higher energy galactic flux increased (Meyer and Vogt, 1963). On this basis, this flux was thought to be of solar rather than galactic origin. Ionization detector measurements beyond the magnetosphere in 1961 on Explorer XII (Bryant et al, 1962) showed agreement with Meyer and Vogt (1963), and established that the low energy proton flux was continuous over long periods of time.

From these experimental results, it appears that two separate effects make up the eleven year variation in cosmic ray intensity. Firstly, there is the removal of galactic cosmic radiation from the vicinity of the earth, more pronounced at times of high solar activity. The modulating region for this effect appears to be

well outside the earth's orbit, and likely centered about the sun. The amount of 'steady state' solar modulation present at solar minimum is as yet uncertain. Secondly, a solar injection of low energy (and therefore rigidity) protons, not detectable in ground equipment, is in effect at times near solar maximum. These low rigidity protons are most likely emitted either continuously or at least very frequently during these times and 'stored' inside the heliocentric modulating region. As can be seen from Figure 2, the proton flux for low rigidities at solar minimum agrees with an extrapolation of the higher rigidity galactic radiation, and is therefore probably galactic in origin. Thus either the solar injection of protons, or perhaps the storage mechanism for these particles, does not seem to be significant at solar minimum.

An early theory of the eleven year solar modulation of galactic cosmic radiation (Morrison, 1956) postulated turbulent 'clouds' of magnetized plasma emitted from the sun at solar active times. The cosmic ray beam was modulated by random diffusion processes inside these clouds, which travelled through the solar system to the region of the outer planets. This proposal of solar-produced magnetized plasma was not startling, as disturbances in the geomagnetic field associated with solar activity had been observed for some time. The existence of steady particle streams from the sun had already been noted by Biermann (1951, 1952, 1957), inferred from the observed acceleration

of particles in comet tails. Many satellite and space probe measurements of these streams and their associated magnetic fields have since been made. Parker used Biermann's observations to develop the concept of a solar 'wind', and later a detailed theory of the state of the interplanetary medium (Parker, 1963). Some consequences of his theory in regard to the eleven year modulation are the following. The physical processes involved in galactic cosmic ray modulation consist of outward convection of the charged particles in moving magnetic fields, balanced against inward leakage of particles by diffusion and drift. The observed eleven year depression is the result of the total integrated cosmic ray convection, diffusion and drift beyond the orbit of the earth. The convection mechanism probably extends out as far as 50 A.U. However, the configuration of the diffusion-producing magnetic fields is as yet unknown. Along with the observed solar wind, the expected perturbations in the interplanetary magnetic field appear sufficient to account for at least a substantial portion of the eleven year attenuation. The possibility of other mechanisms also contributing is recognized. Uncertainty exists in the relative contributions of particle drift and diffusion to the modulation. Time variation studies of cosmic ray particles with different charge to mass ratios, such as the protons and alpha particles, should aid in filling in some of the details of the general mechanism involved.

2.3 Transient Solar Attenuation Phenomena

Superimposed on the eleven year variation in cosmic ray intensity are attenuation phenomena having a much shorter characteristic time scale. These phenomena range from large (20 per cent as measured by sea-level neutron monitors), infrequently occurring decreases, through smaller, much more frequently occurring decreases. Two of these effects have easily identifiable characteristics, and will be discussed in this section.

2.3.1 The Forbush Decrease

An examination of the records of ground level detectors reveals the presence of short-term intensity decreases of a non-repetitive nature. These Forbush decreases, as they are called, are characterized by a sharp decrease, from less than an hour to 24 hours duration, followed by an exponential recovery. The time scale of the recovery increase varies considerably in length, from several days to many weeks. A review article by Webber (1962a) discusses the features of Forbush decreases.

These decreases show a strong correlation with geomagnetic storms, their onset times generally occurring within 1 to 6 hours from the start of a sudden commencement geomagnetic storm. Many of the larger Forbush decreases start one to three days after the occurrence of a large solar flare on the sun. The decrease-associated flares usually are accompanied by a long-lasting intense continuum of low frequency radio noise. There is no

preferred solar longitude zone for these flares, but longer flare-decrease onset times are indicated for flares on the eastern limb of the sun.

The rigidity dependence of Forbush decreases is quite pronounced. However, for the largest decreases, a finite intensity of low-rigidity particles still exists. A comparison of changes in both the proton and alpha particle intensities as measured by Cerenkov-scintillation counters in two balloon flights, one of which was during a Forbush decrease, indicated that the rigidity changes in these two components were the same (McDonald and Webber, 1959). A recent study of the heavier primary cosmic ray nuclei ($Z \geq 3$) by Freier and Waddington (1964), using emulsions flown in balloons before, during, and after four large Forbush decreases, suggested that these nuclei were modulated in a way similar to the alpha particles and protons.

2.3.2 The Twenty-Seven Day Variation

A twenty-seven day variation in cosmic ray intensity which is intimately connected with solar activity and the period of rotation of the sun sometimes occurs. The rigidity dependence of this variation is similar to that of the Forbush decreases, suggesting that the causal mechanisms might be the same. It is possible that the twenty-seven day variation is the result of the superposition of a large number of small decreases, existing inside regions co-rotating with the sun. The demarcation line between repetitive twenty-seven day decreases and non-repetitive Forbush decreases as seen on ground level neutron monitor records is not a clear one.

2.4 Transient Solar Injection Phenomena

Just as the state of the interplanetary medium outside the earth's orbit is revealed by a study of the galactic cosmic radiation, so the interplanetary medium inwards of the earth can be examined by a study of the solar-produced radiation. In addition to the constant presence of low energy particles present during the active phase of the solar cycle, transient solar particle events exist. Observations of these events have been made at ground level, and in balloons, satellites, and space probes. Their characteristics are discussed in detail by Webber (1962b), and will be briefly described here.

2.4.1 Ground-Level Increases

These increases in cosmic radiation occur quite rarely, on the average on one per year, and are seen in the records of ground level neutron monitors. They show a sharp rise, often over 100 per cent, followed by an exponential decrease, and are short in duration, lasting from several hours to a day.

Strong evidence exists for the postulation of certain large solar flares as the 'cause' of these increases. The causal flares are generally accompanied by continuum and slow drift radio noise emission, and X-ray emission. Both these emissions are suggestive of the creation of fast particles.

The characteristics of the increases can differ. A typical ground level increase is initially anisotropic in its arrival direction at the earth, the original intensity rise being recorded only in certain preferred 'impact' zones. Later the

increase becomes isotropic, and contains less high energy particles than previously. Some increases, however, do not have the initial anisotropy. The delay time between the solar flare and arrival time of the anisotropic particles is consistent with the hypothesis of a nearly straight direction of travel between the earth and sun. The impact zones for these particles suggest a source width of $\pm 30^\circ$, although there is uncertainty in the source direction. The later isotropic particles have delay times much longer than those inferred from rectilinear travel. This fact, coupled with the measured isotropy, suggests that the travel mechanism of the later particles is largely one of diffusion.

The causal solar flares for the ground level increases show a strong bias towards the western hemisphere of the sun, perhaps suggesting the linking of magnetic field lines from this hemisphere and the vicinity of the earth. This agrees with present theories of the solar wind (Parker, 1963).

The rigidity spectra of ground level increases are very steep in slope and may differ from event to event. As already indicated, this steepness increases at later times in the event.

2.4.2 Polar Cap Absorption Events

These events are often observed by the occurrence of an increased amount of absorption of galactic radio noise in the ionosphere, as measured by riometers. Bailey (1957) first suggested that the causal mechanism for the enhanced absorption was the arrival of protons, of energies 10 to 100 MeV. Various

balloon and satellite measurements of these particles have since confirmed this. These events, as do the ground level increases, also appear to be strongly associated with radioisotopic solar flares. However, these flares do not show the definite western bias in location that the ground level increase associated flares do, although a small bias is suggested. As well, the delay times between the solar flares and events are much longer than those expected on the basis of rectilinear particle propagation. Both these facts suggest that diffusion plays a much greater role in the propagation of the lower energy polar cap absorption particles than for the ground level increase particles.

2.5 Daily Variation

As well as the transient changes in cosmic ray intensity occurring in connection with solar activity, there is a diurnal variation in cosmic ray intensity as measured by ground level detectors. This variation is quite small, of the order of 0.5 per cent for neutron monitors. The neutron monitor has proved the best tool for examination of the phenomenon of the daily variation.

Considerable variations in the phase and amplitude of the diurnal variation may take place over periods of several days. When the data are averaged over periods of the order of a month, however, the phase seems to settle down to a slowly varying parameter. The amplitude does not, although variations in amplitude are generally of a worldwide character. Latitude studies indicate a slow increase in the diurnal variation with latitude, if any. A definite increase in the time of maximum of the variation, with increase in geomagnetic latitude, occurs.

Up to the present, no direct measurements of the daily variation in the primary radiation have been made.

2.6 Summary: State of Knowledge of the Solar Modulation and Purpose of the Experiment


The solar modulation of cosmic radiation is a time dependent one, consisting of a steady eleven-year variation upon which different types of transient variations are superimposed.

A fair amount is known about the eleven year variation in the cosmic radiation, such as the approximate change in particle rigidity and charge. It is interesting to note that the nature of the modulation appears to have changed from a purely rigidity dependent one for the first part of the last solar cycle, as the maximum in solar activity was being approached, to a partially charge dependent one for the waning phase of the cycle. More observations in this regard are indicated, as they should help in establishing the relative contributions of different mechanisms such as particle drift and diffusion to the eleven year variation, and the time dependences of these mechanisms. As well, it would be helpful to know the residual amount of solar modulation left at solar minimum, in establishing the form of the cosmic radiation outside the solar system. Comparisons of particle rigidities measured near solar minimum from cycle to cycle and also throughout a single minimum period can be of use here.

The shorter-term variations are less well understood. Although the observations of Forbush decreases indicate that the modulation mechanism is mainly a function of rigidity, they are by no means conclusive. More accurate experimental results

than the ones presently in existence are necessary. Not many characteristics of the daily variation other than its ground-level shape are known. Examinations of this effect in the primary radiation, particularly of the relative rigidity dependences of different charge components, would help considerably in determining the possible causal mechanisms.

Therefore, there is a need for further studies of the rigidity and charge dependence of the solar-caused variations in cosmic ray intensity. Further, a greater statistical accuracy than previously obtained is desirable, particularly for studies of the transient variations. The present experiment, designed with this in mind, consisted of a balloon-borne Cerenkov-scintillation counter system, having a relatively high counting rate (approximately 5 counts/second), in which the data was transmitted to the ground for subsequent recording. The theory of the detectors is given in the next chapter.



CHAPTER THREE

THEORY OF THE CERENKOV - SCINTILLATION PARTICLE DETECTION SYSTEM

A Cerenkov-scintillation detector system utilizes the energy losses by two different processes of particles passing through matter, ionization and Cerenkov emission of radiation. The theory for this combination of processes was first discussed by Linsley (1955).

The first process, that of ionization, is discussed at an elementary level in a text by Segre (1964). More sophisticated formulas for this process are collected by White (1965), from calculations of Sternheimer (1952, 1953, 1956). The most probable ionization loss of a relativistic charged particle in a material is given as

$$\epsilon_p = \frac{\alpha x Z^2}{\beta^2} \left(B + 1.06 + 2 \ln \left(\frac{\beta}{\sqrt{1-\beta^2}} \right) + \ln \left(\frac{\alpha x Z^2}{\beta^2} \right) - \beta^2 - \delta \right) \quad (1)$$

where δ is the density correction factor, given by

$$\delta = \begin{cases} 4.606X + C + a(X_1 - X)^n & \text{for } (X_0 < X < X_1) \\ 4.606X + C & \text{for } X > X_1 \end{cases}$$

$$\text{where } X = \log_{10} \left(\frac{\beta}{\sqrt{1-\beta^2}} \right)$$

The symbols are x : thickness of material in g/cm^2 .

Z : charge of particle in units of e .

β : velocity of particle in units of c .

$\alpha, B, C, a, n, X_0, X_1$: constants of the material.

The specific detector we are concerned with uses a 1/2 inch thick piece of plastic scintillator NE102 for an ionization detector. For this material, the constants have the following

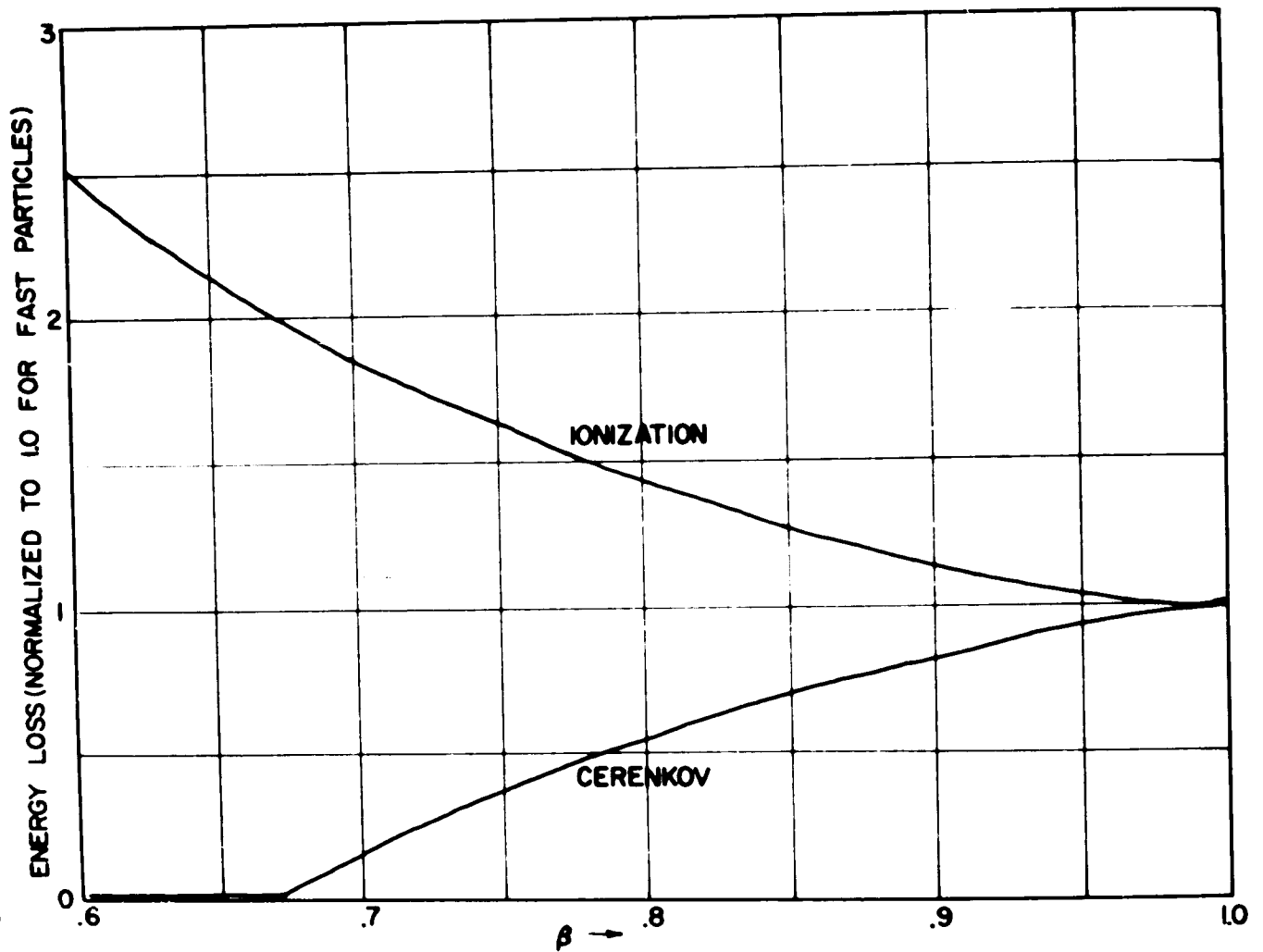


Figure 3a Cerenkov and Ionization Losses of Singly Charged Particles as a Function of Velocity

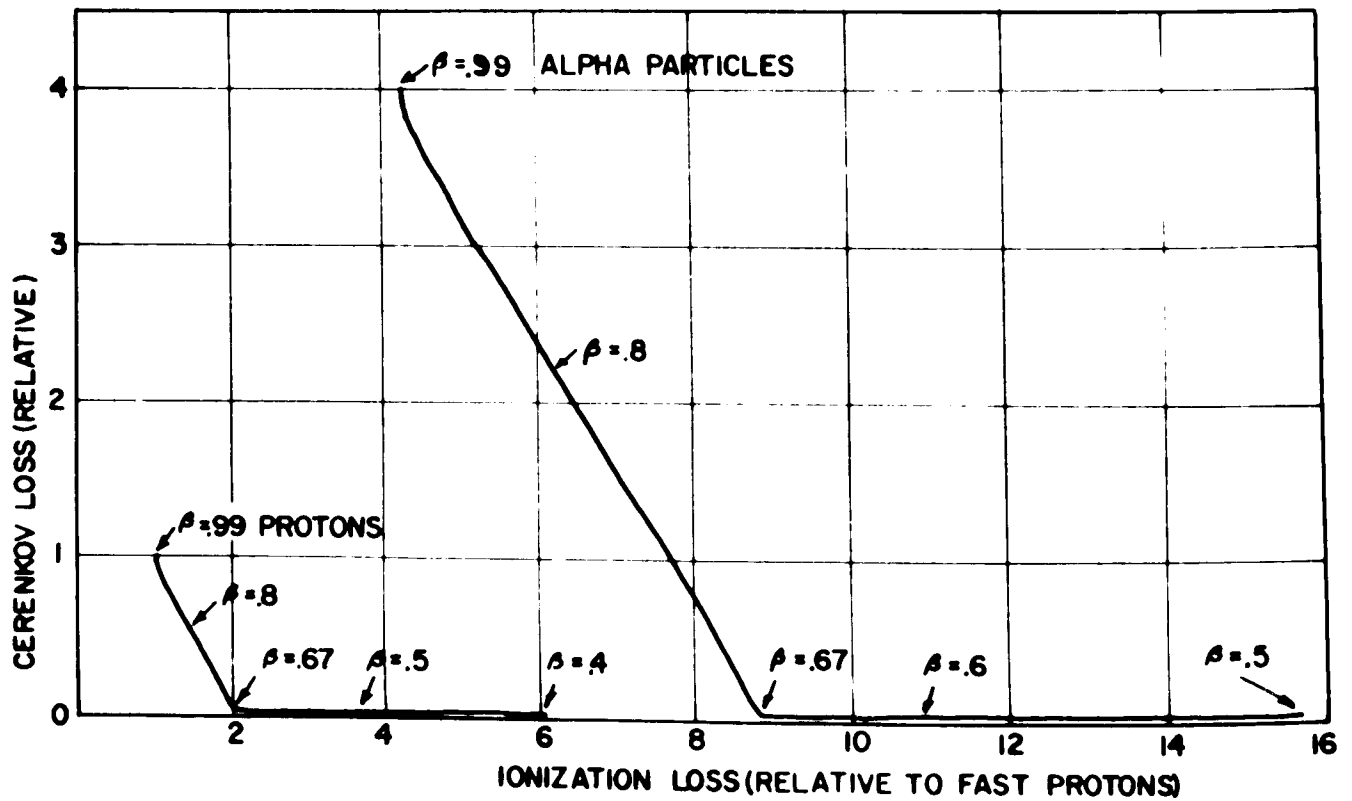


Figure 3b Cerenkov vs. Ionization Loss of Singly and Doubly Charged Particles

values (Crispin and Hayman, 1964):

$$\alpha = 0.0833 \text{ MeV}/(\text{g-cm}^{-2})$$

$$B = 18.69$$

$$C = -3.13$$

$$a = 0.514$$

$$n = 2.595$$

$$X_0 = 0.044$$

$$X_1 = 2.0$$

In Figure 3a, the most probable ionization energy loss for protons in a 1/2 inch thickness of plastic scintillator NE102 is plotted as a function of velocity. This scintillator gives a light output which is a monotonically increasing function of the ionization loss, enabling a determination of the ionization loss to be made from the light output.

The second process, Cerenkov loss, is treated in a classical manner by Schiff (1955). Cerenkov light is of a directional nature, proceeding in a direction fairly close to that of the causal particle. The following formula gives the Cerenkov radiation emitted for a charged particle traversing a material.

$$dN = \frac{2\pi Z^2 d\lambda}{137\lambda^2} \left(1 - \frac{1}{\beta^2 n^2}\right) \quad \text{for } \beta > \frac{1}{n} \quad (2)$$

$$0 \quad \text{for } \beta \leq \frac{1}{n}$$

The symbols are dN : number of quanta emitted per unit
length between wavelengths of λ and $\lambda+d\lambda$
 n : refractive index of material for light
of wavelength λ .

Z, β : as before.

A piece of clear lucite is used as the Cerenkov detector in the present research. This material has a refractive index of 1.5. In Figure 3a, the Cerenkov loss is plotted as a function of particle velocity for this detector.

An examination of formulae (1) and (2) and Figure 3a reveals certain characteristics of the ionization and Cerenkov effects. Both these effects are mainly functions of charge (Z) and velocity (β), being independent of particle mass. Their charge variation is nearly the same, being approximately equal to Z^2 in both cases. The ionization loss, however, is a decreasing function of particle velocity, while the Cerenkov loss is an increasing function of velocity.

Figure 3b shows the Cerenkov loss of a particle as a function of its most probable ionization loss, for both singly and doubly charged particles. The positions along the resultant lines corresponding to certain particle velocities are indicated. Particles passing through a Cerenkov-scintillation detection system will be represented by points clustered about these lines.

From Figure 3b, the ionization losses of both $\beta = 1.0$ to 0.8 doubly charged particles and $\beta = 0.5$ to 0.4 singly charged particles are seen to lie in the same range. An ionization device alone would not be able to discriminate between these particles, but because their Cerenkov losses are different, a Cerenkov detector can. On the other hand, the Cerenkov losses

of $\beta = 0.72$ to 0.5 doubly charged particles cannot be distinguished from those of singly charged particles in the range $\beta = 1.0$ to 0.4, but the ionization losses can. Utilization of both the ionization and Cerenkov effects in a detection device removes ambiguities that either one alone may produce in determining particle charges and energies.

If the particle velocities below 0.4 c are considered, it can be seen that even for the combination of effects, ambiguity will arise between singly and doubly charged particles. Inclusion of a particle absorber to limit the lowest energy detectable in such a system can remove this ambiguity, however.

CHAPTER FOUR

EXPERIMENTAL APPARATUS

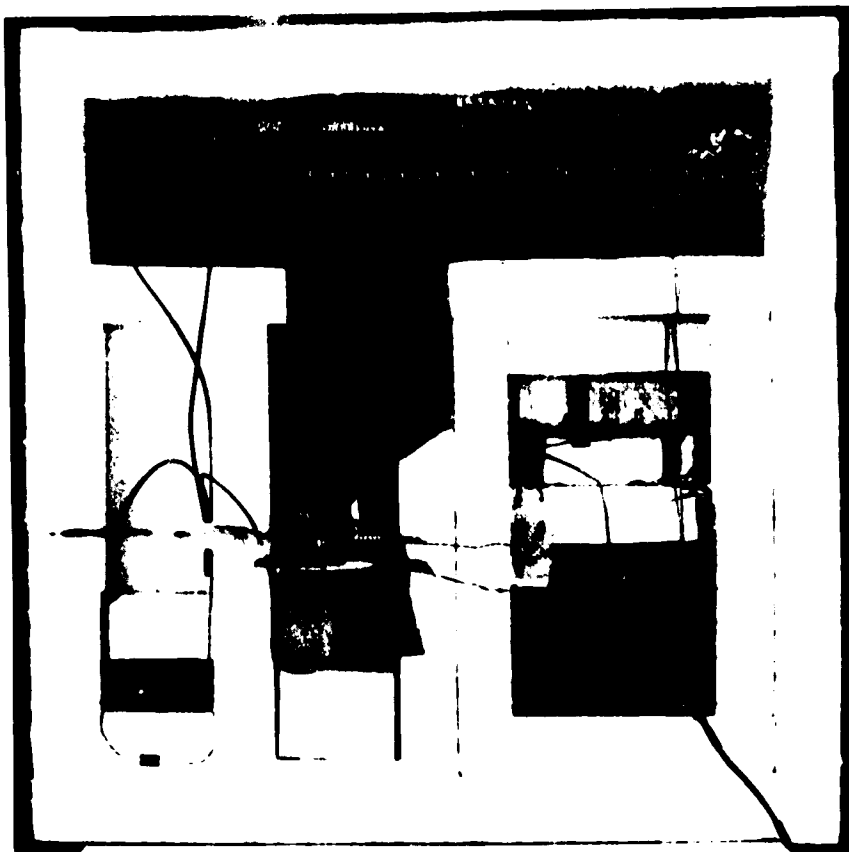


Figure 4a Balloon Package

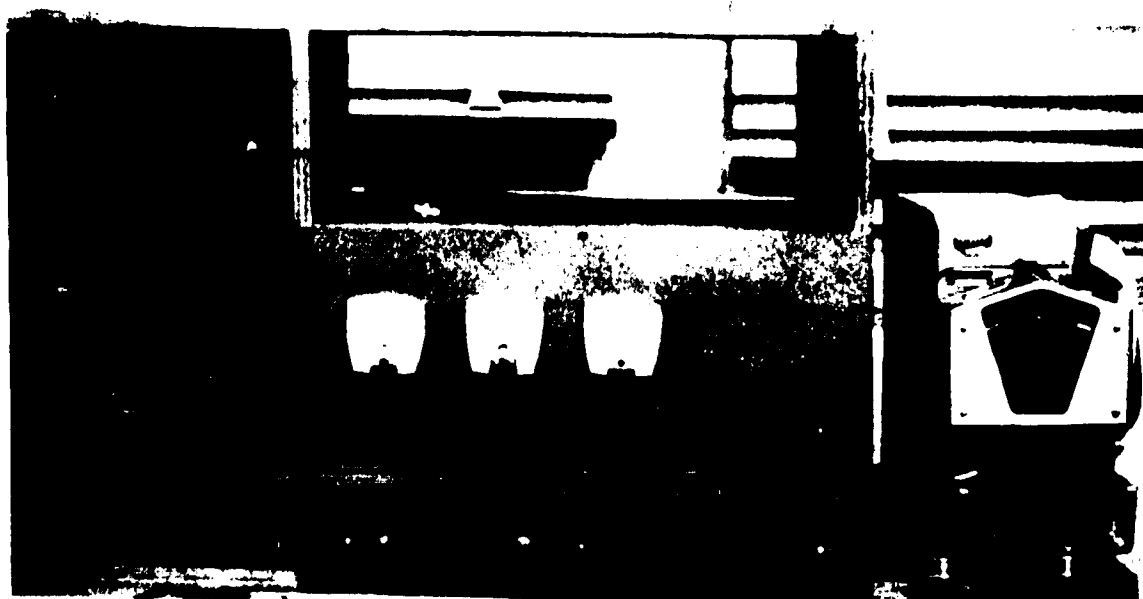


Figure 4b Decoding Electronics and Tape Punch System

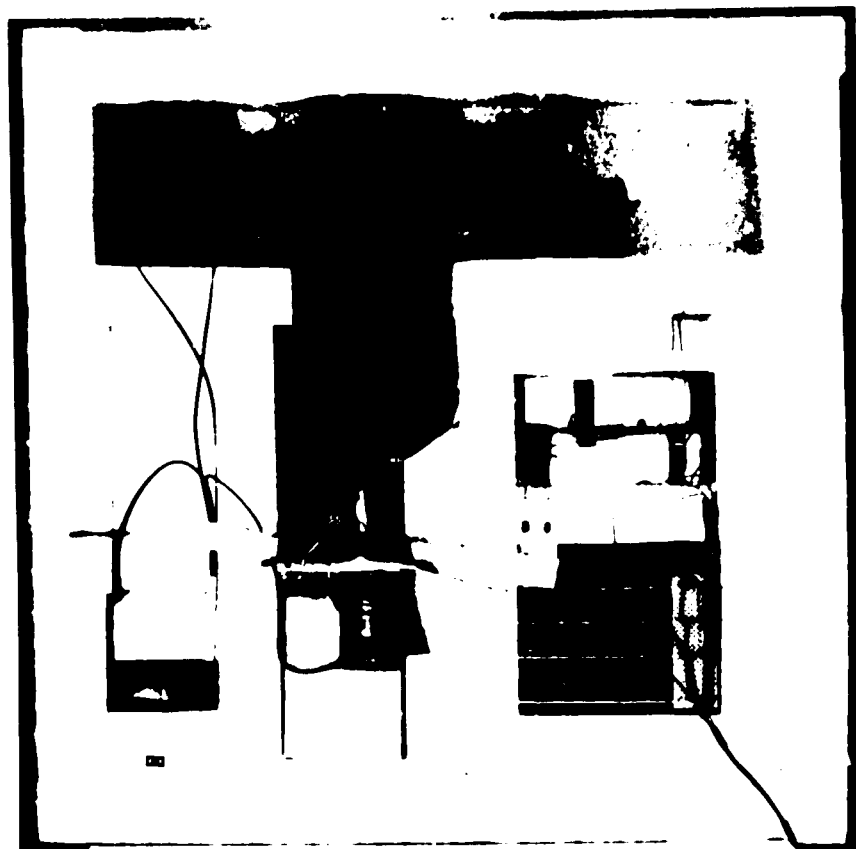


Figure 4a balloon ackare

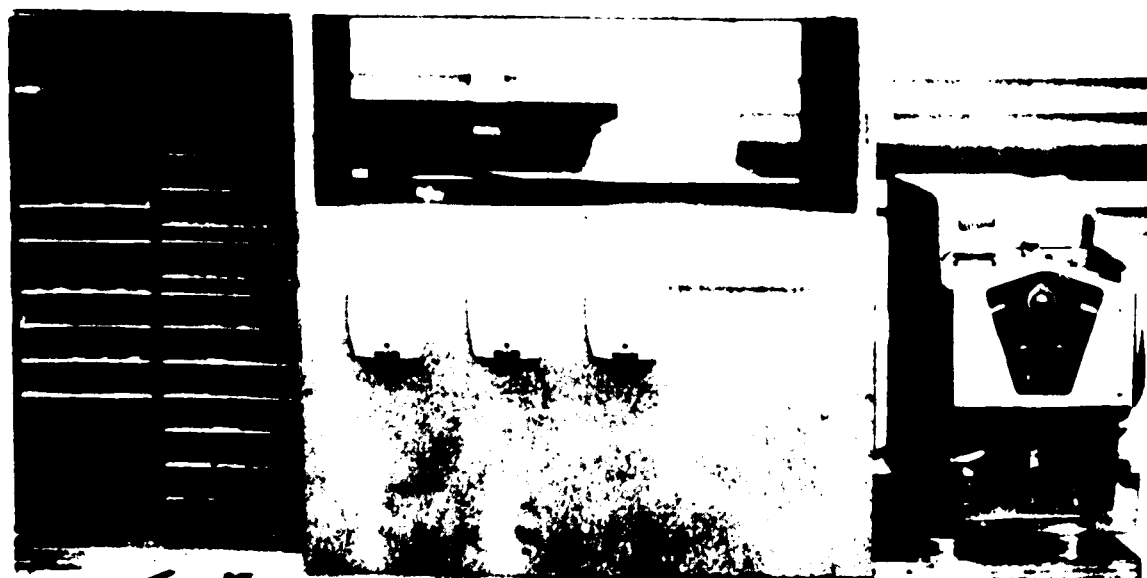


Figure 4b feeding electric and Tape punch system

4.1 General Description of the System

The system used in the course of the present research, for the detection of primary cosmic rays and the subsequent recording of information on these cosmic rays is shown in Figures 4 and 5. It can be seen from Figure 5 that the sole function of the balloon package as far as the cosmic radiation itself is concerned was the detection of the radiation and the transmission of the detection information to the ground. No data was recorded in the balloon package, thus eliminating the need for its recovery.

The antenna-receiver system, the magnetic tape recorder, the pressure and temperature recording system, the crystal chronometer, the balloon-borne transmitter and antenna, and the high voltage supply for the detectors are all components originally developed by the auroral physics group at Calgary under the supervision of Drs Anger and Clark for use with balloon-flown aurora detecting equipment. These components, because of their wide versatility, have become standard equipment, and have since been used in other researches, such as balloon-flown neutron detectors and the present study. The signal decoding and tape punch system, the data display system, the detector array and associated electronics, and the pressure and temperature sensing device were unique to the present study.

In the balloon package, information regarding individual cosmic ray particles as they pass through the detector system was transmitted to the ground, along with the temperature and pressure. A radiating monopole antenna was used for transmission,

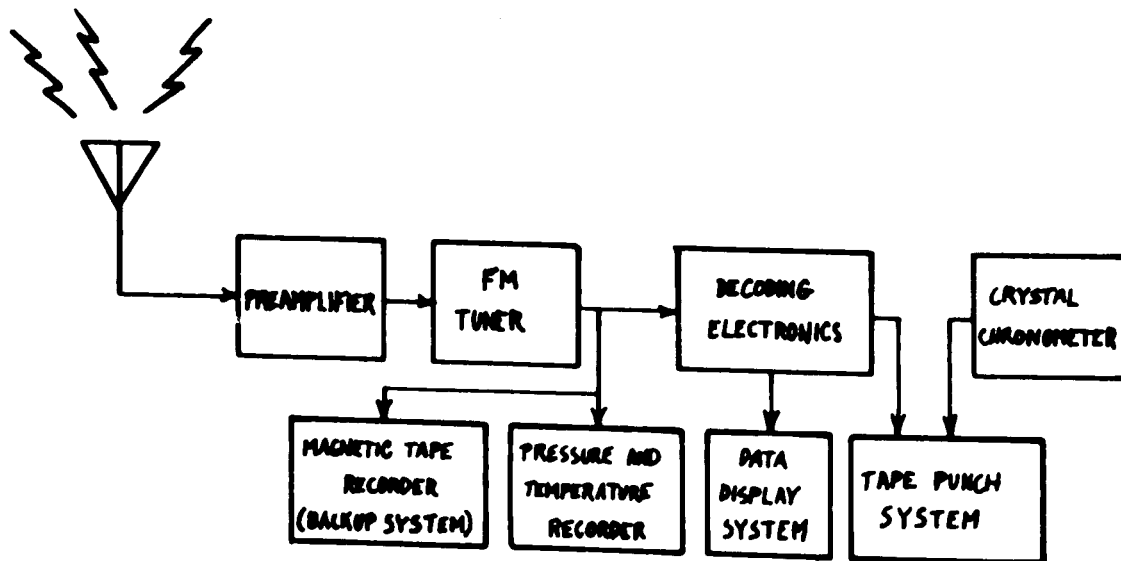
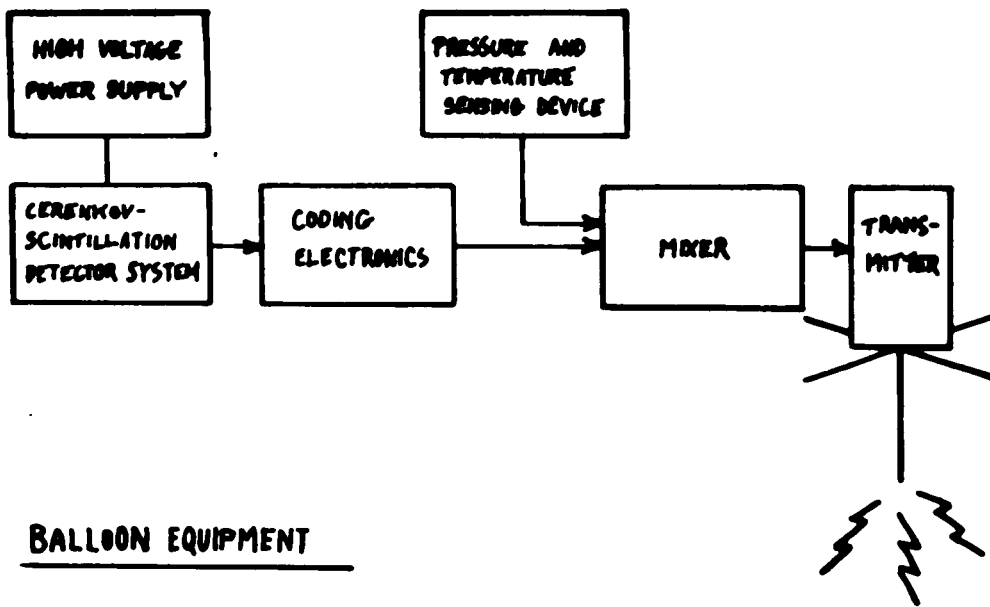


Figure 5 Block Diagram of Apparatus

with a crossed element ground plane to minimize feedback of the transmitted radiation into the detector electronics.

On the ground, the signal was picked up by a double yagi antenna, with a single receiving element and 9 guiding or reflecting elements on each of the two limbs. This antenna, because of its highly directional reception pattern, was attached to a driving motor which would point it in any desired azimuthal direction. The angle of elevation of the antenna was fixed, normally preset to approximately 5° . After passing through a preamplifier, the received signal was demodulated by an F.M. tuner. The demodulated output was fed to a magnetic tape recorder, which acted as a "backup" system from which the received signal might be recovered if any part of the remainder of the ground station broke down during a balloon flight. The output of the receiver was also fed to a pressure and temperature recording system, and to decoding electronics. The decoding electronics separated out the information on the individual cosmic rays which passed through the balloon-borne detectors, and put it into a form in which it could be punched out on paper tape. This electronics also put the data into a display system consisting of an oscilloscope and recording camera.

The next three sections of this chapter examine in greater detail the various components of the system outlined here.

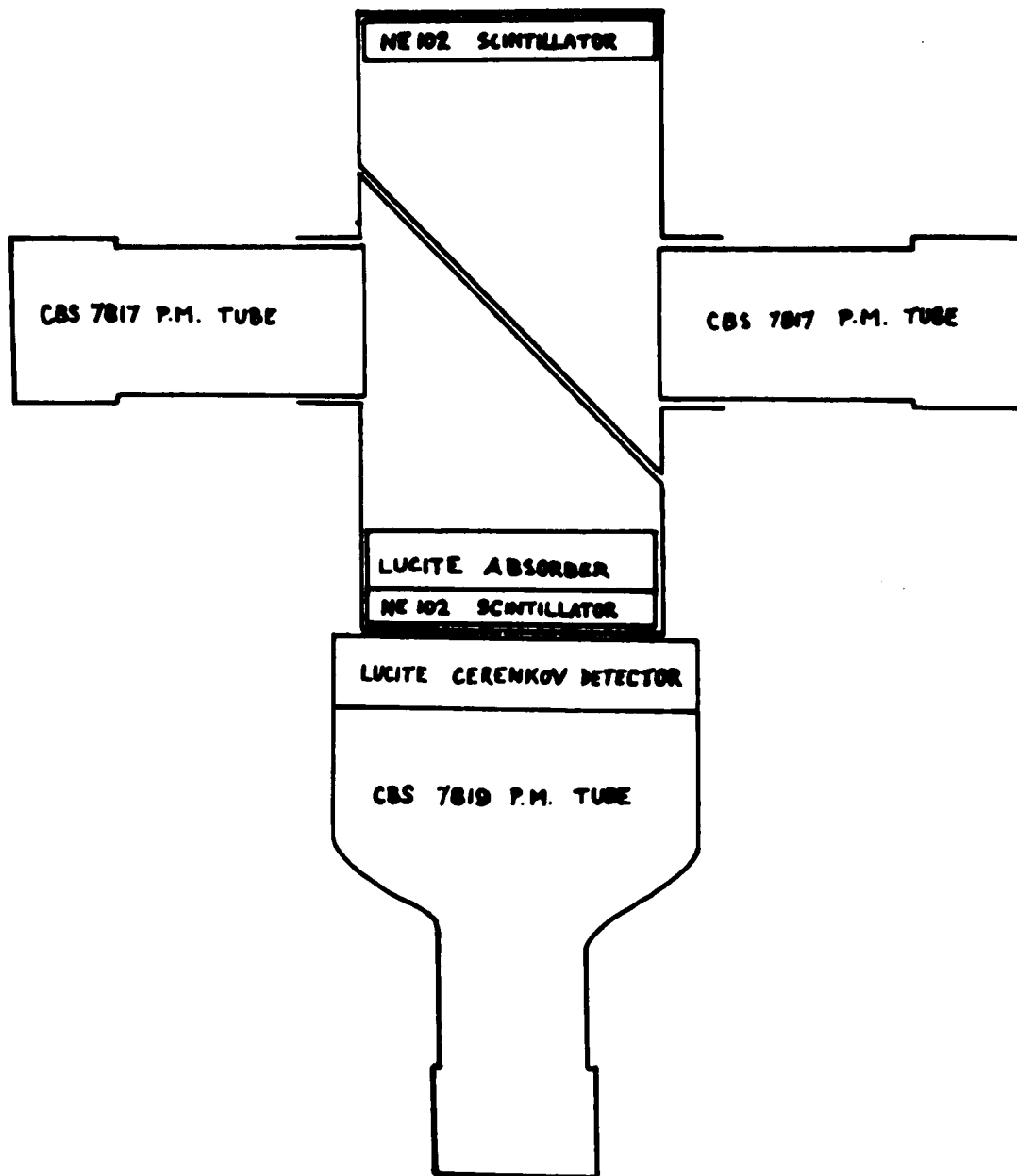


Figure 6 Detector Arrangement

4.2 Detection Apparatus

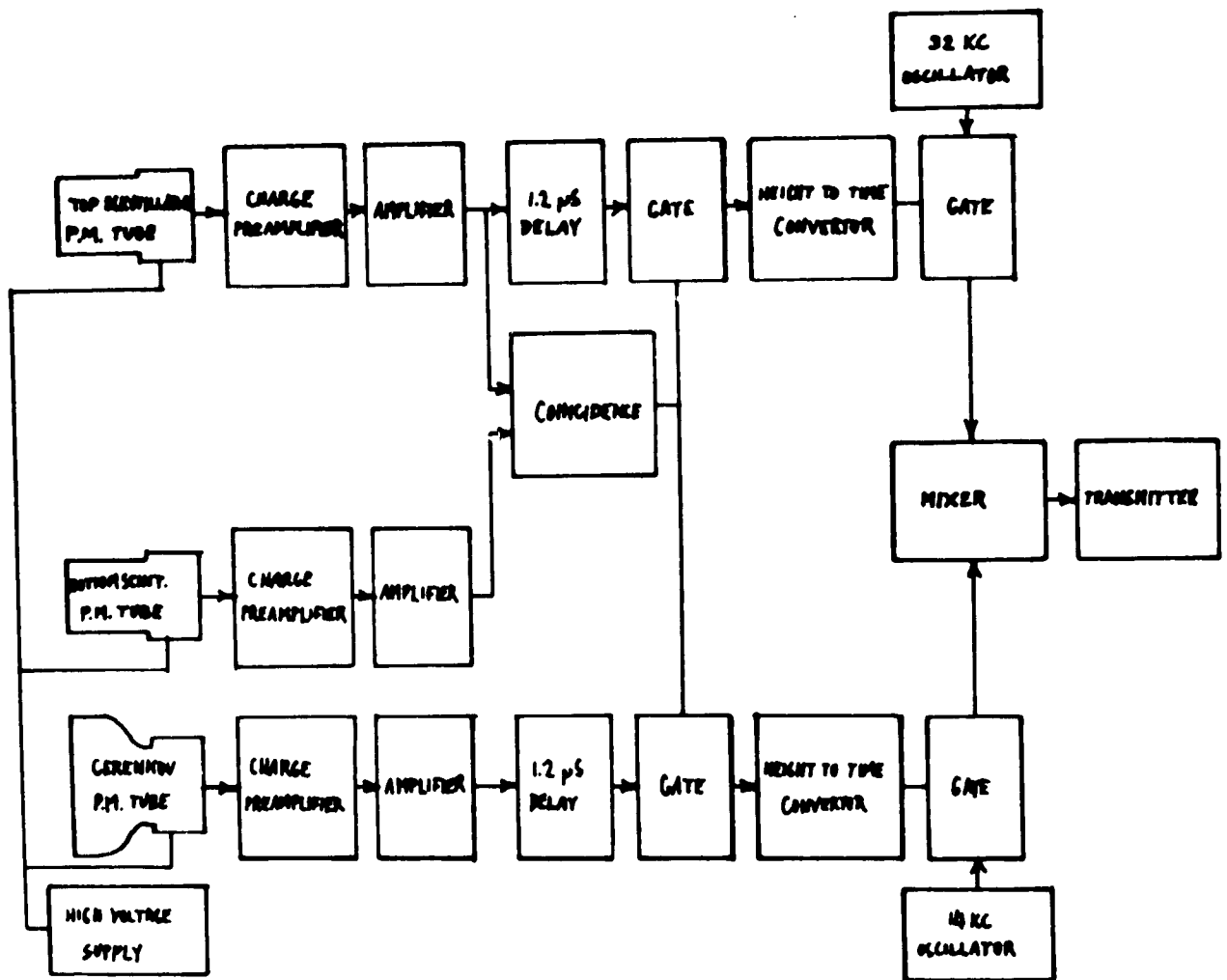
The cosmic ray detection apparatus for this experiment is illustrated in Figure 6.

The detectors consisted of two 4-inch diameter by $\frac{1}{2}$ inch thick NE102 plastic scintillators mounted 8 inches apart in a vertical line through their axes of symmetry, and a 5-inch diameter by 1-inch thick lucite Cerenkov detector placed below the scintillators in such a way that any particle passing through both the scintillators in a straight line also passed through the Cerenkov detector. A cosmic ray event was defined by the simultaneous occurrence of a flash of light from both scintillators.

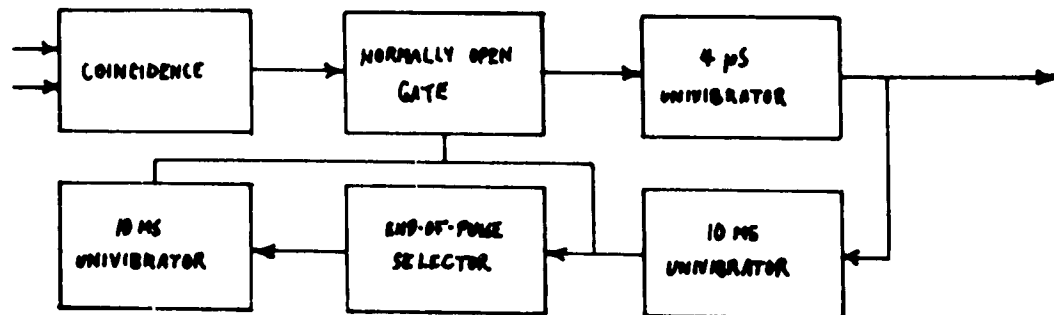
Looking at each scintillator was a 2-inch CBS 7817 photomultiplier tube light-coupled by means of an air cavity, the walls of which were covered by white reflecting paint. A clear lucite particle absorber was placed in the air cavity above the bottom scintillator to remove the possibility of low energy protons being counted. Such protons would have a Cerenkov output (zero) and a scintillator output equal to that of some non-relativistic alpha particles, and thus would be indistinguishable from these particles.

Light-coupled to the lucite Cerenkov detector by means of optical coupling grease was a 5-inch CBS 7819 (sometimes RCA 8055) photomultiplier tube. For the last 3 of the 4 flights made with this equipment, the sides and top of the lucite Cerenkov detector were coated with white reflecting paint. This was found to improve the light-collecting efficiency of the photomultiplier

cathode, and hence the mean number of electrons emitted by the photocathode, which was at a critically low level otherwise. However, this coating did have the disadvantage of destroying the directional properties of the Cerenkov detector.



DETAILS OF COINCIDENCE CIRCUITRY



DETAILS OF HEIGHT TO TIME CONVERTOR

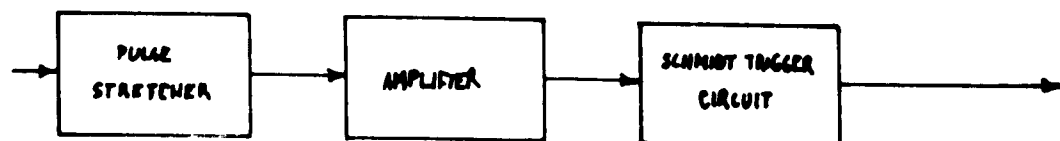


Figure 7 Detailed Block Diagram of Balloon-Borne Electronics

4.3 Balloon-Flown Detector Electronics

The balloon-flown electronics associated with the detectors is shown as a block diagram in Figure 7. Details of the actual electronic circuits used are given in Appendix I.

The outputs of the three photomultiplier tubes, after being amplified in the charge preamplifiers and amplifiers, were handled in the following way. The two pulses originating in the scintillators went to a coincidence system, which gave an output upon the simultaneous arrival of signals from both scintillators. Such an occurrence was considered a cosmic ray event. The coincidence output was used to open two gates, which passed the signals received in the top scintillator and Cerenkov detector, suitably delayed to account for the finite time needed for the coincidence circuitry to work, to height-to-time convertors. These height-to-time convertors changed the input pulses into square output pulses, the lengths of which were proportional to the logarithms of the original pulse heights. The circuitry could pass pulses of up to 11 millisecond output length. The output pulses were used to open gates that passed oscillator outputs of 32 and 14 kc/s frequency. These two gated oscillator outputs, representing the scintillation and Cerenkov signals, were then added together and used to frequency modulate the transmitter.

A refinement in the coincidence circuitry was used to prevent the arrival of a second cosmic ray event while the height-to-time convertors were busy with the first event. This

may be seen in the details of the coincidence circuitry shown in Figure 7. After the first cosmic ray event occurred, and a coincidence signal was produced, this signal passed through a normally open gate to a 4 microsecond univibrator, the output of which was used to gate open the signals from the top scintillator and Cerenkov detector. To prevent further cosmic ray events giving rise to an output while the first event was being "processed", the output of the 4 microsecond univibrator was used to turn on two 10 millisecond univibrators, one after the other, the outputs of which were used to shut the normally open gate described earlier. Two univibrators in succession were employed rather than a single univibrator because of the finite time needed between signals from a single univibrator and the possibility of a third event right after the single univibrator had switched off. The coincidence circuitry thus produced a 4 microsecond long square pulse upon the simultaneous arrival of signals from both scintillators and then "turned itself off" for 20 milliseconds following that event, so that no more events could be seen until the first event was processed.


Details of the height-to-time convertors are shown in Figure 7. The initial signal passed into a pulse-stretching circuit which basically consisted of a diode through which charge was dumped onto a capacitor. The charge was allowed to leak off the capacitor through a resistor. If the voltage across the capacitor as a function of time is considered, it can be seen to consist of an initial sharp increase to a peak proportional in height to the charge dumped onto the capacitor

and in this case the original pulse height as well, followed by a long exponential drop-off, the time constant being given by the resistor and capacitor used. The time from the beginning of this output pulse until it decreases below any arbitrary fixed voltage level can be seen to be directly proportional to the logarithm of the original pulse height. After passing through the pulse stretcher and a following amplifier, the pulse then passed through a Schmidt trigger circuit, which is basically a "flipflop" which changes state when the input signal rises above a certain D.C. voltage level, and changes back when the signal drops below a fixed lesser D.C. level. Thus the output of the Schmidt trigger circuit was a square wave, the length of which was proportional to the logarithm of the height of the exponential pulse which was fed into it, and therefore the height of the original pulse which arrived at the pulse-stretching circuit.

The operation of the balloon-borne electronics may be summarized as follows. When both the top and bottom scintillator in the detector array gave an output pulse, which would happen when a charged cosmic ray particle traversed both, the outputs of the top scintillator and Cerenkov detector were transformed into square pulses, the lengths of which depended on the magnitudes of these two detector outputs. These pulses were used to open gates to pass oscillator signals to a mixer, which provided the modulating signal for a frequency modulated transmitter. This modulating signal then consisted of two different

frequencies, which were present only when the system defined a cosmic ray event, the durations of which were proportional to the logarithms of the outputs of the Cerenkov and top scintillation detectors.

The modulating signal going into the transmitter also carried information on the temperature and pressure at the balloon package on a third oscillator frequency (5.6 kc/s), but as the pertinent system for this was not part of the actual primary cosmic ray detection equipment and consisted mainly of purchased devices, it has not been described here.



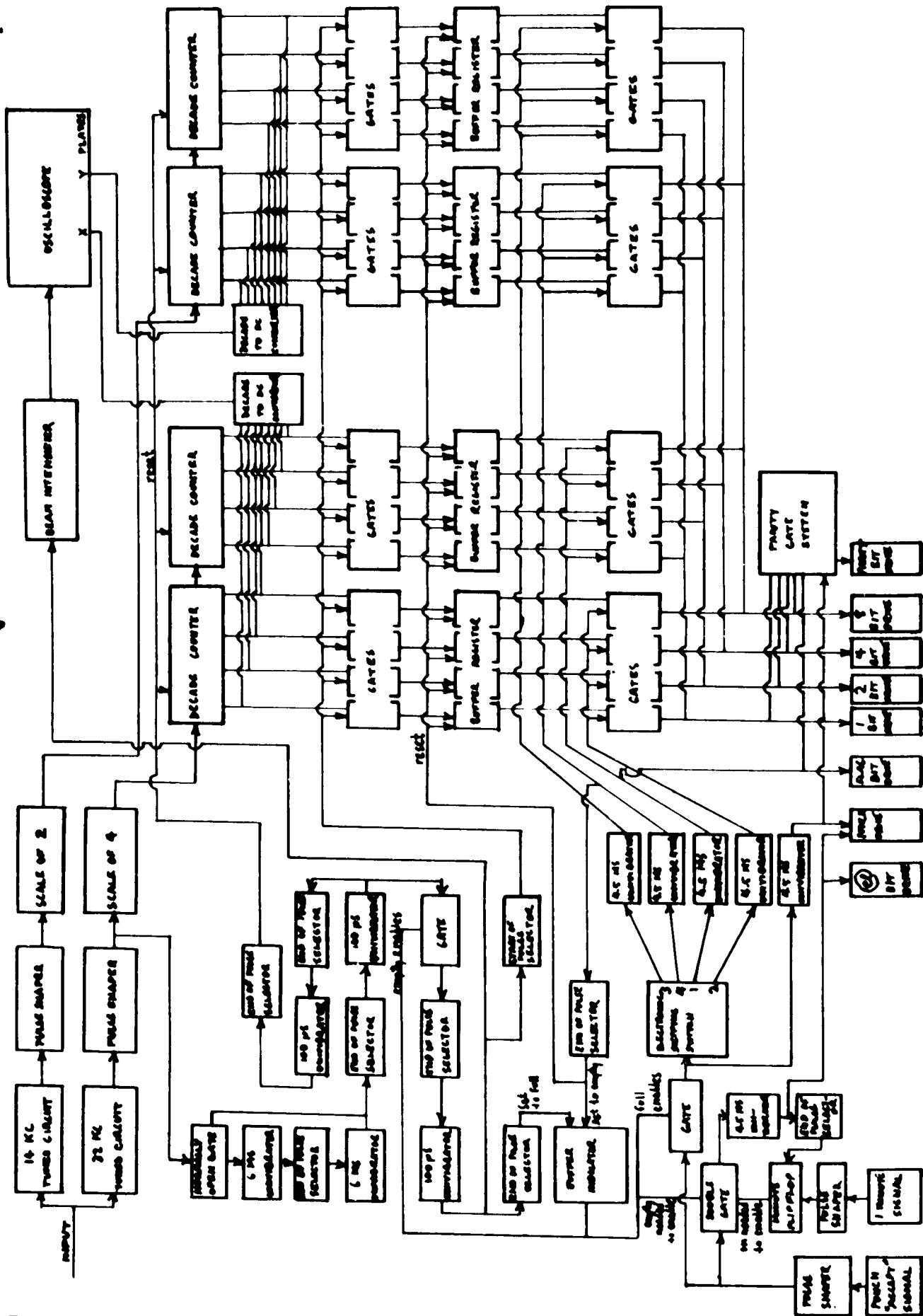


Figure 8 Decoding Electronics

4.4 Decoding Electronics, Display System, and Punch Tape Recorder

The ground-based equipment is shown in Figures 4 and 5. The most complex part of the system was the decoding electronics, which is shown as a block diagram in Figure 8. Reference to Figures 5 and 8 may be found useful in obtaining an understanding of the following discussion.

This decoding electronics performed several functions. It took the demodulated signal from the receiver and separated the cosmic ray information from the pressure and temperature information. It then punched this information onto paper tape. The cosmic ray information punched out consisted of a scintillation output and Cerenkov output for each detected cosmic ray, and was punched out each time an acceptable event was seen in the balloon package. The decoding electronics was also coupled to a display system consisting of an oscilloscope and Polaroid recording camera. Each event recorded on paper tape was also displayed on the oscilloscope screen.

The input signal, arriving at the decoding electronics from the F.M. tuner, was a mixture of three frequencies: 5.6, 14 and 32 kc/s. These frequencies respectively represented the pressure-temperature information, the Cerenkov outputs, and the scintillation outputs of cosmic ray events. The two detector output representations each consisted of a train of oscillations which occurred each time a cosmic ray event was defined by the balloon detector system. The lengths of these oscillation trains and therefore the number of oscillations in each were

proportional to the logarithms of the two original detector output pulse heights.

As the demodulated input signal entered the decoding electronics, it was filtered through two parallel tuned circuits which separated out scintillation and Cerenkov information when a cosmic ray event was transmitted and received. This information, which was then in the form of a train of sine waves in both cases, passed through pulse shapers, which changed the signals to two series of square waves. These signals were scaled by factors of four and two and then each signal was fed to a system consisting of two decade counters. The decade counters counted the number of square waves in each train after scaling. The number in each pair of decade counters then represented the logarithm of the height of the scintillation or Cerenkov output for the cosmic ray event which was just detected in the balloon and received by the ground equipment.

Both sets of decade counters were "looked at" by decade to D.C. convertors, which converted the numbers contained in the counters into proportional voltage levels. These voltage levels, i.e. the scintillation and Cerenkov output representations, were put on the X and Y plates, respectively, of an oscilloscope. When it was certain that the event had finished being received by the decoding electronics, the oscilloscope beam was intensified for 100 microseconds, yielding a point on the screen the position of which was determined by scintillation and Cerenkov light outputs for the particular cosmic ray event being considered. A

Polaroid camera was left open to look at the oscilloscope screen for periods of approximately ten minutes, to get a collection of points representing many cosmic ray events. From the discussion on the theory of the Cerenkov-scintillation counter, it can be seen that these points should be clustered along certain preferred lines similar to those shown in Figure 3 (with allowance for the logarithmic nature of the oscilloscope representation). By taking pictures of the display system from time to time throughout the balloon flight, a running check could be made on the correct operation of the balloon-borne equipment and the ground-based equipment up to the point of observation.

It was necessary to know when the reception of a cosmic ray event had ceased, for the further operation of the decoding electronics and, as already mentioned, for the display system. This was achieved with the knowledge that the transmitted signal could only last as long as 11 milliseconds, and that a second event could not occur until 20 milliseconds after the start of the first (see section on balloon-borne electronics). Following the pulse shaper for the scintillation signal mentioned earlier was a system comprised of a normally open gate, two end-of-pulse selectors, two 6 millisecond univibrators, and a 100 microsecond univibrator which yielded a signal 12 milliseconds after the detectors saw the start of an event after 12 milliseconds, when the event should have ended and no other event could have started.

A system of 100 microsecond univibrators, end-of-pulse selectors, and start-of-pulse selectors were used, following the

end-of-event signal, to yield a sequence of pulses which would perform the next series of operations to be described here, in the right order. A set of sixteen flipflops was used as a "buffer register" to store information to be later punched on paper tape. A "flipflop indicator" was used to indicate whether or not an event was stored in the buffer register.

If the flipflop read "empty", the end-of-event signal initiated a signal which set the buffer register to the same configuration as the decade counters containing the information on the cosmic ray event which had just been read in. At the same time, the oscilloscope beam for the display system was intensified, as mentioned earlier. After the buffer register had been set, the flipflop indicator was set to the full position, and the decade counters were reset to zero so that they would be ready for the next cosmic ray event.

If the flipflop indicator read "full", the only one of these operations that was carried out was the resetting of the decade counters to zero. In this case, the event was lost.

The information in the buffer register was read out onto paper tape in the following manner. The tape punch produced an "accept" signal 110 times a second, at which times it was at the right phase of its operation to punch out information. If the flipflop indicator mentioned earlier read "full", there was information in the buffer register ready to be punched, and the accept signal was passed to an electronic stepping switch. The electronic stepping switch initiated four 4.5 millisecond

univibrators in turn, the outputs of which passed through sets of gates that were open or closed, depending on the configuration of the output register. After passing through the gates, the signals punched on the tape, in order, the tens and units digits representing the scintillation output and the tens and units digits representing the Cerenkov output of the event being processed. At the same time, for each digit, the accept signal initiated a 4.5 millisecond univibrator which drove the punch.

Each digit was punched on the tape in binary-decimal form. The tape consisted of a series of "lines", one after the other, consisting of eight positions or "bits". Four of these bits were used in the representation of a decimal digit: the one, two, four and eight bit. The digit punched out could be found by adding the characteristic numbers of the bits containing a punched hole together. The first digit in the sequence of four to be punched for each event also had a "flag" bit punched along with the appropriate numbered bits, to identify the start of an event. After the fourth digit was punched, an end-of-signal pulse selector on the output of the fourth 4.5 millisecond univibrator to be triggered by the electronic stepping switch reset the flipflop indicator to "empty", so that no more accept signals could trigger the stepping switch, and also set the buffer register to zero, so that it was ready for transfer of the next cosmic ray event from the decade counters.

The punched tape produced was later processed by an I.B.M. 1620 computer, which had the parity requirement that an odd number of holes be punched for each line of tape it read. To

comply with this requirement, a special "parity bit" was reserved on the tape. In the decoding electronics shown in Figure 8 is a parity gate system which produced an output pulse whenever an even number of input pulses was read into it (and also onto the tape), thus making the output tape of this system compatible with the I.B.M. 1620.

A time signal was put onto the tape every minute by the following technique. When the time signal came in from the crystal chronometer, it set a "minute flipflop" which, as soon as the buffer register was denoted by the flipflop indicator to be empty, allowed an end-of-line character to be put on the paper tape by the accept signal. The minute flipflop was then reset. The end-of-line character is another essential feature on punched tapes acceptable to the I.B.M. 1620 computer, as this is the only signal that will automatically stop the computer reading tape once it starts.

A short summary of the decoding electronics is as follows. When a cosmic ray event was received, this event entered the decoding electronics as two pulse trains of different frequencies and lengths mixed together with a third pressure-temperature signal. The electronics separated out the two pulse trains, counted the number of pulses in each, and then transferred the two resultant numbers to a buffer register, provided another event wasn't already stored there. The event was also plotted as a point on an oscilloscope screen in which the X and Y coordinates represented the two numbers in question. The oscilloscope, along

with a Polaroid camera which recorded many such points on a single picture, formed the display system. When the tape punch was ready to accept an event from the buffer register, and when the buffer register contained an event, it was punched out as a series of four digits or lines onto paper tape. Minute signals were also punched onto the tape as a special character (end-of-line). The punched tape was produced in a format acceptable to an I.B.M. 1620 computer, with the aid of parity circuitry which punched an extra hole in each line that would otherwise contain an even number of holes.

Details of the circuitry used in the decoding electronics may be found in Appendix II.

4.5 System Appraisal

This section is intended to be both a discussion of the advantages of the experimental system used, and an examination of its shortcomings, giving thought to how these shortcomings may be overcome in the future.

A major advantage of the system used was the high counting rate of approximately 5 counts per second, which earlier systems relying on photographic recording techniques and manual data analysis could not feasibly have. With this high total count rate, the statistical fluctuation in the hourly proton rate should be less than 1 per cent, and in the alpha rate, less than 3 per cent. If a 24 hour duration balloon flights were achieved, it is then quite possible that the diurnal variation seen previously only at ground level would be distinguishable in both types of particles. Other types of cosmic ray variations such as Forbush decreases and solar flare increases would also be readily seen. Because of the high count rate, it should be possible to observe "fine structure" in these two latter types of events which hasn't been seen before.

To increase the mean counting rate further, the size of the detectors would have to be changed. As it proved desirable to have the best light-coupling possible for the Cerenkov detector to its photomultiplier tube, a large detector implies a correspondingly larger photomultiplier photocathode, with the accompanying drop in photocathode produced electron collection efficiency, as well as increased cost and weight. However, the feasibility of air coupling

A variation of 40° C, which is possible from day to night at high altitudes would cause a change in detector area and hence counting rate of close to 1 per cent.

From the sizes of the possible errors given, it can be seen that a change in counting rate should be accompanied by a refinement of the parts of the system where the possible errors originate, so that either these errors are made smaller or can be corrected for. A possible change in the pressure system is the inclusion of a type of ballast device, designed to keep the balloon at a constant pressure. With the present system it was possible for the combination of a faulty pressure correction of the data and a changing pressure level to give rise to an apparent change in the primary cosmic ray rate. A constant pressure level would eliminate any chance of this.

An important parameter of a system such as the one under consideration is the maximum counting rate it can sustain. In the event of solar increases of the cosmic radiation, both at ground level energies and the lower energies manifested in polar cap absorption events, determinations of the nature of the increases are quite useful. During these events it is possible that the counting rate of the apparatus would increase substantially, and unless the rest of the system could handle this increase its usefulness for such events would be limited.

The maximum possible rate of the system reported on here was given by the tape punch, as this was the slowest component in the system. A synchronous motor allowed the punch to produce

a large Cerenkov detector to a smaller photomultiplier should not be discounted.

An advantage of the present system was the relative lightness of the balloon package compared with other experiments of this type, which enabled it to be carried to acceptable altitudes by means of small (176,000 cubic feet), manually launched balloons. An increase in detector size, and therefore weight, would have necessitated the use of larger balloons.

Increasing the mean count rate would also mean that the rest of the system in addition to the detectors would have had to be modified. The maximum possible counting rate, which was at the time limited by the tape punch, would have had to be increased. Methods for doing this are considered later on in this section.

In the system that was used are certain errors, of a nature other than statistical, which, if the mean count rate were increased very much, would be left the chief contributors to experimental inaccuracies in the system. One such error lies in the pressure detecting device, which in this case was of the order of 0.25 millibars at maximum altitude. This meant that the mean count rate, when corrected for pressure, would have a possible error from this source of 0.2 per cent for protons and 0.5 per cent for alpha particles. These errors were equal to the statistical fluctuations encountered for a 24 hour period with the present system. A second possible error is that of temperature fluctuations causing a change in the detector area because of the large coefficient of expansion for plastics.

110 characters per second and, since the recording of a cosmic ray event required 4 characters, 27.5 events per second could be recorded at most. When a second event arrived before the first one was recorded, it was lost. This "dead time" of $1/27.5$ or .0363 seconds per event resulted in a non-linear response to changes in the counting rate, of the form

$$\text{Rate}_{\text{recorded}} = \text{Rate}_{\text{detected}} (1 - .0363 \text{ Rate}_{\text{detected}}),$$

where the rates were given in events per second. The fraction of the counts recorded for a mean detected rate of 5 counts per second was 0.818. If the detected rate was increased to 10 counts per second, the fraction recorded became 0.636. This type of change limited the mean rates at which changes in rate could be seen with any reasonable sensitivity.

On the other hand, the dead time per event in this system was determined by a synchronous motor and was therefore constant. If the tape punch had been made much faster, then the balloon electronics would have become the slowest component in the system. The dead time determined in the electronics was slightly dependent on the battery voltage and ambient temperature. Changes in these two variables would have yielded apparent changes in a cosmic ray rate which might actually have been constant.

There are several ways of speeding up a system such as the one used here. These include the following:

1. Use a faster tape punch. This has the disadvantage mentioned in the last paragraph, and also the added disadvantage of cost. Tape punches much faster than the one presently in use

2. Add a buffer memory to the system. With this memory, a large number of events could pile up in the ground station before being actually recorded. This technique has the disadvantage mentioned in the last paragraph, and also that of complexity.
3. Play back the magnetic tape recording at a slower speed than recorded, into the decoding electronics and tape punch system. In this way the tape punch would have a longer time to punch out the same event than previously. Again the disadvantage of having the dead time determined by the balloon electronics occurs. However, very little extra cost or electronics is incurred by this method.

In all these methods, the dead time becomes that of the balloon electronics, provided the speeding up is great enough. However, the last method is such that it need be invoked only when considered necessary. For most cosmic ray data, the time variations should be small and the importance of eliminating non-real variations are therefore great. For such data the present system sufficed. If large increases which make the present data recording system much more nonlinear were seen, then it was possible for the last method (3) to be invoked, using the magnetic tape from the backup system. During these large increases, much larger fluctuations than usual can be expected to occur, and therefore for such events any small changes in dead time per event would be negligible.

If it were considered desirable to speed up the system more than that allowed by changing the mode of data recording, then the dead time of the balloon electronics would have to be decreased.

The method of transmitting pulse lengths from balloon to ground is such that the minimum dead time is limited by the time of response of the ground-based electronics to changes in amplitude of the subcarrier frequencies which convey the cosmic ray information. This response time depends on the Q of the initial tuned circuits in the decoding electronics, which has to be large enough to eliminate cross-talk between subcarrier frequencies and also noise signals. In the present system, a Q of 8 was used, thus limiting the response time to approximately 0.3 milliseconds for the 32 kc/s signal. For reasonable accuracy of transmission this meant that the maximum signal length had to be at least 10 milliseconds, and therefore the dead time slightly larger, or about 11 milliseconds. If higher subcarrier frequencies were used, the response time and therefore the necessary dead time would decrease. However, the present subcarrier frequencies were limited by the response of the tape recorder in the backup system, and also by the bandwidth of the transmitter.

An alternate method of decreasing the dead time lies in changing the transmission technique altogether. Instead of transmitting the cosmic ray information as time-length pulses, information could be transmitted in coded digital form. This technique is already used by researchers in similar balloon and satellite experiments (Hubbard, 1962). For this method, however, a large amount of additional balloon electronics was required, thus raising the cost of a balloon package considerably. Major revisions in the decoding electronics would also be necessary.

The present system had an advantage over older systems in that data was analyzed automatically. The higher count rate made this more essential. With the system reported on here, the recordings produced showed each individual event, and the subsequent automatic analysis required some time (about 12 hours I.B.M. 1620 computer time for 24 hours data) to put it into a more useable form. However, if a two-dimensional pulse height analyzer were incorporated as part of the decoding electronics, its output would already lie in this more useable form. As well, the dead time of the system would not be limited by the tape punch. However, two-dimensional pulse height analyzers are at present extremely expensive and therefore out of the range of most small research groups.

The detector arrangement itself should be commented upon in this section. One needs to consider the various types of cosmic ray events in addition to single primary cosmic rays, and the corrections necessary to account for these additional events. Such events are as follows:

1. Accidental coincidences. These depend on the total counting rates and the resolving time of the electronics. A calculation of their expected rate, given later in Chapter 7 of this thesis, yields a value of 5% for the fraction of the total rate expected to be due to accidental coincidences.
2. Secondary particles produced in the air above the detectors. These particles should fall about the lines shown in Figure 3 and should therefore not cause any difficulty in the initial analysis of the various particles. Later on, of course, it was necessary to make correction for this.

3. Showers occurring above the apparatus. These events, as they consist of more than one particle were expected to cause points off the single particle lines shown in Figure 3. Correction for this effect would therefore be difficult, as statistical fluctuations in the detectors also caused a spreading of points, and both effects had to be removed. However, earlier experiments by MacDonald (1956) with Cerenkov scintillation counters having a large shower detecting area in comparison to the scintillation detector area used have shown that events such as this are few in number at balloon altitudes.
4. Nuclear collisions in the detector system. These events, similar to 3, were expected to cause difficulty in the initial analysis.

Effect 4 could be lessened by making the top scintillator as thin as possible, so that this effect would happen only rarely in this scintillator. On the other hand, the output of the top scintillator, as already mentioned was used in the subsequent analysis. Its thickness, therefore, had to be sufficiently great to yield a reasonable amount of light for all events, so that hard-to-calculate photomultiplier statistics did not play too great a role. Further work on the best thickness of the top scintillator is clearly indicated.

A change in the detector system used here from earlier systems used by other workers was the presence of a clear plastic absorber between the two scintillators. This absorber limited the lowest particle energy that could be detected to 60 MeV for protons, and

in this way removed the possible ambiguity that could occur between very low energy protons and medium energy alpha particles. It was expected to have the effect of removing part of the albedo electron contribution to the data obtained. The addition of an absorber was also a feature of the Cerenkov-Scintillation counter detectors recently reported on by Hedgecock (1964).

The relatively low cost of the present type of system is an important advantage, particularly for small university groups with limited resources. The cost was kept to a minimum by several features:

1. All the recording apparatus was on the ground. This made the balloon package lighter and less expensive, and also had the added advantage of eliminating the need for recovery. The cost of flying light packages is much less than that of heavier packages, as the amount of helium and the size of the balloon needed are much less than that needed for only slightly heavier packages, and manual balloon launches are possible only with the smaller balloons. The loss of a balloon package was a very probable occurrence in the isolated regions in which these packages were normally flown, and the cost of immediate recovery of the ones that could be found, i.e. the ones that could be located and have fallen in an accessible area, could be more expensive than the value of the recovered balloon packages. It was therefore advantageous, from the points of view of economics and data recovery, to have as little as possible in the balloon package, thus keeping its cost and weight fairly low.

2. The data was analyzed automatically. Because of the high counting rate, manual analysis would have been lengthy and therefore expensive.
3. The scintillators used were plastic, as compared to the more expensive sodium iodide detectors used in earlier studies. As well, plastic scintillators are easier to work with. The nonlinearities of plastic scintillator (Prescott and Rupaal, 1961) are not too important in studies of primary protons and alpha particles at velocities detectable with the present system. If this system were to be adapted for a study of heavy nuclei such as that carried out by MacDonald and Webber (1962), then the nonlinearities of plastic would require that it be replaced by sodium iodide or some other sufficiently linear scintillator.

The system developed in this study had the advantage of versatility. Various types of detection system could be flown using the same transmission and decoding-recording system with only slight modifications. Some possible experiments making use of the same system are as follows:

1. dE/dx by E detectors. These are normally used to look for particles with energies below 100 MeV, and thus are very useful in studies of polar cap absorption events.
2. Cerenkov-scintillation studies of heavier nuclei.

In general, any detection system with at most two outputs of which it is necessary to know the size and which is meant for operation at balloon altitudes or less, could be adopted for use with the present system.

CHAPTER FIVE

PREFLIGHT ADJUSTMENT AND CALIBRATION OF THE APPARATUS

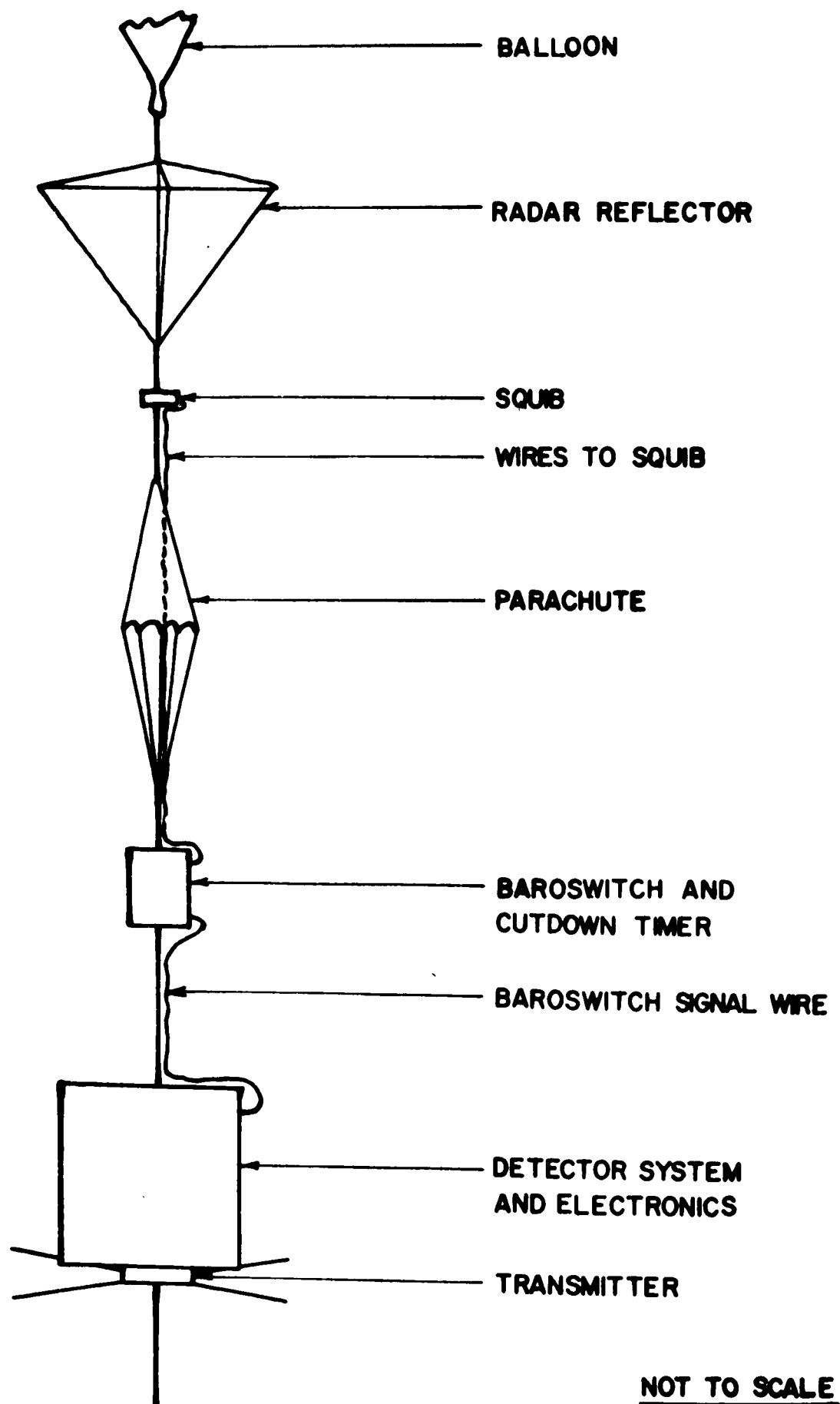
Although the Cerenkov-scintillation system used was basically a self-calibrating one, it was still necessary, owing to the mode of data retrieval and electronic limitations, to make certain ground measurements on, and adjustments to, this system.

Such a measurement was involved in the examination of the height-to-time convertors. Theoretically, the output should be a logarithmic function of the input with the appropriate conversion parameters being given by the values of the electronic components used. However, the convertors were by no means ideal, and the values of the electronic components not known to an accuracy greater than 10%. To derive an exact relationship between input pulse height and output pulse length, the output of each convertor was examined over a wide range of inputs. The relationship found was then graphed, and later used in analysis of the data at altitude. A check was made on the temperature stability of the height-to-time convertors as well, and any necessary adjustments made on a special compensation circuit incorporated into the convertors. Finally, the 'zero output' of the convertor, i.e. the output corresponding to the gating pedestal arising from the firing of the coincidence circuit alone, was adjusted so as to be approximately 0.5 milliseconds in length. This was more than sufficient to allow for any shifts due to changes in battery voltage and temperature.

The gains of the individual detectors in the system had to be adjusted for each flight. This adjustment ensured that the output pulse heights of interest were not so large as to be

distorted in the electronics, or, on the other hand, so small as to lose their resolution in the transmission. For this purpose, the detection system was placed under 10 cm of lead, so that nearly all the particles traversing it were relativistic muons. The output of each detector was examined with the aid of a 400 channel pulse height analyzer, gated by the balloon coincidence circuitry. Knowing the detector output distributions for this 'control group' of relativistic muons, the output distributions for all particles of interest, in this case protons and alpha particles of energies down to the cutoff defined by the detecting system, were inferred. The detector gain in question was then adjusted so that these outputs fell within an allowable range, with a safety factor of 2 times to take care of any temperature changes in photomultiplier gain. The discrimination levels of the event-defining coincidence circuit were also suitably adjusted on this basis.

A final test run of each balloon package was made, again under 10 cm of lead, to check the overall operation of the system. This run was used to look at the resolutions of the detectors in the system as well. The data for this run was recorded using the ground-based electronics and tape punch unit intended for use later on during the actual balloon flight.



NOT TO SCALE

Figure 9 Balloon Package Train Assembly

In the course of this research, four balloon packages were assembled and flown. The first flight was made from the Calgary region on December 9, 1964, and the second and third from Fort Churchill on March 29 and April 6, 1965, and the fourth, from Calgary on July 27, 1965. All four flights had radar coverage, and pressure and temperature were measured by a "baroswitch" contained in a small package separate from the main detector pack. The balloon train assembly for a typical flight is shown in Figure 9.

The pressures and flight path for each flight are shown in Figures 10 and 11. Table 1 gives the radar position as a function of time for each flight. A summary of each flight is given below.

Flight 1

Flight 1 was launched at 2122 LT, December 9, 1964. A 135,000 cu. ft., 3/4 mil polyethylene balloon was used. The time of this flight was limited by air regulations, and for this reason the cutdown timer was set to operate at 0400 LT the next day. The package reached an altitude corresponding to 9 mb pressure, and later settled to a pressure of 13 mb by 0400 LT. The lowest temperature recorded was -58°C , towards the end of the flight.

The operation of the balloon package was good for the most part, but there were shortcomings. The baroswitch signal did not modulate the appropriate subcarrier as it should have, possibly due to the baroswitch signal cable becoming disconnected

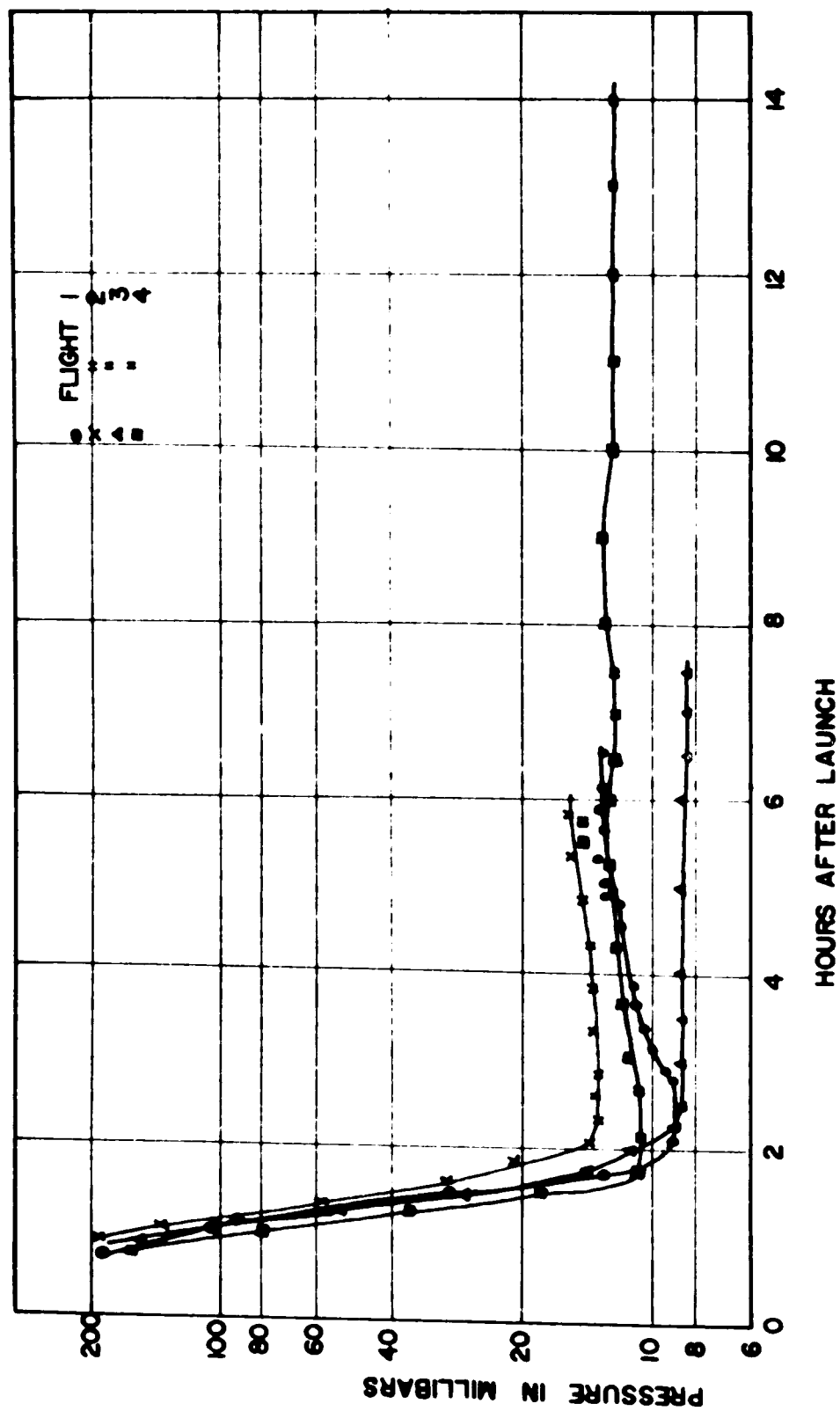


Figure 10 Pressure-Time Curves for Balloon Flights

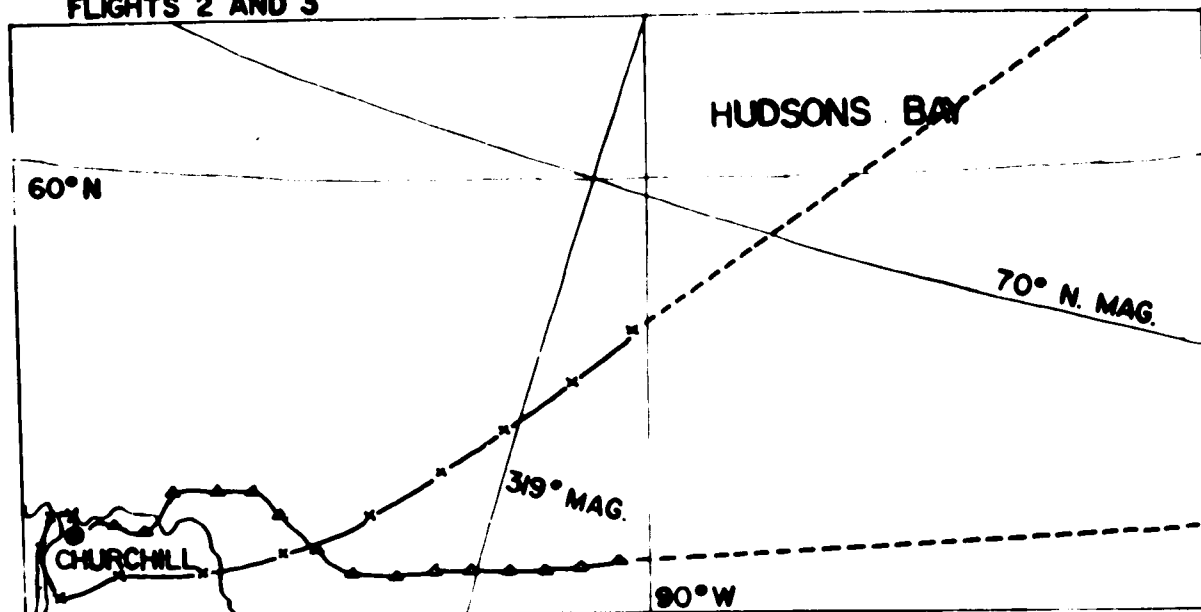
at the time of launch. However, pressure and temperature data was still obtainable, as the D.C. level of the receiver discriminator output was seen to shift slightly when the baroswitch contacts closed. The system was observed to be susceptible to ignition noise from automobiles as well. The modulation level was less than it could have been. A fading in signal occurred when the balloon was about 100 miles away, at which point the noise signal was able to compete successfully with the information. It was later discovered that this decrease in signal was a feature of either the transmitting or receiving antenna patterns, as it occurred for every flight at about this distance. After 100 miles, the signal would improve again and would remain at a reasonable level until the balloon was close to the horizon, about 350 miles away. However, for this particular flight, the cutdown timer operated at 0403 LT, when the balloon was only 120 miles away, and the signal strength had not yet come back up to any great extent. The equipment flown on this flight was found and returned to the university four months later, in surprisingly good condition.

About three hours of useful data at altitude was obtained on this flight.

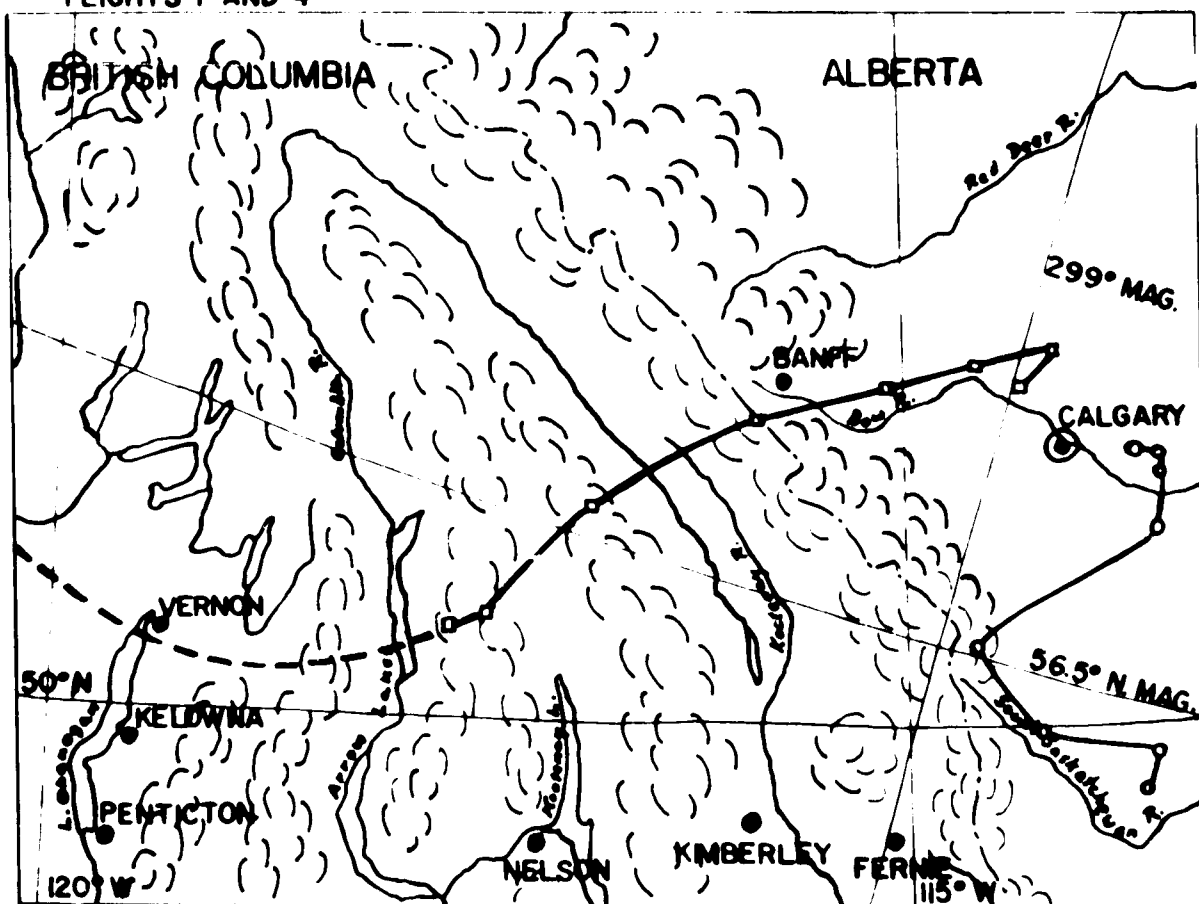
Flight 2

Flight 2 was launched from Fort Churchill at 1939 LT on March 29, 1965. A 170,000 cu. ft., 3/4 mil polyethylene balloon was used for the flight. The cutdown timer was set to operate 24 hours from the time of launching. An altitude corresponding

FLIGHTS 2 AND 3



FLIGHTS 1 AND 4



| ○ | FLIGHT | 1 | RADAR | READINGS |
|---|--------|---|-------|----------|
| x | " | 2 | " | " |
| ▲ | " | 3 | " | " |
| ◻ | " | 4 | " | " |

Figure II Balloon Flight Paths

Table 1: Supplement to Figure 11Times of radar readings shown in Figure

| | <u>Reading No.</u> | <u>Time</u> | <u>No.</u> | <u>Time</u> |
|-----------------------|--------------------|-------------|------------|-------------|
| <u>Flight 1</u> | 1 | 2205 LT | 5 | 0055 LT |
| | 2 | 2250 | 6 | 0143 |
| | 3 | 2320 | 7 | 0220 |
| | 4 | 2357 | 8 | 0245 |
| (Launch time 2122 LT) | | | | |
| <u>Flight 2</u> | 1 | 2000 LT | 7 | 2130 LT |
| | 2 | 2015 LT | 8 | 2145 |
| | 3 | 2030 | 9 | 2200 |
| | 4 | 2045 | 10 | 2215 |
| | 5 | 2100 | 11 | 2230 |
| | 6 | 2115 | 12 | 2245 |
| (Launch time 1939 LT) | | | | |
| <u>Flight 3</u> | 1 | 0930 LT | 9 | 1130 LT |
| | 2 | 0945 | 10 | 1145 |
| | 3 | 1000 | 11 | 1200 |
| | 4 | 1015 | 12 | 1215 |
| | 5 | 1030 | 13 | 1230 |
| | 6 | 1045 | 14 | 1245 |
| | 7 | 1100 | 15 | 1300 |
| | 8 | 1115 | | |
| (Launch time 0914 LT) | | | | |
| <u>Flight 4</u> | 1 | 2318 LT | 5 | 0341 LT |
| | 2 | 2350 | 6 | 0641 |
| | 3 | 0128 | 7 | 0740 |
| | 4 | 0210 | 8 | 0802 |
| (Launch time 2246 LT) | | | | |

Dotted parts of balloon flight paths are inferred from ground antenna directions, along with the assumption of a constant balloon speed.

to a pressure of 13.5 mb was reached, and eventually the balloon settled back to a pressure of 15.5 mb. The lowest temperature recorded was -48° C. Extremely fast high altitude winds prevailed at this time, and the package was carried beyond the horizon 3 hours from the time it reached altitude.

Operation of the equipment seemed satisfactory for this flight, although the counting rate was $1\frac{1}{2}$ times faster than on the other flights. A strong signal, fairly well above the noise level, was received for most of the flight, even through the "100 mile decrease" noted earlier.

About $2\frac{3}{4}$ hours of useful data at altitude was received on this flight.

Flight 3

This flight was launched from Fort Churchill at 0914 LT, April 6, 1965. A 170,000 cu. ft., $\frac{3}{4}$ mil polyethylene balloon was used. The cutdown timer was set for a 24 hour flight. The lowest pressure reached was 8.4 mb, and the balloon remained very close to this pressure for the entire time that it was at altitude and a signal being received. The lowest temperature recorded during this daytime flight was -22° C. Fast high altitude winds carried the balloon beyond the horizon at about 1700 LT.

The operation of the balloon package was very good for this flight. The signal was above the noise level, even through the "100 mile dip" in signal strength, until the horizon was reached.

Five hours of useful data at altitude was obtained on this flight.

Flight 4

This flight was launched from Calgary at 2246 LT, July 27. (A previous attempt had been made to launch this balloon package, but it had failed to reach altitude and came back down. The equipment was recovered the next day and found to be in good working condition.) A 135,000 cu. ft., 1/2 mil polyethylene balloon was used. The cutdown timer for flight 4 was set for 24 hour operation.

A pressure of 10.9 millibars was reached on this flight. After initially reaching this pressure at 0300 LT, July 28, the balloon settled back to a pressure of 14.6 millibars by 0400 LT, to rise again after sunrise to a pressure of 12.4 millibars. This latter pressure was maintained throughout the daytime part of the flight.

High altitude winds were fairly slow at the time of flight 4, and a signal was received from the balloon pack until 1500 LT, July 28, at which time it appeared that the balloon had dropped beneath the horizon.

Signal reception was not good. The initial part of the flight was marred by the fact that the balloon was very nearly overhead, and in this position could not be received very well, because of the design of the ground station antenna. For this reason no useful data was obtained until sometime after the balloon reached altitude. Later in the flight, several dips in signal strength were experienced, where the noise level rose sufficiently to interfere with data recording. Thunderstorms and motorized vehicles also caused some interference.

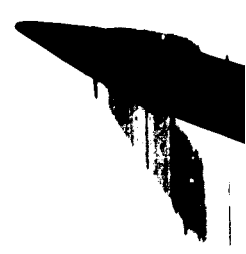
Despite the difficulties in reception, a considerable amount of useful data extending over a 12 hour period at altitude was received during this flight.

CHAPTER SEVEN

ANALYSIS OF THE DATA

Analysis of the data taken with the Cerenkov-scintillation counter system is an involved process. From the data, originally for each cosmic ray event in the form of two numbers representing the scintillation and Cerenkov outputs of different detectors, such things as an absolute counting rate, charge spectrum, and energy spectra must be obtained. The derivation of these representations of the data is complicated both by the statistical nature of the detector outputs and the presence of cosmic ray interactions, both in the atmosphere above the detector and in the detector itself.

Owing to the large number of events, manual analysis would be an extremely lengthy process. For this reason, an I.B.M. 1620 computer was used in nearly all phases of the analysis. The output of the experiment, on punched paper tape as mentioned earlier, lent itself well to this.



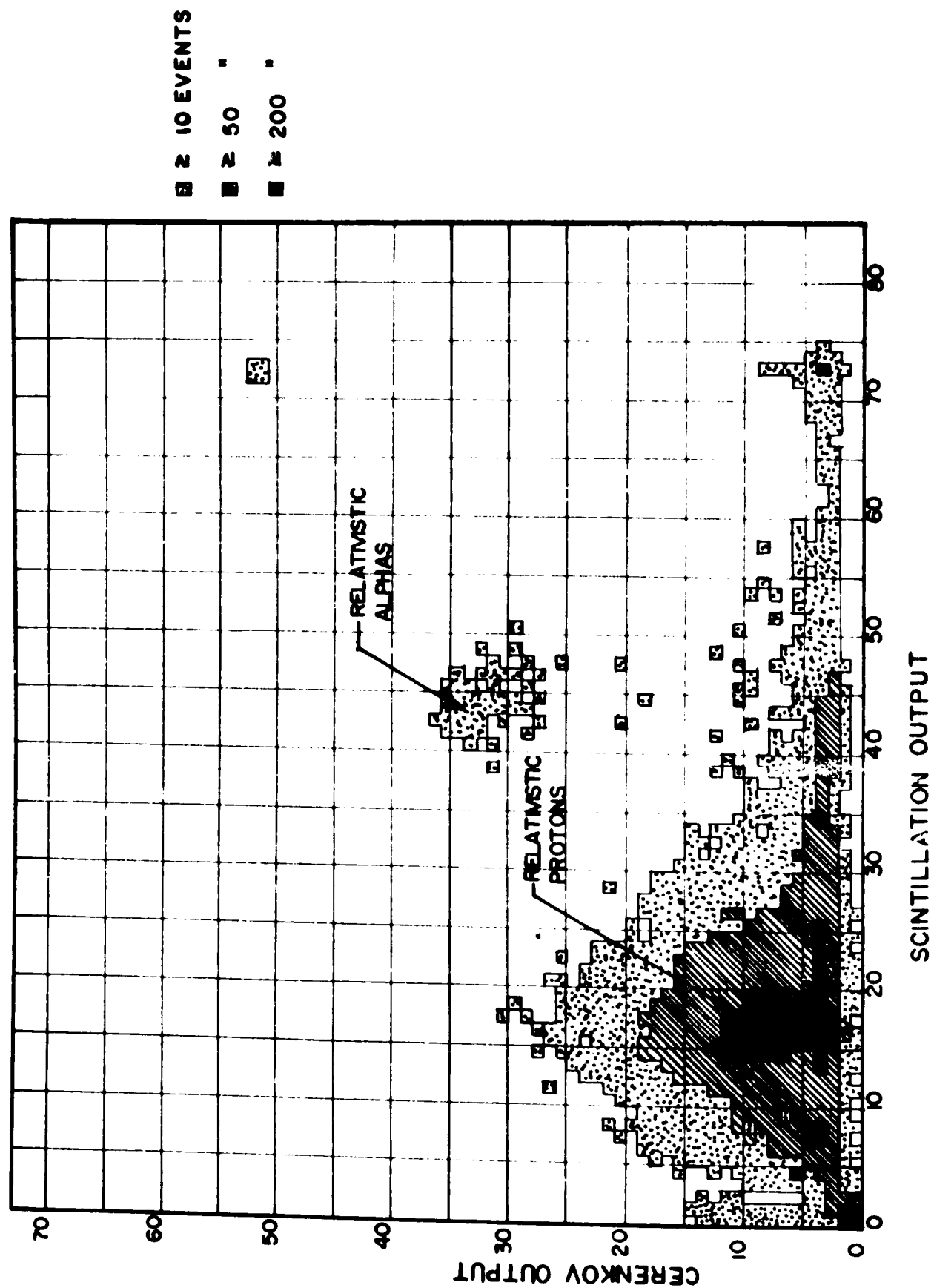


Figure 12 Cerenkov - Scintillation Diagram for Flight 1

7.1 Organization of the Data into an Easily Analyzable Representation

The first phase of the data analysis put the individual cosmic ray events into a more collective representation. At this point, the data was in the form of two two-digit numbers, representing the Cerenkov and scintillation light outputs, for each cosmic ray event. An area in the memory of the computer was defined, consisting of an array of 100 by 100 positions, each position capable of holding any number of events up to 9999. Depending on the values of its two detector output numbers, an event was entered into one of these positions. In this way, the computer was made to act like a two-dimensional pulse height analyzer, and the individual data grouped together into a collective, more easily analyzable representation. This representation could be plotted on paper and compared with the theoretical lines shown in Figure 3 (b). A modified example of such a representation is given for flight 1 in Figure 12. The paper was divided into a grid. The channel number along the x axis represented the scintillator output, and along the y axis, the Cerenkov output. The number in a square was the number of events having the two particular outputs the square corresponded to. In the example shown in Figure 12, the counts can be seen to be clustered about two points, corresponding to the combined outputs for relativistic protons and alpha particles. A third cluster, occurring at the points of combined saturation of the scintillation and Cerenkov detectors, most likely owes its existence to fast particles of charge (2) greater than 2.

The computer output for this representation was in the form of 400 punch cards. Using this representation, the data at altitude was put into approximately 1 1/2 hour intervals, and the data during ascent, into 10 minute intervals. A representation for the total data at altitude was also drawn up, for each flight.

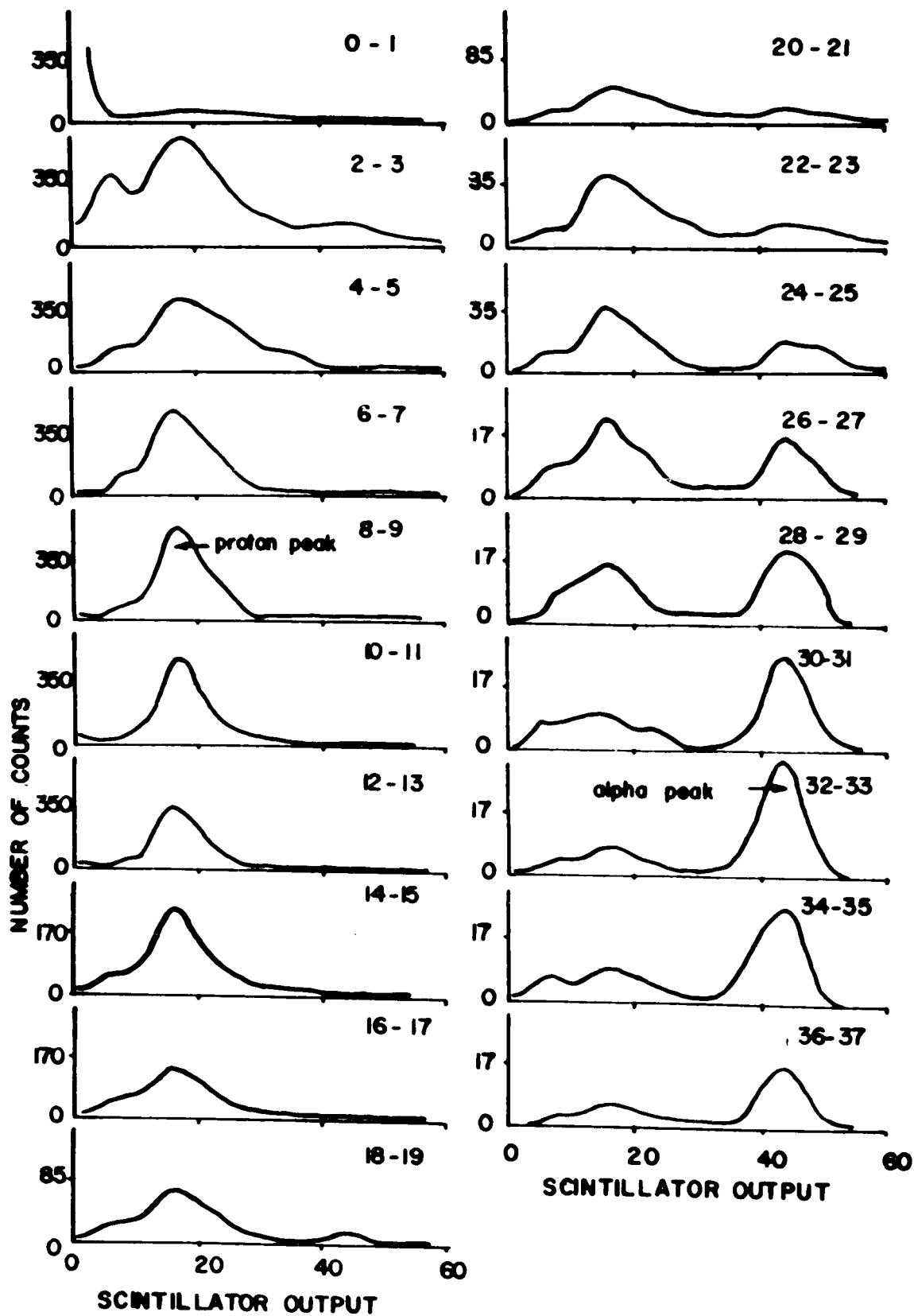


Figure 13 Scintillator Output Distributions for Various Cerenkov Outputs for Flight 1

7.2 Calibration of the Scintillation Detection System

The second phase of the analysis involved an examination of the scintillation part of the data. Using the computer output of the first phase, scintillation distributions for various Cerenkov intervals were plotted. These distributions for flight 1 are shown in Figure 13. In this figure, peaks corresponding to the relative proton and alpha distributions emerge quite clearly when the Cerenkov output gets sufficiently large. The scintillation outputs at these peaks approach asymptotic values for large Cerenkov outputs. These values were taken to be the most probable scintillation outputs for relativistic protons and alpha particles.

From these two values, the knowledge of what their ratio should be, and the preflight calibration on the height-to-time convertors, a "zero voltage", i.e. a voltage corresponding to a zero time output of the height to time convertors, could be inferred for each flight. This zero voltage was subtracted from the input voltages deduced from the height-to-time graph to obtain the actual detector output voltages. With this information, the voltage corresponding to each scintillation output channel during the flight was deduced.

This procedure was not repeated for the Cerenkov output channels, as it was not necessary to use this information in an exact form in this experiment.

The scintillation output channels were then grouped together into particle energy intervals, for both protons and alpha particles, on the basis of most probable scintillation light output. The

formulae used in this calculation were (1) appearing in Chapter 3, for the most probable ionization loss of particles in a medium, and also

$$L_{\text{out}} = \frac{a\epsilon_p}{1 + b\epsilon_p/x} \quad (3)$$

for the light output (L_{out}) of a scintillating material of thickness x in terms of the ionization loss, taken to be the most probable energy loss (ϵ_p). 'a' and 'b' are constants of the scintillation material. This formula was originally given by Birks (1951) and is qualitatively explained in a text edited by Ritson (1961). It was not necessary to know the value of 'a' as this was merely a proportionality constant. The value used for 'b' was $.0091 \text{ g cm}^{-2} \text{ MeV}^{-1}$, found by Prescott and Rupaal (1961) for plastic scintillator NE102.

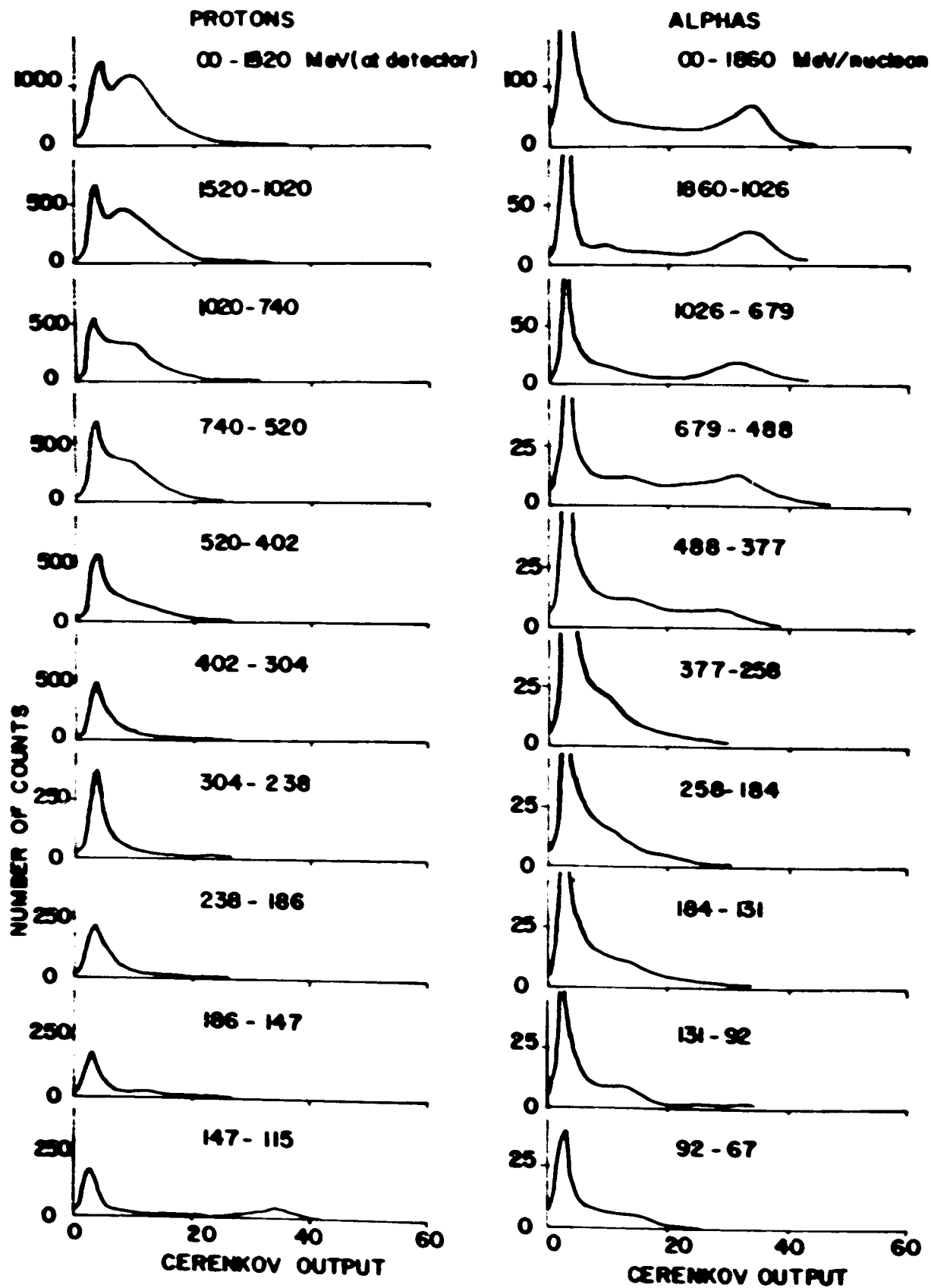


Figure 14 Cerenkov Output Distributions for Various Scintillation Outputs Defined in Terms of Particle Energy for Flight I

7.3 Preliminary Examination of the Cerenkov Distributions

To aid in the identification of particles, the Cerenkov distributions for the scintillation intervals derived as mentioned in the last section were plotted. An example (flight 1) is shown in Figure 14. An examination of this figure proved enlightening, both in regard to the operation of the apparatus, and the corrections to be made to the counts in these intervals in order to derive a primary spectrum, both for protons and alpha particles.

The relativistic proton curves show two peaks, corresponding to a Cerenkov output of zero (situated at 3 on the output scale) and a Cerenkov output situated at 10. Judging by its pronounced presence only for the fast proton intervals, the 10 peak corresponds to the Cerenkov output for relativistic protons. In flight 1, the Cerenkov detector was directional, so that upwards-moving particles would not be seen by it. Since a cosmic ray albedo, for the most part consisting of fast electrons, exists in reasonable amounts (McDonald and Webber, 1959), it should contribute to the zero Cerenkov peak. Other effects, such as chance coincidences between the two scintillators in the detector telescope, may also contribute to this peak. Such effects will be discussed more fully later on.

In the lower energy proton intervals, the relativistic peak disappears, and the zero Cerenkov peak remains. This is to be expected, as the particles falling in these intervals will not have a resolvable Cerenkov output. (A slight amount of scintillation occurs in the lucite Cerenkov detector, but for singly charged particles it is not sufficiently large to be resolved.)

The lowest energy interval defined for the protons shows a new peak at 34, owing to the appearance of relativistic alpha particles.

The high energy alpha particle intervals have several interesting features. As well as the alpha peak at 34, there is a zero Cerenkov peak. This may be partly due to low energy protons but, as it extends past the detector cut-off energy for such particles, the zero peak must also contain other events. Speculation on what these events might be is included later. A slight peak at about 10 also occurs. This may be due to the Landau tail in the scintillation distribution of relativistic protons.

As the alpha energies decrease, the alpha peak tends towards a lower value, but not zero. This may be expected because, as mentioned earlier, a small amount of scintillation occurs in the Cerenkov detector. It appears that, for the doubly charged lower energy alpha particles, a sufficient amount of light is emitted to partially distinguish them from zero output events.

The zero Cerenkov peak also persists throughout all the alpha energy intervals. In fact, this peak is quite large in comparison with the rest of the counts in each of the alpha energy intervals.

7.4 Initial Correction of the Data

In deriving primary cosmic ray spectra from distributions such as those shown in Figure 14, several corrections were necessary. The first type of correction was applied to these distributions, and transformed this data into a spectral representation of the cosmic radiation as seen by the detector. The second type of correction was made upon this spectral representation in order to derive the actual form of the primary cosmic radiation at the top of the atmosphere. This section will consider only the first type of correction, the second being considered in a later section.

At this point, the data was in the form of Cerenkov output distributions for different particle energy intervals, defined in terms of the most probable light output of the scintillation detector, both for protons and alpha particles. It now became convenient to consider protons and alpha particles separately, applying different corrections to each of them.

7.4.1 Background Correction in Alpha Region

The large 'zero output peak' which is apparent over the entire alpha particle region as shown in Figure 14, is symptomatic of a large number of 'background events' of uncertain origin which occurred in the detectors during all balloon flights. McDonald (1956) has also noted the existence of similar events but, for the particular apparatus and balloon flights he was concerned with, they do not form as large a fraction of the total number of counts as they do here. (See Figures 15 and 17.) This increase was perhaps due to the higher geomagnetic latitudes at

which the present flights were made, but much more likely due to the composition and configuration of the detectors used, and perhaps certain electronic parameters.

Possible mechanisms which may have given rise to these background events are the following:

Accidental coincidences between the two telescope elements.

The fraction of such events depends on the total counting rate of each of the two scintillators in the telescope, and hence their areas. It also depends on the resolving time of the coincidence circuitry. The vertical particle flux found by Winckler and Anderson* for the 1955 solar minimum period, at a latitude of 64.5° N. magnetic and an altitude corresponding to 10 g.cm^{-2} of air pressure, was $0.52 \text{ particles/cm}^2\text{.sr.sec.}$ If the flux is assumed to be isotropic, then this measured value leads one to expect a total count rate of 162 counts/second for each of the scintillators in the present experiment. The resolving time of the coincidence circuitry was typically about 5 microseconds. With the expected total rate, this yields a value of 0.26 counts/second for accidental coincidences. This number of accidental coincidences is only 5 per cent of the total expected particle rate and therefore cannot account for most of the observed background counts.

Electrons in the cosmic ray beam. A certain number of cosmic ray electrons passing through the telescope, but stopping

* Winckler, J. R., and Anderson, K. A., 1957, Phys. Rev., 108, 148.

before or in the Cerenkov detector will produce some of the background events. These electrons may be either primary electrons, re-entrant albedo electrons, or secondary electrons produced in the air and material above the detectors. A crude spectrum of the re-entrant plus secondary electrons has been determined from the results of several workers by Schmoker and Earl*. These authors find only a negligible contribution from primary electrons. From their work, the total flux of downwards electrons for the present experiment is estimated to be 0.02 particles/cm².sr.sec. Of this flux, 40 per cent should stop before the Cerenkov detector, thus having no Cerenkov output, 20 per cent should stop in the Cerenkov detector and thus have an "intermediate" Cerenkov output, and the remainder will pass through the Cerenkov detector, and therefore have an output similar to that of relativistic protons. The downwards-moving electrons can account for approximately 4 per cent of the total counting rate of the present experiment.

Nuclear interactions of cosmic rays in the scintillator.

These events are expected to form 2 or 3 per cent of the total counting rate. They are likely to have large scintillation outputs which would place them in the alpha regions. Their fraction of the total rate is independent of the detector area, but depends on the thickness and type of material used in the detectors, being greater for lighter materials. For this reason,

* Schmoker, J. W., and Earl, J. A., 1965, Phys. Rev., 138, B300.

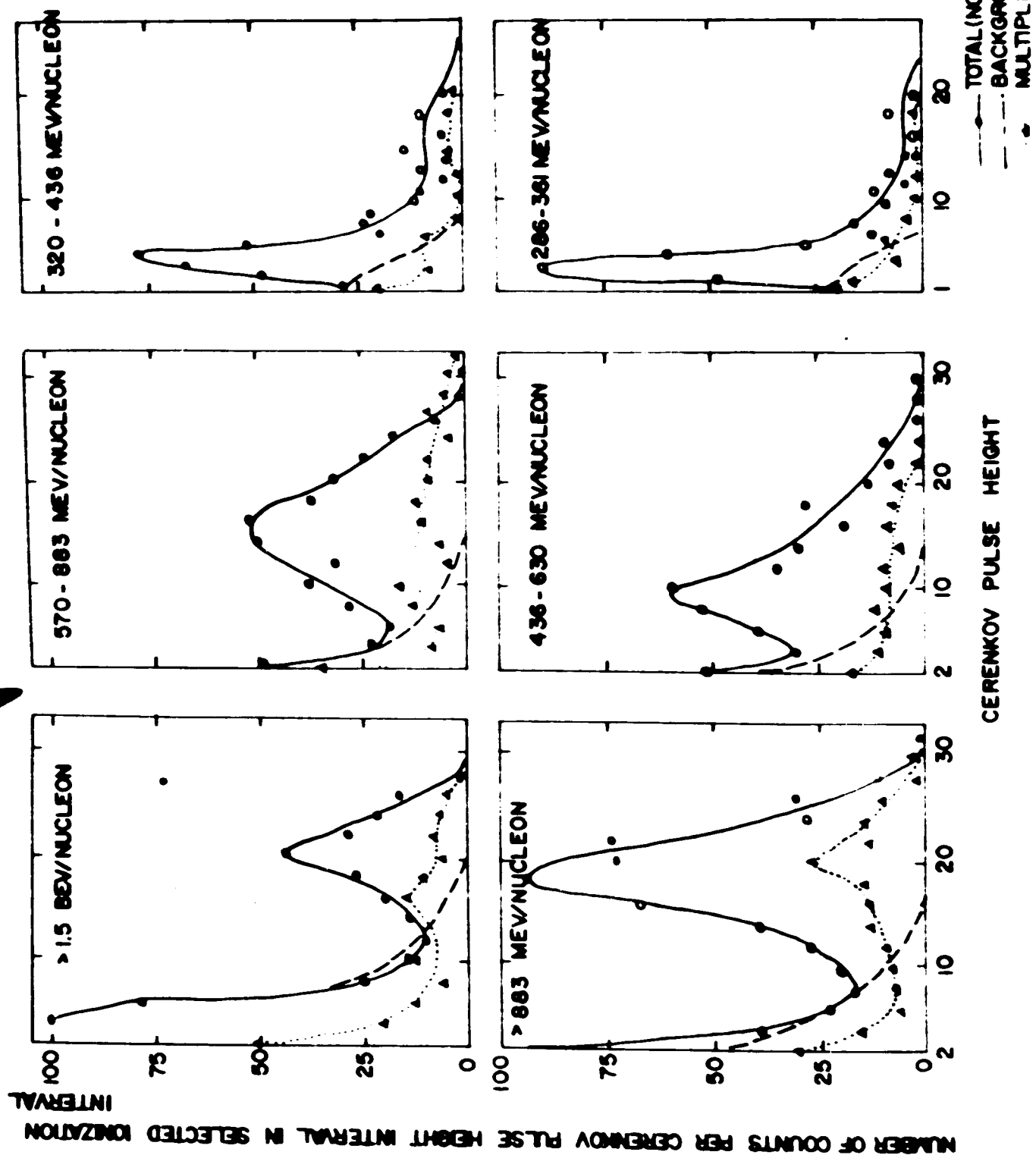


Figure 15 Cerenkov Distributions Found by McDonald (1956) over Alpha Ionization Intervals

the fraction of such events should be about $2 \frac{1}{2}$ times greater than those seen by McDonald. This is not large enough to explain the difference in fraction of background between the two experiments.

Showers above the detectors.

In McDonald's experiment, multiple particle events were detected with an efficiency of 0.5, and the number of such events found to be reasonably small in comparison to the rest of the events in each scintillation output interval. The generally lower pressures achieved for the present experiment should tend to reduce the shower rate to a value below what McDonald detected. His results are shown in Figure 15.

Thus it is not feasible that the background is composed entirely of these four phenomena alone. The total intensities in $\left[\frac{\text{particles}}{\text{cm}^2 \cdot \text{sec} \cdot \text{ster}} \right]$ at floating altitude for the four flights, with the transmission noise counts removed where possible, are shown below along with the rates observed by Winckler and Anderson (reference at bottom of page 70) for similar geomagnetic latitudes.

| | Present results | Present results minus 10 per cent | Winckler and Anderson |
|----------|-----------------|--------------------------------------|--------------------------|
| Flight 1 | .49 | .44 | .46 |
| Flight 2 | .78 | .70 | .52 |
| Flight 3 | .62 | .56 | .52 |
| Flight 4 | .67 | .60 | .46 |

71a

An extra contribution to the rates of the present flights comes from the accidental coincidences (5 per cent) and the presence of extra material in the detectors. An upper limit to the contribution of nuclear interactions in the extra detector thickness to increases in the counting rate is 5 per cent, neglecting evaporation particles, as they will not be able to pass through the telescope absorber and be detected as events. Thus, a 10 per cent excess at most can be expected for the present flights over those of Winckler and Anderson. Agreement is found for flights 1 and 3, but the other two flights show total rates significantly higher than expected. For these flights, an additional source of background not present in the other two flights, or in Winckler and Anderson's flights, may have existed. Noise originating in the electronics is a likely such source.

It is, in any case, extremely difficult to make a theoretical calculation on the amount of background in any scintillation output interval, and the accuracy of such a calculation would be doubtful. Experimental techniques show more promise for inferring the background rates.

McDonald (1956), in making a correction for the background radiation in the alpha particle region, observed that the shape of the background Cerenkov distribution remained the same across

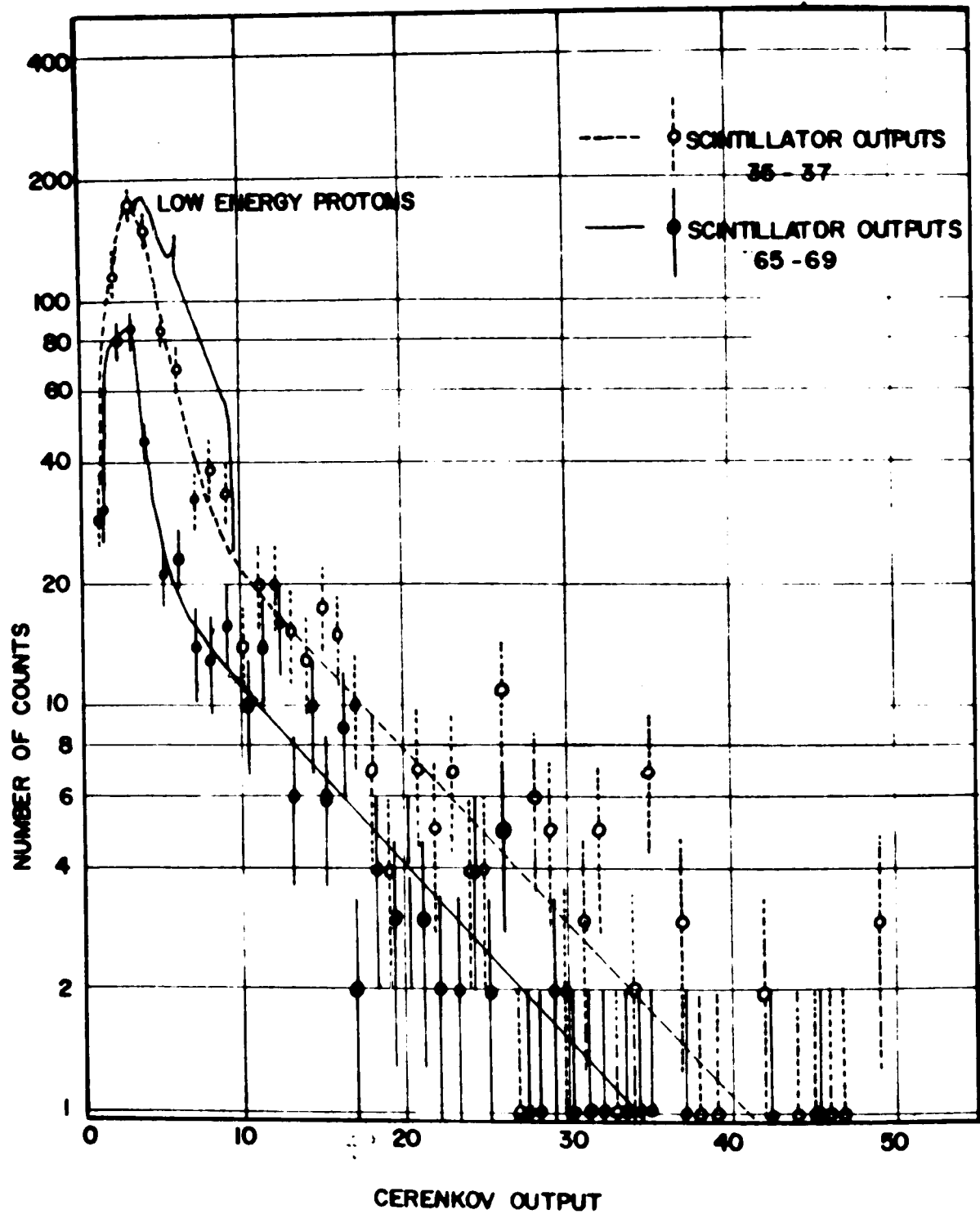


Figure 16 Cerenkov Distributions in Scintillation Regions Containing Mostly Background Counts, for Flight 1

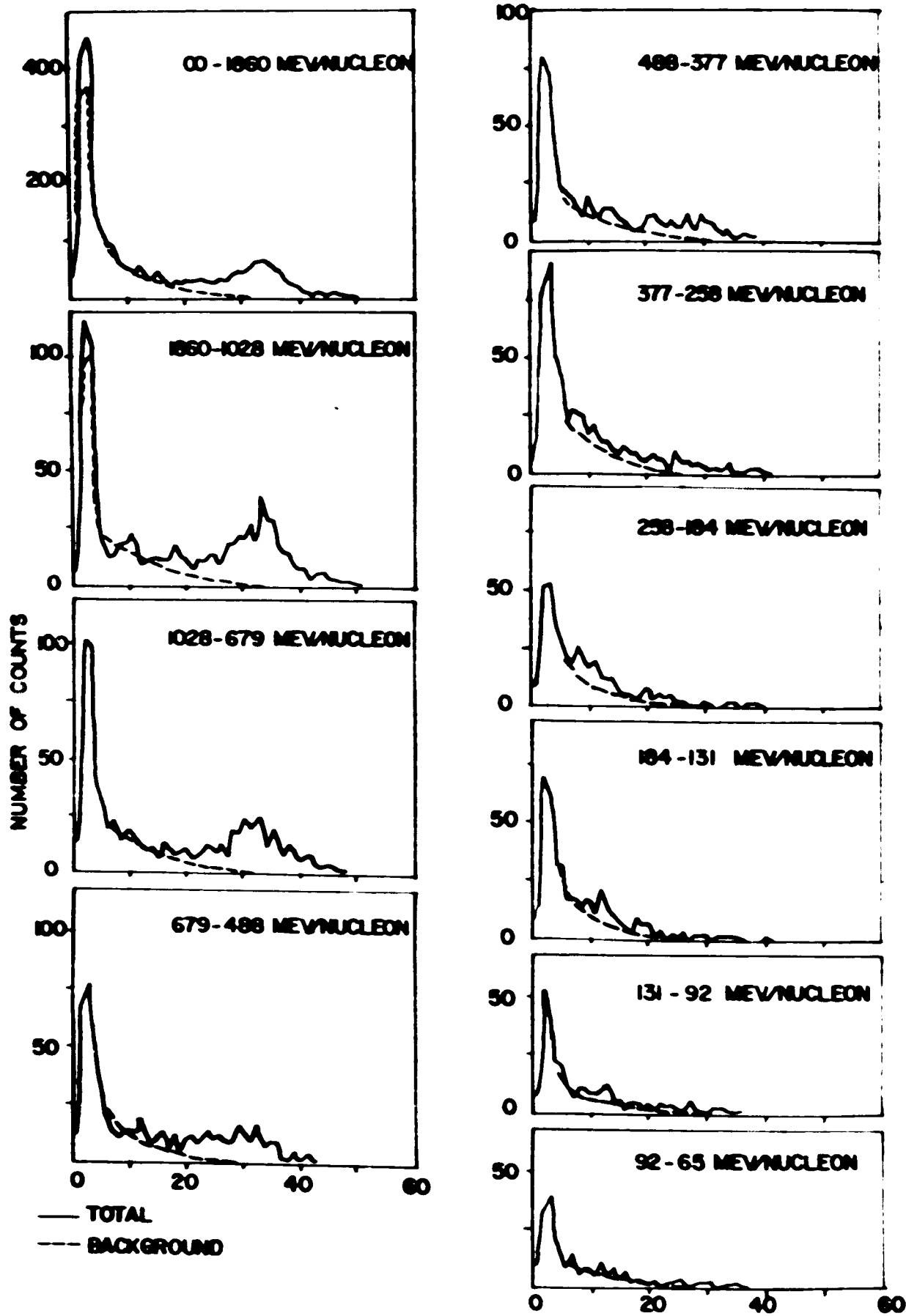


Figure 17 Cerenkov Distributions for Alpha Scintillation Intervals, for Flight 1

the alpha region. From the similar Cerenkov distributions on both sides of the alpha scintillation output region, he determined the shape of the background correction. The alpha particle Cerenkov output peaks in each energy interval were then identified, and the background correction normalized to this interval on the low Cerenkov output side of the alpha peaks. Figure 15 shows examples of his work.

A similar procedure was attempted for this experiment. The shape of the background Cerenkov distribution was inferred from the scintillation output region just above that corresponding to alpha particles, and compared to that of the region just below the alpha particles, to check the constancy of the shape of the background correction. The results for flight 1 are shown in Figure 16.

In normalizing the background distribution to each of the alpha energy intervals, for each flight, the zero Cerenkov output peaks were used, except for the highly relativistic intervals where proton contamination could occur. From the results, shown in Figure 17, the background curves seem a reasonably good fit to the data, except of course for the alpha peaks. For the highly relativistic alpha region, the portion between the alpha and zero Cerenkov peaks was used for normalization. Only the counts above this portion were considered to be due to alpha particles. The certainty of this correction in the low energy intervals appears dubious, as the alpha particle resolution here is low, as can be seen in Figure 17.

7.4.2 Background Correction in Proton Region

In the relativistic proton region, the background correction problem was a little different. The majority of the background counts in this region were thought to be some form of 'noise' originating in the transmission of data, and also accidental coincidences between the scintillators. Most of these events could not be expected to have a large Cerenkov output, and were therefore separated from the relativistic protons on this basis. A background Cerenkov distribution was determined from the scintillation output region immediately below that of the relativistic protons. The fast proton scintillation output region was corrected for background by normalizing this distribution to the counts in the low output Cerenkov channels, and then subtracting it from the fast proton region. A systematic error in the background correction arose in flight 1, in which a directional Cerenkov detector was employed, yielding a contribution to the low output Cerenkov channels in the fast proton region from albedo particles. This is discussed in the next chapter.

For the lower energy proton region, a combination of both 'noise' and nuclear interaction background pulses were expected. Furthermore these pulses could not be removed on the basis of their Cerenkov distributions as before, since the protons were also expected to have low Cerenkov outputs in this region. For lack of a better method, an interpolation of the background rate was used. The background used for other regions of scintillator output was plotted and a smooth line drawn between the relativistic

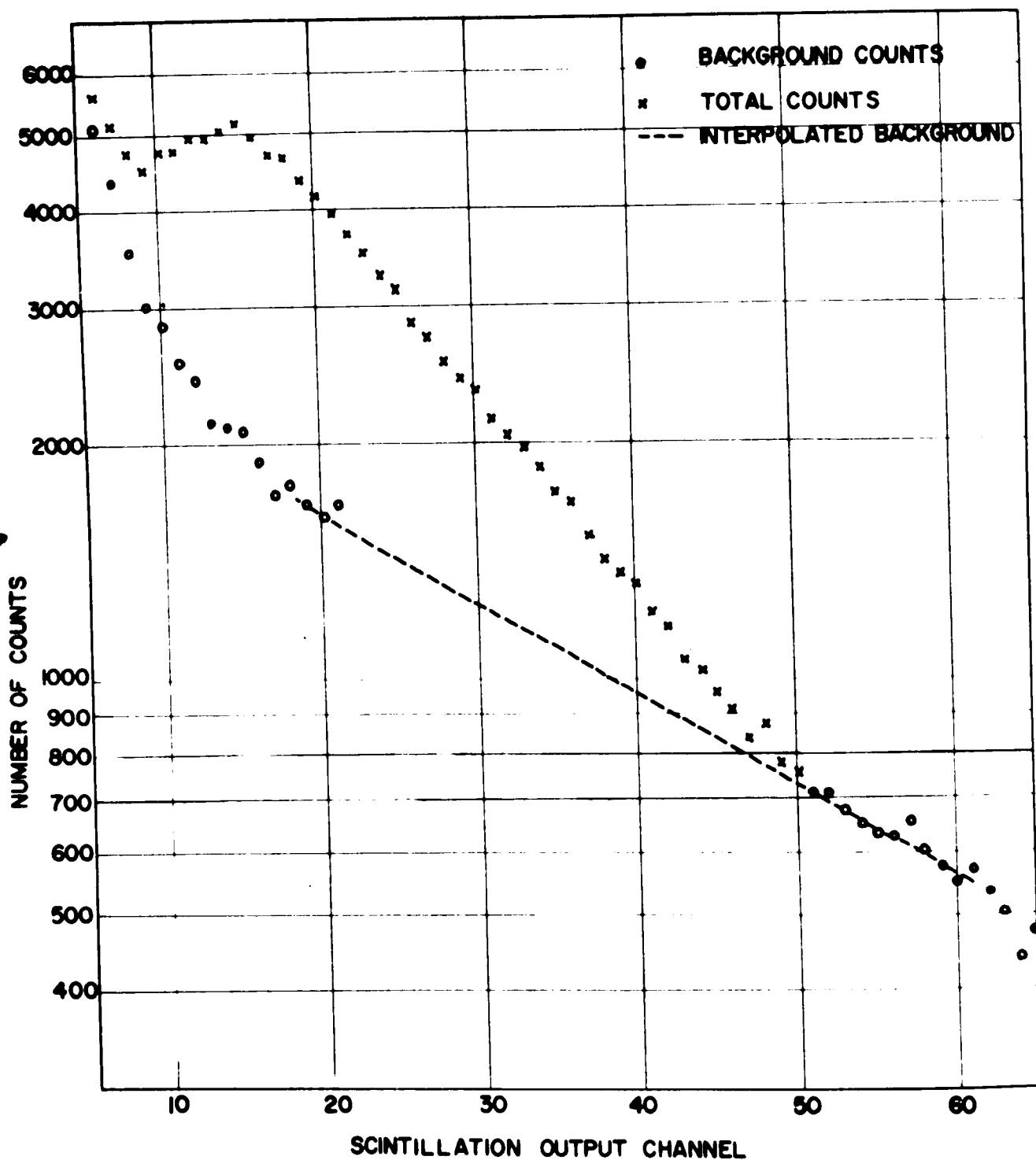


Figure 18 Background Correction over Proton Region for Flight 4

proton region, and the alpha regions, to get the background for the low energy proton region. An example for flight 4 is shown in Figure 18. As the number of proton counts was quite high, the accuracy of the background correction for the proton region was not as vital as that for the alpha region.

7.4.3 Detector Correction

Because of the statistical nature of ionization losses and therefore light output in the scintillators, there was not a one-to-one correspondence between particle velocity and light outputs for any one velocity distributions for any flight; it was necessary to know the output distributions of the system for fixed particle velocities. Calculations of these distributions have been carried out by Symon (1948) and are discussed in a text by Rossi (1956).

The theory of the convolution procedure used to obtain particle spectra from detector output spectra, using distributions such as mentioned above is now given.

Suppose a particle velocity β_i . Write the output distribution of this velocity as $f_j(\beta_i)$, corresponding to a detector output of O_j . If there are $N(\beta_i)\Delta\beta_i$ particles with velocities between β_i and $\beta_i + \Delta\beta_i$, then the number of outputs between O_j and $O_j + \Delta O_j$ is given by

$$[N(O_j)\Delta O_j]_i = f_j(\beta_i)N(\beta_i)\Delta\beta_i$$

for this particular small range of velocities. To include all velocities, sum:

$$N(O_j)\Delta O_j = \sum_i f_j(\beta_i)N(\beta_i)\Delta\beta_i$$

Set $c_{ji} = \begin{cases} f_j(\beta_i) & \text{for } i = j \\ f_j(\beta_i) - 1 & \text{for } i \neq j. \end{cases}$ (4)

Then, $N(O_j)\Delta O_j = N(\beta_j)\Delta\beta_j + \sum_i c_{ji}N(\beta_i)\Delta\beta_i$.

Therefore,
$$\begin{aligned} N(\beta_j) &= N(O_j)\Delta O_j - \sum_i c_{ji}N(\beta_i)\Delta\beta_i \\ &= N(O_j)\Delta_j - \sum_i c_{ji}(N(O_i)\Delta O_i \\ &\quad - \sum_k c_{ik}N(\beta_k)\Delta\beta_k). \end{aligned}$$

Continuing this procedure, we get the infinite series,

$$\begin{aligned} N(\beta_j)\Delta\beta_j &= N(O_j)\Delta O_j - \sum_i c_{ji}N(O_i)\Delta O_i + \sum_{i,k} c_{ji}c_{ik}N(O_k)\Delta O_k \\ &\quad - \sum_{i,k,l} c_{ji}c_{ik}c_{kl}N(O_l)\Delta O_l \\ &\quad + \text{----- etc.} \end{aligned}$$

This equation gives the original velocity spectrum $N(\beta_j)$ in terms of the output spectrum $N(O_j)$. If the intervals $\Delta O_j, \Delta\beta_j$ are such that the c_{ji} are small, then we can approximate:

$$N(\beta_j)\Delta\beta_j = N(O_j)\Delta O_j - \sum_i c_{ji}N(O_i)\Delta O_i. \quad (5)$$

From equation 4, this is seen to happen when the $f_j(\beta_i)$ are large for $i = j$, and small for other values. Now the scintillator output is in the form of numbers, so the ΔO_i can be taken to be 1. $f_i(\beta_i)$ is largest when the $\Delta\beta_i$ interval is that corresponding to the ΔO_i interval on the basis of most probable scintillation output. However, even with this representation the detector output distributions $f_j(\beta_i)$ for a fixed β are sufficiently wide compared to a single scintillation output channel that some c_{ij} are still fairly large. When several channels are taken together, and equation 5 applied to

these groupings of channels, the size of the c_{ij} is reduced considerably.

The elements $f_j(\beta_i)$ for the detector correction were found from ionization distribution curves drawn up for different particle velocities by Symon (1948), a knowledge of the nonlinearity properties of plastic scintillator NE102 (Prescott and Rupaal, 1961), and the calibration curves found for the scintillation outputs for each flight (Section 7.2). The positions of the most probable outputs of relativistic protons and alpha particles found as outlined in Section 7.2 were also instrumental to this calculation. These elements were found for each channel of scintillation output.

The next step was the division of the output channels into intervals, several channels per interval, for each flight. For the higher velocity intervals, between .95 and 0.8 c where the output distributions were wide and the number of counts high, the interval widths were about half to two-thirds that of a theoretical single velocity distribution in this region. Slow changes in the primary spectrum for these velocities could therefore be reasonably well produced, but the first order correction would not be sufficient to resolve abrupt changes in a single interval. For the lower velocity regions, the intervals were wider in general than the distributions, thereby allowing abrupt changes in spectra to be observed.

Then, using the $f_j(\beta_i)$ found for each channel, and equation 5, the contribution to each velocity loss interval

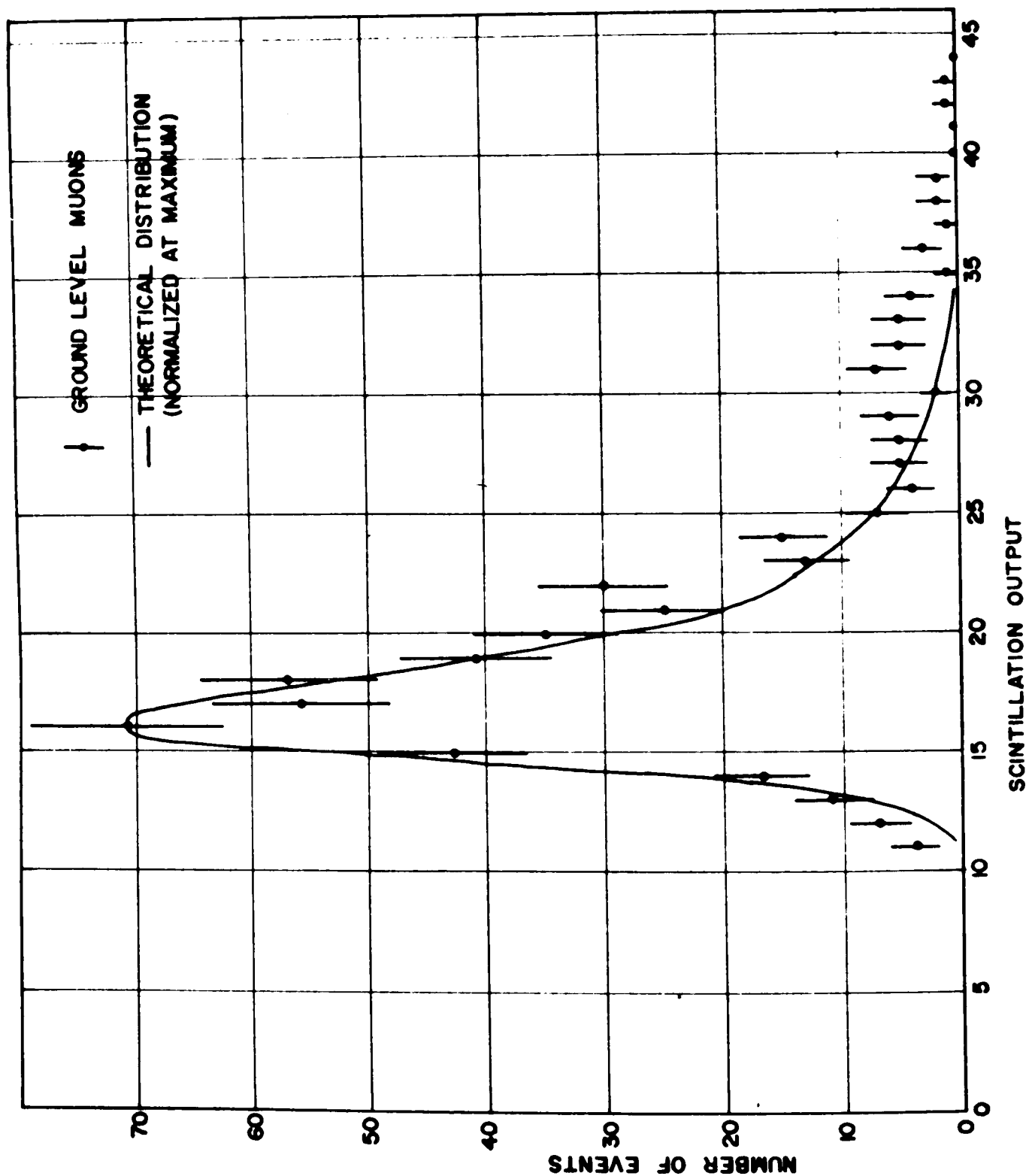


Figure 19 Ground Level Muon Scintillation Distribution for Flight I Compared with Theoretical Curve

was ascertained from the output rates of each channel.

As a check on the theoretical light output distribution, $f_j(\beta_i)$, the calculated distribution for fast singly charged particles was compared to the experimental distribution found for ground level muons, as mentioned in Chapter 5, for all four flights. An example for flight 1 is shown in Figure 19.

7.4.4 Recording Correction

A small amount of uncertainty arose in the changing of the analogue pulse length transmitted to the ground into a digital number, owing to the electronics involved in this process. A pulse whose length under ideal conditions should have yielded a certain number had a 50 per cent probability of yielding that number, and a 25 per cent probability of yielding each of the two adjacent numbers. This uncertainty was taken into consideration by including it in the detector correction. The distribution element $f_j(\beta_i)$ then became $0.5f_j(\beta_i) + 0.25f_{j-1}(\beta_i) + 0.25f_{j+1}(\beta_i)$.

7.5 Atmospheric Correction of the Data

The data at this point was in the form of two velocity spectra for each flight, those of the singly and doubly charged particles present in the vicinity of the detector. Because of the occurrence of various types of cosmic ray interaction in the atmosphere above the detector, it was necessary to make several different corrections to this data in order to arrive at spectra for particles above the earth's atmosphere.

7.5.1 Ionization Loss in the Atmosphere

This type of correction applied to both protons and alpha particles. The velocity intervals for the particle and flight concerned were put in terms of particle energy. Then, using the measured pressure along with range-energy curves for particles in air (Ritson, 1961), the energy intervals were corrected for ionization loss to the top of the atmosphere. This correction neglected the effects of fluctuations in ionization loss, which were generally smaller than other uncertainties in the energy intervals arising from instrument calibration.

7.5.2 Alpha Particle Absorption

The alpha particles were corrected for absorption in the air and material above the detector. By using the data taken while the balloon was ascending, a mean interaction length could be found. The technique used for this is described in a later section. Using the value found, the alpha particle data was corrected to the top of the atmosphere for this effect.

Owing to a large number of competing effects for protons, the proton data was not corrected in this manner, but rather in a manner described later on.

7.5.3 Production of Alpha Particles by Fragmentation of Heavier Nuclei

A significant number of alpha particles is produced in the interaction of the heavier cosmic ray nuclei with the atmosphere. As the absorption lengths for these nuclei are less than that for alpha particles as well as there being a reasonably large difference in intensity, this effect should not cause any large error in the determination of the absorption length of alpha particles. However, in determinations of absolute alpha particle counting rate, the production effect is large enough at balloon altitudes to warrant correction. This correction was combined with the absorption correction, in the manner outlined theoretically below.

A traditional experimental division of cosmic ray nuclei with charge (Z) greater than 2 is the following:

light nuclei (L) : $3 \leq Z \leq 5$

medium nuclei (M) : $6 \leq Z \leq 9$

heavy nuclei (H) : $10 \leq Z$

Let the ratio of light, medium, and heavy nuclei to alpha particles be $R_{L\alpha}$, $R_{M\alpha}$, and $R_{H\alpha}$ respectively; their interaction mean free paths, λ_L , λ_M and λ_H ; their alpha fragmentation parameters (mean number of alpha particles produced in one interaction with an "average" air nucleus), $P_{L\alpha}$, $P_{M\alpha}$, and $P_{H\alpha}$.

Consider the flux of light nuclei, $N_\alpha(0) R_{L\alpha}$ at the top of the atmosphere, where $N_\alpha(0)$ is the flux of alpha particles at

the top of the atmosphere. The fraction interacting between 0 and $x \text{ g/cm}^2$ depth of atmosphere is $(1 - e^{-x/\lambda_L})$, and the number of interactions, $N_\alpha(0)R_{L\alpha}(1 - e^{-x/\lambda_L})$. Therefore the number of alpha particles produced in $x \text{ g/cm}^2$ of atmosphere by interactions of light primary cosmic ray nuclei is

$$N_{L\alpha}(x) = N_\alpha(0)R_{L\alpha}P_{L\alpha}(1 - e^{-x/\lambda_L}) \quad (6)$$

Similar expressions to (6) may be found for the medium and heavy nuclei-produced alphas, $N_{M\alpha}(x)$ and $N_{H\alpha}(x)$, if the production of alpha particles in second or higher reactions, e.g. the fragmentation of a heavy nucleus producing a medium nucleus and the interaction of this medium nucleus producing an alpha particle, is neglected.

The number of original primary alpha particles at a depth x is given by

$$N_{\alpha\alpha}(x) = N_\alpha(0)e^{-x/\lambda_\alpha} \quad (7)$$

where λ_α is the mean interaction length of alpha particles in the atmosphere.

If the absorption of fragmentation alphas in the air is neglected, as this is a second-order effect, the total number of alpha particles present at depth x is given by

$$N_\alpha(x) = N_{\alpha\alpha}(x) + N_{L\alpha}(x) + N_{M\alpha}(x) + N_{H\alpha}(x) \quad (8)$$

Substituting (6) and (7) into (8), we obtain

$$\begin{aligned} N_\alpha(x) = & N_\alpha(0)e^{-x/\lambda_\alpha} + N_\alpha(0)R_{L\alpha}(1 - e^{-x/\lambda_L}) \\ & + N_\alpha(0)R_{M\alpha}P_{M\alpha}(1 - e^{-x/\lambda_M}) \\ & + N_\alpha(0)R_{H\alpha}P_{H\alpha}(1 - e^{-x/\lambda_H}). \end{aligned}$$

Rearranging,

$$N_{\alpha}(0) = N_{\alpha}(x) / (e^{-x/\lambda_{\alpha}} + R_{L\alpha} P_{L\alpha} (1 - e^{-x/\lambda_L}) + R_{M\alpha} P_{M\alpha} (1 - e^{-x/\lambda_M}) + R_{H\alpha} P_{H\alpha} (1 - e^{-x/\lambda_H})) \quad (9)$$

Equation (9) gives the alpha flux at the top of the atmosphere in terms of the measured flux at a small depth x in the atmosphere.

Equation (9) was used to correct the measured alpha flux for absorption and production by fragmentation of heavier nuclei to the top of the atmosphere. Values for the interaction lengths and alpha fragmentation parameters for the L, M, and H nuclei found by Noon and Kaplon (1955) from emulsion studies were used. The values given for the ratios $R_{L\alpha}$, $R_{M\alpha}$, and $R_{H\alpha}$ in terms of energy per nucleon by Waddington (1963) were used. Implicit in the usage of these ratios was the assumption that the fragmentation alpha particles emerged from the collision with the same energies per nucleon or velocities as the primary parent particles. λ_{α} , the alpha particle interaction length, was determined experimentally as outlined in section 7.6.

7.5.4 Secondary Effects Involving Singly Charged Particles

As the production of secondary singly charged particles, which could not be distinguished from protons by the apparatus, arises from several different processes involving complex and uncertain calculation, the proton data was not corrected for either absorption or production of secondaries by any theory-based method. Instead, the data taken while going to altitude was divided into three proton energy intervals on the basis of proton scintillator

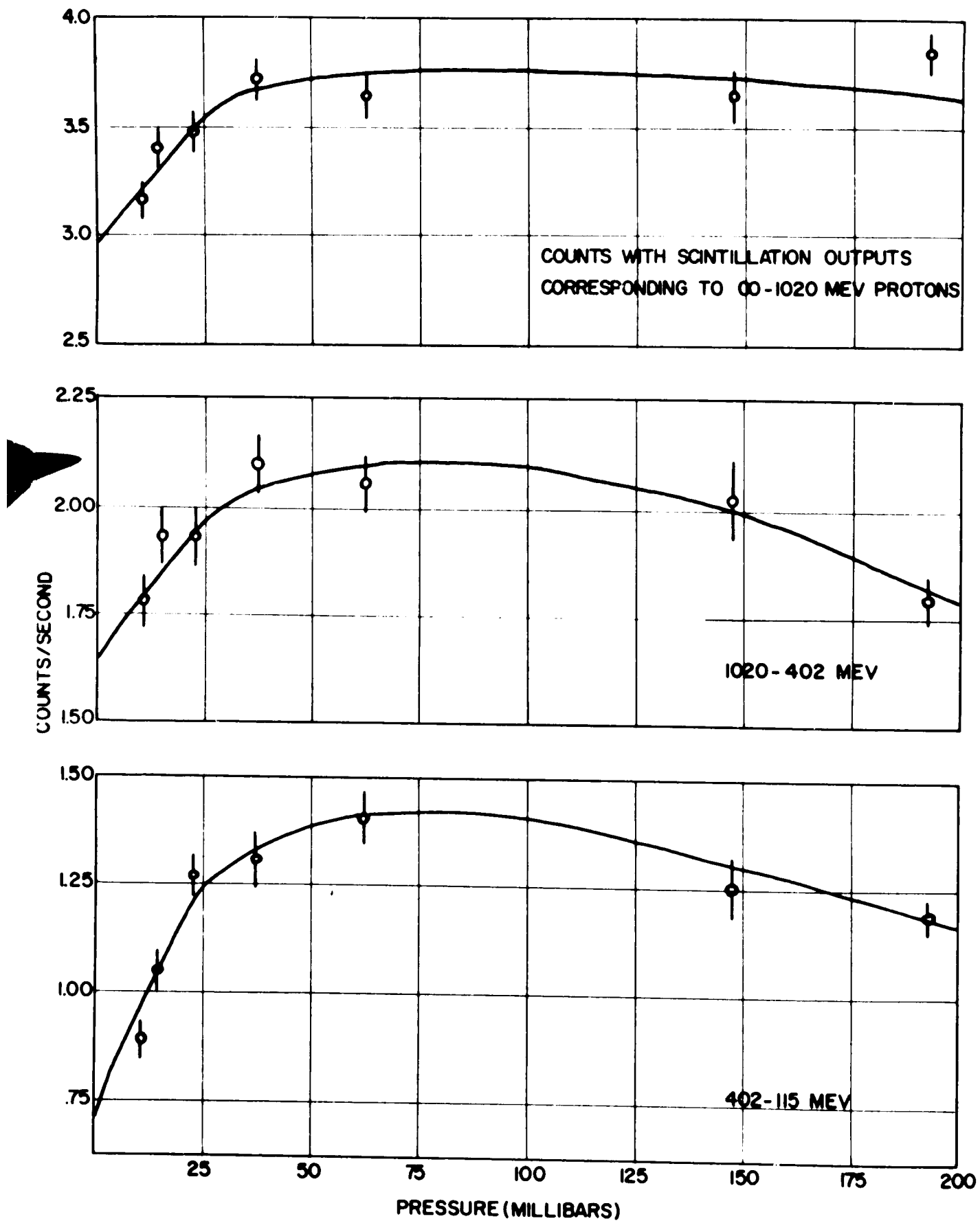


Figure 20 Counting Rates during Ascent for Flight I Proton Scintillation Output Region

output. The counts in these intervals were plotted as a function of atmospheric pressure, and the resultant curves extrapolated to the top of the atmosphere. An example is shown in Figure 20.

This method was similar to that employed by McDonald and Webber (1959). However, it was hampered by the existence of a large background in the present study. As statistics were not good enough to allow a separation of the particle counts and background to be made, it was assumed that these counts varied in the same way as the protons. The curves obtained during the three flights used were compared, and average correction factors obtained for the three energy regions. Flight 4 was not used here, as signal reception difficulties occurred during ascent of this flight.

No correction has been made to the data for albedo protons, or electrons. The electrons are expected to be highly relativistic and therefore have outputs in the relativistic proton region (MacDonald and Webber, 1959). The protons, on the other hand, should lie in the slow proton region, and should be partially distinguishable on the Calgary flights, as some of them should extend below the geomagnetic cut-off, down to the lowest observable energies. An examination of these two flights gave an indication of the magnitude of this effect for the Calgary vicinity.

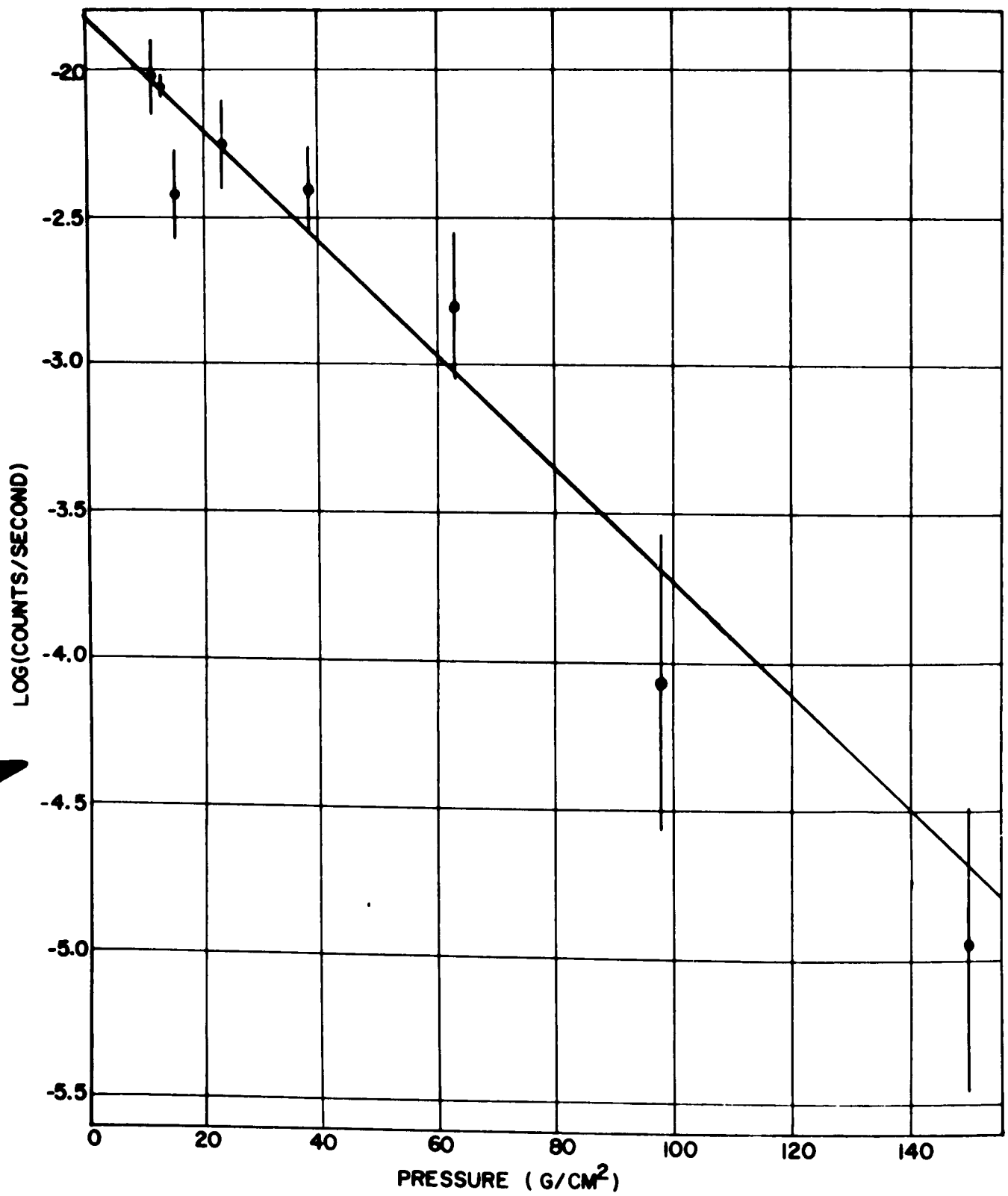


Figure 21 Counting Rate in Fast Alpha Region during Ascent for Flight 1

7.6 Determination of the Alpha Particle Mean Free Path in Air

Using the data obtained during balloon ascents, it was possible to calculate a mean free path for alpha particles in the atmosphere.

As the number of counts in each interval chosen for this calculation had to be necessarily small, it was essential to use a portion of the combined Cerenkov scintillation output spectrum (see Figures 3b and 12) which consisted nearly entirely of alpha particles. The only such region was that corresponding to relativistic alphas. By examining diagrams similar to Figures 13 and 14, the boundaries of this region were chosen for each flight. In each of these relativistic alpha regions, the non-alpha particle counts were less than 3 per cent of the total counts at altitude.

The number of counts in this chosen region of the Cerenkov-scintillation output spectrum was taken over 10 minute intervals as the balloon was ascending and, from these numbers and the counting time of each interval, alpha rates computed. The logarithms of the alpha rates were plotted against the mean pressure recorded in each interval, and a straight line fitted to the data. An example is shown in Figure 21. From the slope of the straight line, the alpha particle mean free path was determined. This procedure was carried out for Flights 1, 2, and 3.

CHAPTER EIGHT

EXPERIMENTAL RESULTS

8.1 Scintillation Output Calibration and Particle Energy Intervals

The data taken on the ground were compared with the theoretical scintillation distributions calculated with the aid of the relativistic proton and alpha positions at altitude, as described in Section 7.4.3. The first three flights showed a reasonable fit, as typified by Figure 19, except for the small fraction of the distribution in the higher output channels.

The fourth flight, however, yielded relativistic proton and alpha points which indicated a substantially higher zero correction (See Section 7.2.) than the other flights. The resultant theoretical relativistic particle distribution was appreciably wider than the experimental one, suggesting that the mode of zero correction was in error, and that the calibration for this flight was incorrect. Very little zero correction was needed on the other flights, so that the error introduced for them must have been quite small. A new relativistic distribution was calculated for flight 4 on the basis of the half-width of the ground distribution. However, there was no obvious way of inferring a new energy calibration for the scintillator output regions for this flight. Examination of the Cerenkov distributions for the various scintillation output intervals, such as those shown for flight 1 in Figure 14, particularly of the point at which the proton Cerenkov outputs become zero, yielded agreement for all four flights, with a value somewhere between 300 and 400 MeV as was expected on the basis of theory. From this inspection, it was concluded that

the energy calibration for flight 4 could not have been out by more than 60 MeV, at the 350 MeV point. As the theoretical distributions were extremely sensitive to small changes in calibration, they were considered a good check on the accuracy of the calibration. For flights 1, 2, and 3 it could be concluded that the calibrations were accurate to within one channel of scintillation output, and for flights 4, to within 2 or 3 channels at a point midway between the relativistic proton and alpha particles, decreasing to 1 at these two points.

Table 2 gives the energy intervals used for the protons and alpha particles for all four flights, both at the balloon altitude, and corrected for ionization loss to the top of the atmosphere.

Table 2: Particle Energy Intervals, Defined in Terms of Most Probable Scintillation Output

| <u>Interval No.</u> | <u>Channels</u> | <u>Velocity (β)</u> | <u>Energy at detector</u> | <u>Rigidity, corrected to top of atmosphere</u> |
|---------------------|-----------------|--------------------------------------|---------------------------|---|
|---------------------|-----------------|--------------------------------------|---------------------------|---|

Flight 1 Protons:

| | | | | |
|----|-------|-----------|----------------|----------------|
| 1 | 10-17 | 1.00-.925 | ∞ -1520 | ∞ -2290 |
| 2 | 18-19 | .925-.880 | 1520-1020 | 2290-1738 |
| 3 | 20-21 | .880-.830 | 1020- 740 | 1738-1414 |
| 4 | 22-24 | .830-.768 | 740- 520 | 1414-1145 |
| 5 | 25-27 | .768-.716 | 520- 402 | 1145- 992 |
| 6 | 28-30 | .716-.658 | 402- 304 | 992- 857 |
| 7 | 31-33 | .658-.605 | 304- 238 | 857- 764 |
| 8 | 34-36 | .605-.533 | 238- 186 | 764- 690 |
| 9 | 37-39 | .533-.505 | 186- 147 | 690- 631 |
| 10 | 40-42 | .505-.459 | 147- 115 | 631- 584 |

(10.7 g/cm² of atm.)

Flight 2 Protons:

| | | | | |
|----|-------|-----------|----------------|----------------|
| 1 | 6-10 | 1.00-.915 | ∞ -1380 | ∞ -2145 |
| 2 | 11 | .915-.860 | 1380- 891 | 2145-1599 |
| 3 | 12 | .860-.810 | 891- 656 | 1599-1322 |
| 4 | 13 | .810-.767 | 656- 519 | 1322-1152 |
| 5 | 14-15 | .767-.698 | 519- 368 | 1152- 956 |
| 6 | 16-17 | .698-.644 | 368- 286 | 956- 849 |
| 7 | 18-19 | .644-.580 | 286- 211 | 849- 746 |
| 8 | 20-21 | .580-.530 | 211- 167 | 746- 684 |
| 9 | 22-23 | .530-.478 | 167- 129 | 684- 625 |
| 10 | 24-25 | .478-.439 | 129- 105 | 625- 595 |

(14.1 g/cm² of atmosphere)

Table 2 (cont.)

| <u>Interval No.</u> | <u>Channels</u> | <u>Velocity (β)</u> | <u>Energy at detector</u> | <u>Rigidity, corrected to top of atmosphere</u> |
|-------------------------|-----------------|--------------------------------------|-------------------------------|---|
|-------------------------|-----------------|--------------------------------------|-------------------------------|---|

Flight 3 Protons:

| | | | | |
|----|-------|-----------|----------------|----------------|
| 1 | 8-16 | 1.00-.947 | ∞ -2105 | ∞ -2905 |
| 2 | 17-20 | .947-.895 | 2105-1160 | 2905-1892 |
| 3 | 21-24 | .895-.838 | 1160- 775 | 1892-1452 |
| 4 | 25-28 | .838-.783 | 775- 566 | 1452-1197 |
| 5 | 29-32 | .783-.734 | 566- 440 | 1197-1038 |
| 6 | 33-37 | .734-.674 | 440- 328 | 1038- 885 |
| 7 | 38-42 | .674-.616 | 328- 252 | 885- 775 |
| 8 | 43-47 | .616-.560 | 252- 194 | 775- 693 |
| 9 | 48-52 | .560-.495 | 194- 141 | 693- 607 |
| 10 | 53-57 | .495-.430 | 141- 101 | 607- 544 |

(8.8 g/cm² of atmosphere)Flight 4 Protons:

| | | | | |
|----|-------|-----------|----------------|----------------|
| 1 | 6-15 | 1.00-.960 | ∞ -2380 | ∞ -3210 |
| 2 | 16-18 | .960-.933 | 2380-1652 | 3210-2435 |
| 3 | 19-21 | .933-.905 | 1652-1260 | 2435-2008 |
| 4 | 22-25 | .905-.863 | 1260- 908 | 2008-1617 |
| 5 | 26-29 | .863-.822 | 908- 708 | 1617-1381 |
| 6 | 30-34 | .822-.760 | 708- 503 | 1381-1130 |
| 7 | 35-40 | .760-.690 | 503- 354 | 1130- 938 |
| 8 | 41-47 | .690-.595 | 354- 227 | 938- 759 |
| 9 | 48-54 | .595-.495 | 227- 141 | 759- 630 |
| 10 | 55-61 | .495-.411 | 141- 89 | 630- 555 |

(12.8 g/cm² of atmosphere)

MeV

MV

Table 2 (cont.)

| <u>Interval No.</u> | <u>Channels</u> | <u>Velocity (β)</u> | <u>Energy at detector</u> | <u>Rigidity, corrected to top of atmosphere</u> |
|--|-----------------|--------------------------------------|-------------------------------|---|
| <u>Flight 1 Alphas:</u> | | | | |
| 1 | 37-43 | 1.00-.943 | ∞ -1860 | ∞ -5300 |
| 2 | 44-45 | .943-.880 | 1860-1028 | 5300-3496 |
| 3 | 46-47 | .880-.816 | 1028- 679 | 3496-2638 |
| 4 | 48-49 | .816-.755 | 679- 488 | 2638-2208 |
| 5 | 50-51 | .755-.702 | 488- 377 | 2208-1918 |
| 6 | 52-54 | .702-.624 | 377- 258 | 1918-1592 |
| 7 | 55-57 | .624-.551 | 258- 184 | 1592-1372 |
| 8 | 58-60 | .551-.482 | 184- 131 | 1372-1218 |
| 9 | 61-63 | .482-.416 | 131- 92 | 1218-1108 |
| 10 | 64-66 | .416-.353 | 92- 62 | 1108-1034 |
| (10.7 g/cm ² of atmosphere) | | | | |

Flight 2 Alphas

| | | | | |
|--|-------|-----------|----------------|----------------|
| 1 | 20-25 | 1.00-.943 | ∞ -1600 | ∞ -4760 |
| 2 | 25-27 | .943-.847 | 1600- 818 | 4760-3024 |
| 3 | 28-29 | .847-.774 | 818- 540 | 3024-2362 |
| 4 | 30-31 | .774-.711 | 540- 393 | 2362-1986 |
| 5 | 32-33 | .711-.648 | 393- 290 | 1986-1708 |
| 6 | 34-35 | .648-.598 | 290- 229 | 1708-1538 |
| 7 | 36-37 | .598-.549 | 229- 182 | 1538-1412 |
| 8 | 38-40 | .549-.480 | 182- 127 | 1412-1254 |
| 9 | 41-43 | .480-.410 | 127- 90 | 1254-1156 |
| 10 | 44-46 | .410-.356 | 90- 66 | 1156-1100 |
| (14.1 g/cm ² of atmosphere) | | | | |
| | | | MeV/nucleon | MV |

Table 2 (cont)

| <u>Interval No.</u> | <u>Channels</u> | <u>Velocity (β)</u> | <u>Energy at detector</u> | <u>Rigidity, corrected to top of atmosphere</u> |
|-------------------------|-----------------|--------------------------------------|-------------------------------|---|
|-------------------------|-----------------|--------------------------------------|-------------------------------|---|

Flight 3 Alphas:

| | | | | |
|----|-------|-----------|----------------|----------------|
| 1 | 48-56 | 1.00-.949 | ∞ -2170 | ∞ -6040 |
| 2 | 57-58 | .949-.892 | 2170-1122 | 6040-3736 |
| 3 | 59-60 | .892-.838 | 1122- 774 | 3736-2998 |
| 4 | 61-62 | .838-.780 | 774-556 | 2998-2366 |
| 5 | 63-65 | .780-.699 | 556- 369 | 2366-1882 |
| 6 | 66-68 | .699-.622 | 369- 258 | 1882-1568 |
| 7 | 69-71 | .622-.552 | 258- 186 | 1568-1366 |
| 8 | 72-74 | .552-.489 | 186- 136 | 1366-1196 |
| 9 | 75-77 | .489-.431 | 136- 101 | 1196-1090 |
| 10 | 78-80 | .431-.377 | 101- 74 | 1090- 990 |

(8.8 g/cm² of atmosphere)Flight 4 Alphas:

| | | | | |
|---|-------|-----------|----------------|----------------|
| 1 | 50-58 | 1.00-.952 | ∞ -2100 | ∞ -5810 |
| 2 | 59-60 | .952-.900 | 2100-1204 | 5810-3886 |
| 3 | 61-62 | .900-.850 | 1204- 838 | 3886-3070 |
| 4 | 63-65 | .850-.781 | 838- 559 | 3070-2398 |
| 5 | 66-68 | .781-.717 | 559- 403 | 2398-2000 |
| 6 | 69-74 | .717-.596 | 403- 228 | 2000-1520 |
| 7 | 75-83 | .596-.447 | 228- 110 | 1520-1186 |

(12.8 g/cm² of atmosphere)

c

MeV/nucleon

MV

8.2 Background and Detector Correction; Particle Counts at the Detector

Table 3 gives the total counts, background counts, particle counts, and redistributed particle counts after correction for the detector and recording statistical distributions, for each of the intervals defined in Table 2. The errors included are the resultant of statistical error and uncertainty of the background correction, amplified by the convolution procedure necessary to correct for detector-recording distributions. The number of 'zero' Cerenkov output counts used in determination of the background distribution magnitude is indicated for the pertinent proton regions. As well, the background magnitude-determining counts are shown for all alpha particle regions.

Table 3: Counts per Interval: Total, Background, Particle, and Particle after Correction for Statistical Spreads in Output

| <u>Interval No.</u> | <u>Total</u> | <u>Background in particle zone</u> | <u>Particles</u> | <u>Particles after statistics correct.</u> |
|---------------------|--------------|------------------------------------|------------------|--|
|---------------------|--------------|------------------------------------|------------------|--|

Flight 1 Protons:

| | | | | |
|----|-------|------|------|-----------------|
| 1 | 19991 | 6426 | 8738 | 11331 \pm 570 |
| 2 | 6038 | 1968 | 2898 | 3114 280 |
| 3 | 4835 | 1766 | 2240 | 2032 230 |
| 4 | 5351 | 3075 | 2276 | 1644 390 |
| 5 | 3524 | 2320 | 1204 | 355 150 |
| 6 | 2385 | 1737 | 648 | 20 100 |
| 7 | 1590 | 1295 | 295 | -55 100 |
| 8 | 1114 | 990 | 124 | -10 90 |
| 9 | 988 | 864 | 124 | 123 80 |
| 10 | 1253 | 1142 | 111 | 101 70 |

Flight 2 Protons:

| | | | | |
|----|-------|------|------|----------------|
| 1 | 25017 | 4915 | 7012 | 8830 \pm 710 |
| 2 | 5769 | 825 | 2519 | 2773 290 |
| 3 | 4358 | 665 | 1808 | 1619 210 |
| 4 | 3285 | 2050 | 1235 | 934 180 |
| 5 | 4306 | 2950 | 1356 | 705 140 |
| 6 | 2602 | 2000 | 602 | 97 80 |
| 7 | 1608 | 1370 | 238 | 92 80 |
| 8 | 1187 | 1112 | 75 | -6 70 |
| 9 | 1073 | 1030 | 43 | 29 60 |
| 10 | 1070 | 966 | 104 | 103 60 |

Table 3 (cont.)

| <u>Interval</u> <u>No.</u> | <u>Total</u> | <u>Background in</u> <u>particle zone</u> | <u>Particles</u> | <u>Particles after</u> <u>statistics correct.</u> |
|-------------------------------|--------------|--|------------------|--|
|-------------------------------|--------------|--|------------------|--|

Flight 3 Protons:

| | | | | |
|----|-------|------|-------|-------------|
| 1 | 24904 | 7821 | 12753 | 17181 ± 850 |
| 2 | 12391 | 3915 | 6881 | 7805 720 |
| 3 | 9993 | 3909 | 5268 | 4944 550 |
| 4 | 7875 | 4075 | 3800 | 2781 400 |
| 5 | 6629 | 3510 | 3119 | 2030 350 |
| 6 | 6838 | 4332 | 2506 | 1423 260 |
| 7 | 5208 | 3195 | 2013 | 1237 230 |
| 8 | 3626 | 2286 | 1340 | 708 180 |
| 9 | 2850 | 2235 | 615 | 327 160 |
| 10 | 2801 | 2415 | 386 | 242 110 |

Flight 4 Protons:

| | | | | |
|----|-------|-------|-------|-------------|
| 1 | 49753 | 10397 | 19473 | 24502 ± 980 |
| 2 | 14350 | 1820 | 8916 | 9676 450 |
| 3 | 12534 | 1690 | 7636 | 7330 720 |
| 4 | 13664 | 5920 | 7744 | 6582 730 |
| 5 | 9998 | 4715 | 5283 | 3866 600 |
| 6 | 10430 | 5905 | 4525 | 3320 680 |
| 7 | 9088 | 6135 | 2953 | 1819 700 |
| 8 | 7194 | 6045 | 1149 | 611 450 |
| 9 | 5458 | 5333 | 125 | 99 200 |
| 10 | 5680 | 5680 | 0 | 0 150 |

Table 3 (cont.)

| <u>Interval</u> <u>No.</u> | <u>Total</u> | <u>Background in</u> <u>particle zone</u> | <u>Particles</u> | <u>Particles after</u> <u>statistics correct.</u> |
|-------------------------------|--------------|--|------------------|--|
|-------------------------------|--------------|--|------------------|--|

Flight 1 Alphas:

| | | | | |
|----|------|-----|-----|--------------|
| 1 | 2733 | 208 | 725 | 948 \pm 72 |
| 2 | 873 | 100 | 366 | 418 48 |
| 3 | 770 | 97 | 282 | 260 45 |
| 4 | 599 | 141 | 206 | 155 39 |
| 5 | 509 | 137 | 122 | 45 35 |
| 6 | 568 | 166 | 99 | 13 33 |
| 7 | 402 | 112 | 86 | 60 26 |
| 8 | 393 | 120 | 53 | 36 25 |
| 9 | 275 | 80 | 48 | 47 25 |
| 10 | 246 | 72 | 43 | 42 20 |

Flight 2 Alphas:

| | | | | |
|----|------|-----|-----|--------------|
| 1 | 3330 | 56 | 641 | 793 \pm 76 |
| 2 | 965 | 19 | 397 | 463 48 |
| 3 | 725 | 15 | 290 | 274 50 |
| 4 | 509 | 146 | 167 | 90 40 |
| 5 | 442 | 142 | 107 | 45 36 |
| 6 | 309 | 102 | 73 | 33 30 |
| 7 | 256 | 76 | 79 | 71 27 |
| 8 | 301 | 91 | 89 | 72 30 |
| 9 | 250 | 76 | 71 | 69 25 |
| 10 | 270 | 75 | 85 | 85 24 |

Table 3 (cont.)

| <u>Interval</u> <u>No.</u> | <u>Total</u> | <u>Background</u> <u>particle zone</u> | <u>Particles</u> | <u>Particles after</u> <u>statistics correct.</u> |
|-------------------------------|--------------|---|------------------|--|
|-------------------------------|--------------|---|------------------|--|

Flight 3 Alphas:

| | | | | |
|----|------|-----|-----|----------------------|
| 1 | 5056 | 362 | 805 | 1025 ⁺ 97 |
| 2 | 1144 | 455 | 477 | 601 60 |
| 3 | 1007 | 79 | 402 | 408 58 |
| 4 | 1059 | 117 | 455 | 475 60 |
| 5 | 1225 | 362 | 471 | 342 55 |
| 6 | 999 | 311 | 309 | 168 48 |
| 7 | 757 | 242 | 219 | 151 40 |
| 8 | 639 | 204 | 154 | 125 35 |
| 9 | 496 | 179 | 86 | 76 30 |
| 10 | 436 | 135 | 120 | 123 27 |

Flight 4 Alphas:

| | | | | |
|---|------|------|-----|-----------------------|
| 1 | 6976 | 641 | 937 | 1186 ⁺ 114 |
| 2 | 1676 | 185 | 555 | 704 71 |
| 3 | 1606 | 178 | 500 | 553 70 |
| 4 | 2089 | 345 | 675 | 678 75 |
| 5 | 1843 | 323 | 515 | 396 70 |
| 6 | 2901 | 1107 | 629 | 367 70 |
| 7 | 3924 | 677 | 358 | 281 75 |

8.3 Atmospheric Corrections

8.3.1 Proton Correction

Flights 1 and 3 were used for the proton correction of the data to the top of the atmosphere. An inspection of flight 2 ascent data revealed that a change in gain took place during the ascent, so that this data could not be sensibly used. The results are listed in Table 4a.

The proton change was found to be reasonably linear over the last 30 mb of air, so that extrapolation to the top of the atmosphere seemed reasonable. However, the errors in the Table 4a results for each flight were considered large enough to remove the significance of any difference between flights. For this reason, the mean values were used. Multiplying factors were deduced for each proton region for all four flights. These factors are listed in Table 4b.

8.3.2 Alpha Correction

The values for the alpha particle absorption length found during the ascents of flights 1, 2, and 3 are listed in Table 5a, along with the output region of the Cerenkov-scintillation representation used for this investigation. The mean value is also listed, along with values obtained by Webber and McDonald (1955), and McDonald (1956). These values are in agreement within the given errors, although the mean value is consistently higher.

The mean value was used, along with the fragmentation parameters and mean free paths given by Noon and Kaplon (1955) and charge ratios by Waddington (1963), to deduce correction

factors for the alpha data, as described in Section 7.5.3. A check showed that the difference in experimental absorption lengths quoted in Table 5a produced little change in any of these correction factors (.025 at most). The correction factors are given in Table 5b.

Table 4a: Change in Proton Rate from 20 to 10 mb Pressure

| | Velocity (β) | | |
|-------------|----------------------|------------------|------------------|
| | <u>1.0 - .90</u> | <u>.90 - .72</u> | <u>.72 - .45</u> |
| Flight 1 | -6.7 | -6.7 | -21.1 |
| Flight 3 | -9.3 | -13.7 | -20.3 |
| Mean values | -8.0 | -10.2 | -20.7 |
| | % | % | % |

Table 4b: Proton Atmospheric Correction Factors

| | Velocity (β) | | |
|--------------------|----------------------|------------------|------------------|
| | <u>1.0 - .90</u> | <u>.90 - .72</u> | <u>.72 - .45</u> |
| Flight 1 (10.5 mb) | .92 | .89 | .79 |
| Flight 2 (13.8 mb) | .89 | .86 | .72 |
| Flight 3 (8.6 mb) | .93 | .91 | .83 |
| Flight 4 (12.5 mb) | .90 | .87 | .75 |
| (mean pressure) | | | |

Table 5a: Observed Alpha Particle Absorption Lengths

| | Output Region Boundary | | Absorption Length Observed in Output Region |
|-----------------------------|---------------------------|----------------------|---|
| | <u>Scint. Channels</u> | <u>Cer. Channels</u> | |
| Flight 1 | 37-45 | 26-70 | $53 \pm 5 \text{ g/cm}^2$ |
| Flight 2 | 20-27 | 44-70 | $45 \pm 3 \text{ g/cm}^2$ |
| Flight 3 | 48-60 | 30-70 | $55 \pm 3 \text{ g/cm}^2$ |
| Mean value: | $51 \pm 3 \text{ g/cm}^2$ | | |
| Webber and McDonald (1955): | $43 \pm 8 \text{ g/cm}^2$ | | |
| McDonald (1956): | $45 \pm 7 \text{ g/cm}^2$ | | |

Table 5b: Alpha Atmospheric Correction Factors

| | <u>Absorption</u> | <u>Fragmentation Production</u> | <u>Total</u> |
|--------------------|-------------------|-------------------------------------|--------------|
| Flight 1 (10.5 mb) | 1.233 | -.073 | 1.160 |
| Flight 2 (13.8 mb) | 1.300 | -.100 | 1.200 |
| Flight 3 (8.6 mb) | 1.190 | -.060 | 1.130 |
| Flight 4 (12.5 mb) | 1.283 | -.089 | 1.194 |

Table 6: Balloon Flight Parameters

| | <u>Flight 1</u> | <u>Flight 2</u> | <u>Flight 3</u> | <u>Flight 4</u> |
|------------------------------------|------------------|------------------|-----------------|------------------|
| Location | Calgary | Churchill | Churchill | Calgary |
| Date (U.T.) | Dec. 10, 1964 | Mar. 30, 1965 | Apr. 6, 1965 | July 28, 1965 |
| Geomagnetic cut-off* | 1.2-1.3 | 0.19 | 0.19 | 1.2-1.3 GV |
| Mean pressure at altitude | 10.5 | 13.8 | 8.6 | 12.5 mb |
| Total counting time at altitude | 7822 | 5051 | 12111 | 20480 sec. |
| Duration at altitude | 3 | 2-3/4 | 5 | 11-1/4 hr |

Geometric factor: $1.43 \times 10^{-3} \text{ m}^2$ sr for all flights.

* Given by Quenby and Webber (1962)

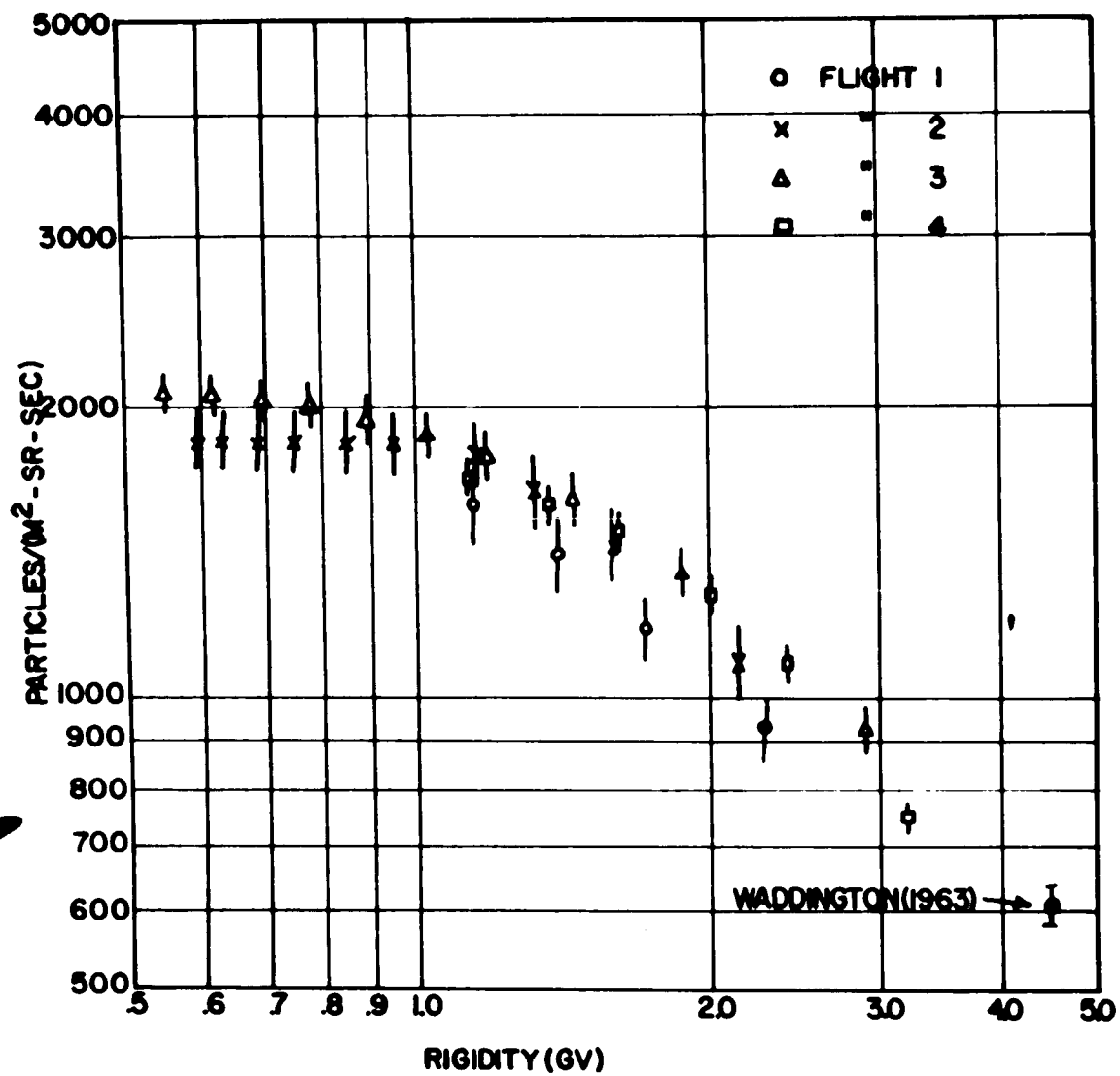


Figure 22 Proton Integral Rigidity Spectra for All Balloon Flights

8.4 Proton and Alpha Particle Integral Rigidity Spectra

8.4.1 Proton Integral Rigidity Spectra

The proton integral rigidity spectra for all four flights, corrected to the top of the atmosphere, are shown in Figure 22. Table 6 gives the counting times and geometric factors which were essential to the calculation of these spectra, along with other parameters of the flights. In the figure, the data below the geomagnetic cut-off for the Calgary flights, 1 and 4, have been omitted.

Towards the high rigidity end, flights 2, 3, and 4 were in agreement within their limits of error. Flight 1 was consistently lower. An examination of the Sulphur Mountain neutron monitor rate, which is reasonably sensitive to primary particles in the pertinent rigidity range, showed that the ground level nucleon intensity at the time of flight 1 was 0.5 per cent less than that of flight 2, 1.2 per cent less than that of flight 3, and 1.8 per cent greater than that of flight 4. It therefore seems that this difference between flight 1 and the other flights was instrumental, rather than real. As well, the Cerenkov detector for flight 1 was directional, and had poorer resolution than for the other three flights. Both these things would contribute to an overly large background correction for the relativistic protons, as the background distribution was normalized to the particular relativistic proton scintillation output interval at the low Cerenkov output end, and for flight 1, albedo particles and poorly resolved fast protons could be expected

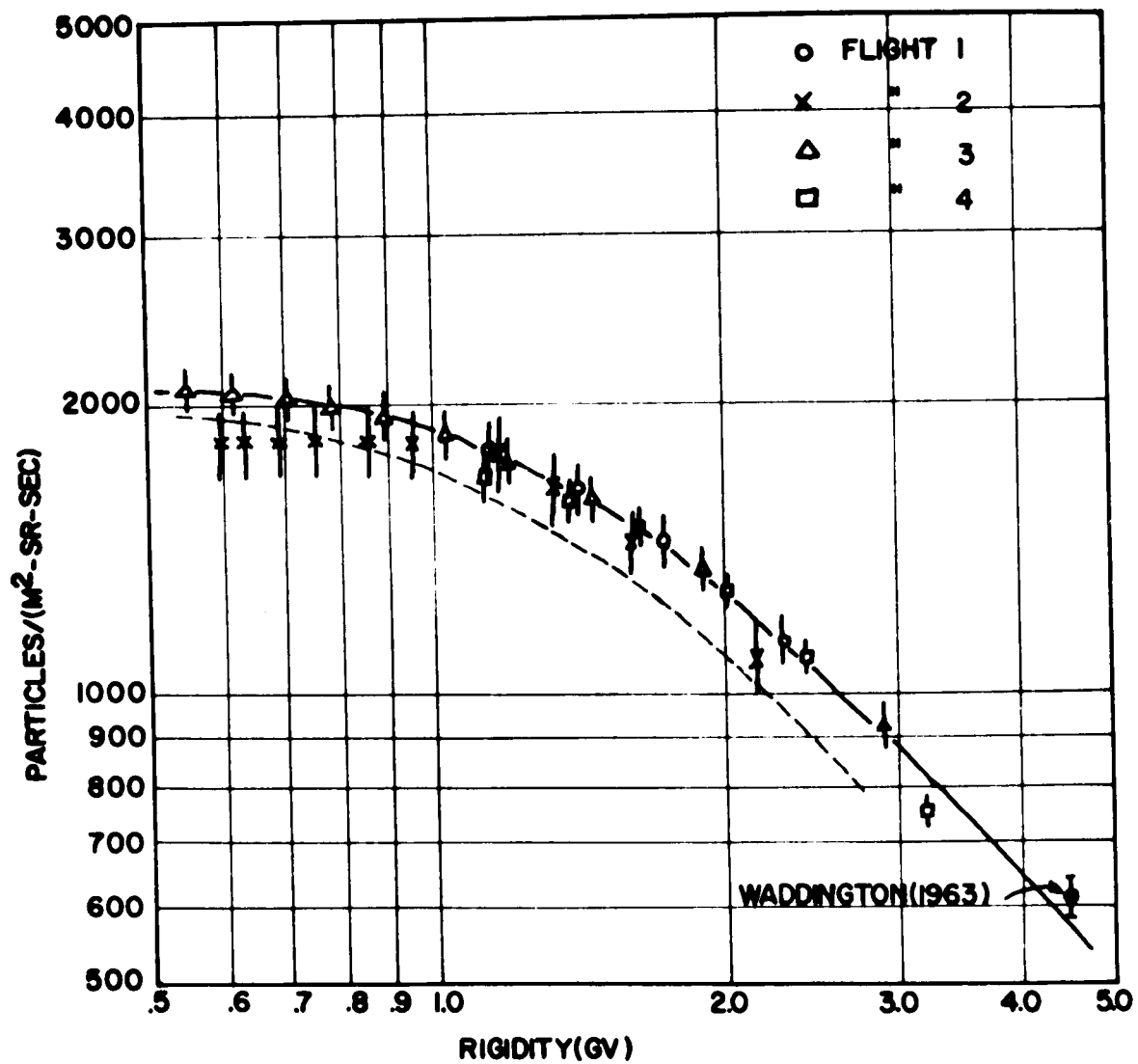


Figure 23 Preton Integral Rigidity Spectra for All Flights, with Flight 1
Normalized to Other Flights at High Rigidity End

here as well as background counts. The effects of poor Cerenkov resolution on the backgrounds of the other three flights was not thought to be too great, as differences in the resolutions of these non-directional detectors produced little change in the relativistic proton intensities measured.

Flight 1 was normalized to the other flights at the high rigidity end, and a new background in its relativistic proton region inferred from this. This new background correction was then used in a reinterpolation of the background counts over the lower energy proton region, to obtain a more reasonable correction for this region. Figure 23 shows the corrected integral data for flight 1, along with that of the other three flights.

The data in Figure 23 contains both primary cosmic ray protons and cosmic ray albedo. This albedo is expected to consist mainly of fast electrons and therefore yield a contribution to the apparent high rigidity proton flux.

Determinations of the intensity of the fast upwards albedo by McDonald and Webber (1959), yielded a value of 89 ± 8 particles/m²sr.sec. at 55°N. magnetic. An increase of upwards albedo with latitude from near the equator to this value was also indicated, although the magnitude of such an increase was uncertain (McDonald and Webber, 1959; Anderson, 1957). Above this latitude, however, there should be little, if any increase in fast electron production, because all the primaries sufficiently fast to produce such particles would be already allowed to enter the earth's atmosphere at 55°N. The steeper inclination of the

magnetic field lines at high latitudes, on the other hand, should constrain the production of upwards moving albedo to the cosmic rays coming in at large zenith angles, as is indicated in a study made by Anderson (1957). It is unlikely that upwards fast albedo will increase much above 55°N., and, in fact, at very high latitudes, it should decrease considerably.

The re-entrant albedo at the top of the atmosphere, as it was originally upwards albedo at the conjugate geomagnetic position, must be less than or equal to the upwards flux. Therefore twice the upwards albedo is an upper limit to the total albedo. The argument in the last paragraph also suggests that the upper limit of 178 particles/m²sr.sec. determined for 55°N. magnetic is also a good upper limit for all latitudes further north.

Application of any fast albedo correction to the data in Figure 23 would lower the whole curve by a fixed amount, as this correction applies to the high rigidity end of the spectrum only. The lower limits to the proton curve, based on the solid line drawn through the measured data and the fast albedo upper limit, is shown by the dotted curve in Figure 23. The real curve should lie somewhere in between these two curves.

An examination of the Calgary flights for particles below the geomagnetic cut-off, which should reflect in part the low energy proton albedo, was indefinite. An indication of protons in the 100 to 200 MeV range was suggested for flight 1, but not

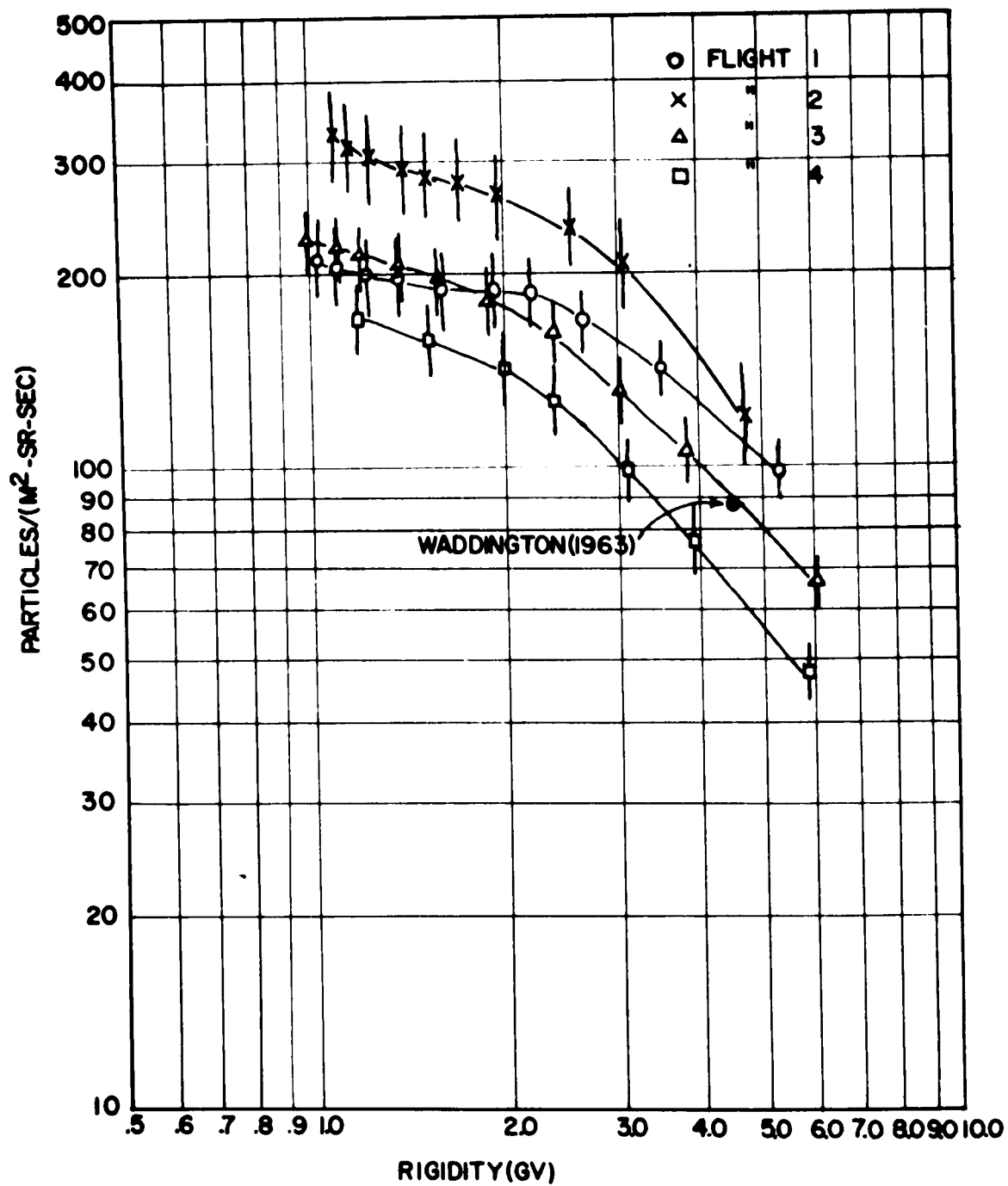


Figure 24 Alpha Particle Integral Rigidity Spectra, for All Flights

flight 4. The background correction was sufficiently inaccurate to mask any small contributions to this region, however. More is said about this in section 8.5.1.1.

The value for the primary proton intensity at rigidities greater than 4.5 GV has been inferred by Waddington (1963) from observations of several workers during the last solar minimum period, 1955 to 1956. This value is plotted in Figures 22 and 23. A rather uncertain extrapolation of the present data, in Figure 23, suggests a lower value for this cycle.

8.4.2 Alpha Integral Rigidity Spectra

Figure 24 shows the alpha particle integral rigidity spectra, corrected to the top of the atmosphere, for all four flights. A fair amount of difference between the flights occurs which does not correlate with the proton differences, or ground level neutron monitor differences. Also shown is the flux value, 88 ± 2 particles/m²sr.sec., found for alphas with rigidity greater than 4.5 GV during the previous solar minimum (Waddington, 1963). An average of the four flights yields the value 99 ± 26 particles/m²sr.sec., which is in agreement with Waddington's figure.

A change in slope is noted for all the four balloon flights, at a point well above the geomagnetic cut-offs of any of the flights as given in Table 6. The reality of this change in slope is doubtful, because of the possibility of poorly resolved alpha Cerenkov outputs causing an overcorrection of the very

large background. (The mode of correction is described in Section 7.4.1.) This would reduce the apparent number of low rigidity alpha particles, thus changing the slope. The point at which this effect is expected to become noticeable is that at which the Cerenkov-emitted light becomes zero and the only output from the Cerenkov detector is due to a small amount of scintillation, which is utilized in the same way as the Cerenkov light to discriminate against background. This point corresponds to a primary alpha rigidity of approximately 1.8 GV and agrees with the roll-over seen in Figure 24. Flight 1 seems to have the flattest slope at this point, which is expected on the basis of the poor resolution of the Cerenkov detector. A later increase in slope occurs, which is also expected, as the scintillation light emitted in the Cerenkov detector will increase, therefore causing a better separation between particles and background. For flights 3 and 4 these later increases do not occur, and the slopes at 1.8 GV rigidity are comparatively steep. This suggests that the particle removal via background is not as pronounced for these flights as the others.

8.4.3 Determination of $\Gamma_{p\alpha}(R)$

A rough estimate of the ratio of protons to alphas above a fixed rigidity, $\Gamma_{p\alpha}(R)$, can be made with this data. It is limited by the observed differences between alpha particles in the different flights. The value found is 5.9 ± 2.1 , for particles with rigidities greater than 2.5 GV. The proton value used in this calculation was one lying halfway between the solid curve

and the lower limit dotted curve, both of which are given in Figure 23. The ratio found is in agreement with the value given by Waddington (1963) of 6.2 ± 0.7 for such rigidities. For reasons which will be made clear in Section 8.5.2, ratios for lower rigidity ranges cannot be determined from the present data.

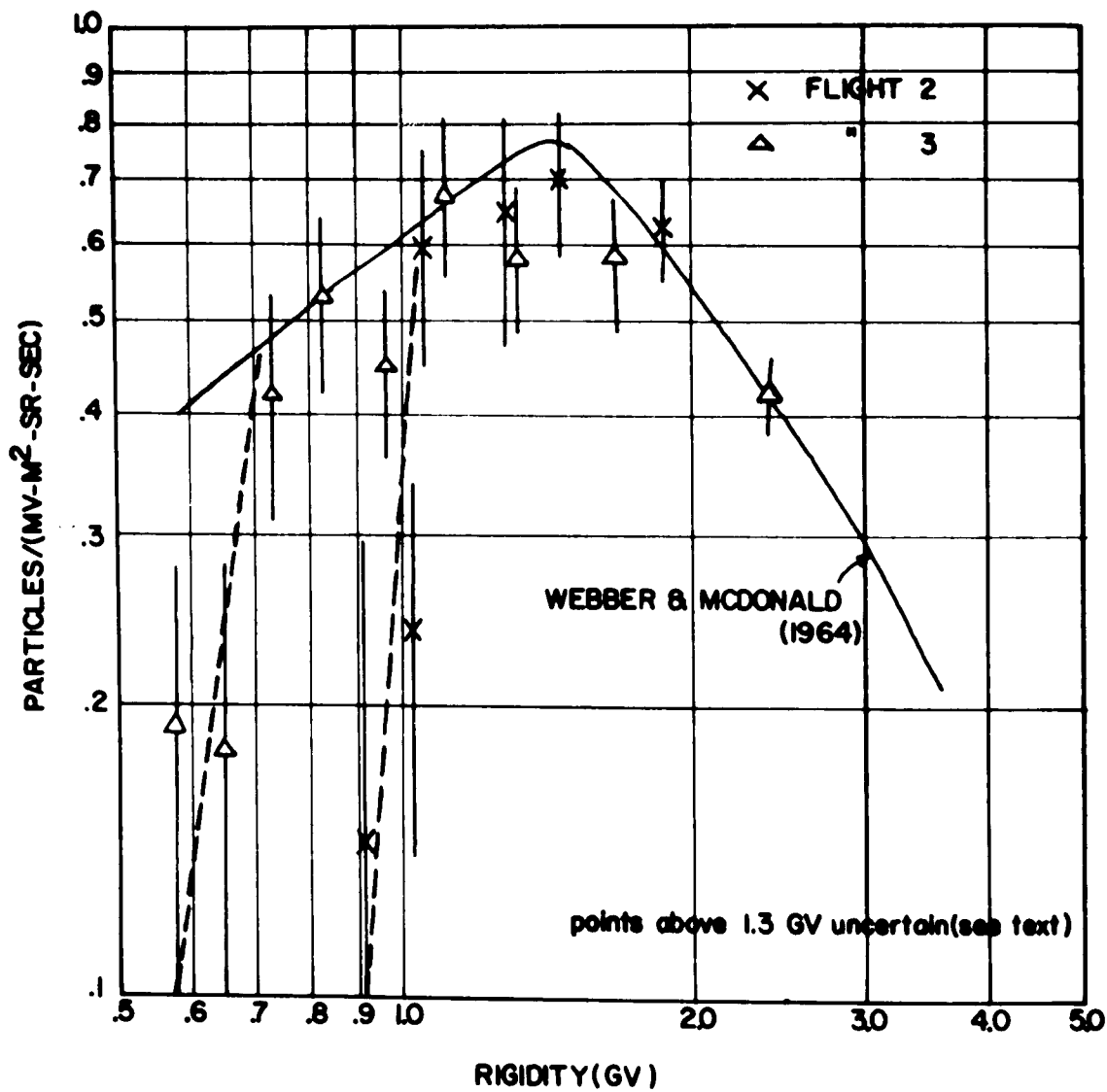


Figure 25 Proton Differential Rigidity Spectra, for Churchill Flights

8.5 Differential Rigidity Spectra

8.5.1 Protons

8.5.1.1 Churchill Flights

Figure 25 shows the proton differential rigidity spectra for Fort Churchill. Also shown is a curve obtained by Webber and McDonald (1964) from the combined proton and alpha particle spectra measured during a balloon flight on September 7, 1956 (See Figure 1, as well.). Both the present flights show approximate agreement with this curve at rigidities greater than 1.0 GV, although uncertainty on the points between 1.3 and 2.5 GV rigidity exists, owing to the inaccuracy of the first-order detector correction for statistical fluctuations in this region (See Section 7.4.3.). An examination of Figure 1 shows that this portion of the curve was originally obtained with alpha particle data, multiplied by a normalizing factor ($\Gamma_{p\alpha}(r)$) of 7.2.

Flight 3 shows agreement with the Webber and McDonald curve down to 0.7 GV rigidity, below which decrease occurs. Flight 2, on the other hand, shows a decrease immediately below 1.0 GV.

It is possible that these decreases could be due to an overly large background correction, particularly in the region below 1.0 GV. The present equipment cannot discriminate against low energy upwards moving albedo, which can yield scintillation outputs corresponding to rigidities below the downwards cut-off of the detector, approximately 0.4 GV. As this large

scintillation output region is the one at which the high output end of the proton background is determined, for a subsequent interpolation across the low energy proton region (see Figure 18), very low energy upwards moving particles may cause an overly large background correction, particularly for the low energy proton region. If this were the case, the low rigidity difference between flights 2 and 3 would suggest a difference in upwards moving albedo between the two flights, leading to a difference in the 'overcorrections' of their backgrounds. Examination of the background scintillation distribution for flight 2 shows however that this effect (the removal of a flux greater than $200 \text{ counts/m}^2 \text{sr.sec.}$) is far too large to be explained on the basis of a difference in upwards albedo. However, the upwards albedo could perhaps explain the removal of particles below 0.7 GV for flight 3.

It is possible that a linear interpolation of the background is not the correct procedure for all flights. The difference between flights 2 and 3 could then be explained by a decrease in the background level for flight 2 of 30 per cent from the interpolated background, over the pertinent scintillation output region. It is unlikely that such a difference between flights would occur, but the possibility cannot be overlooked. The high ratio of extrapolated background to proton counts in the low energy proton region severely limits the validity of the results for these particles.

The difference in low rigidity proton flux between flight 2 and 3 may be due to an actual removal of primary particles below 1 GV. A difference of 0.7 per cent in the Sulphur Mountain

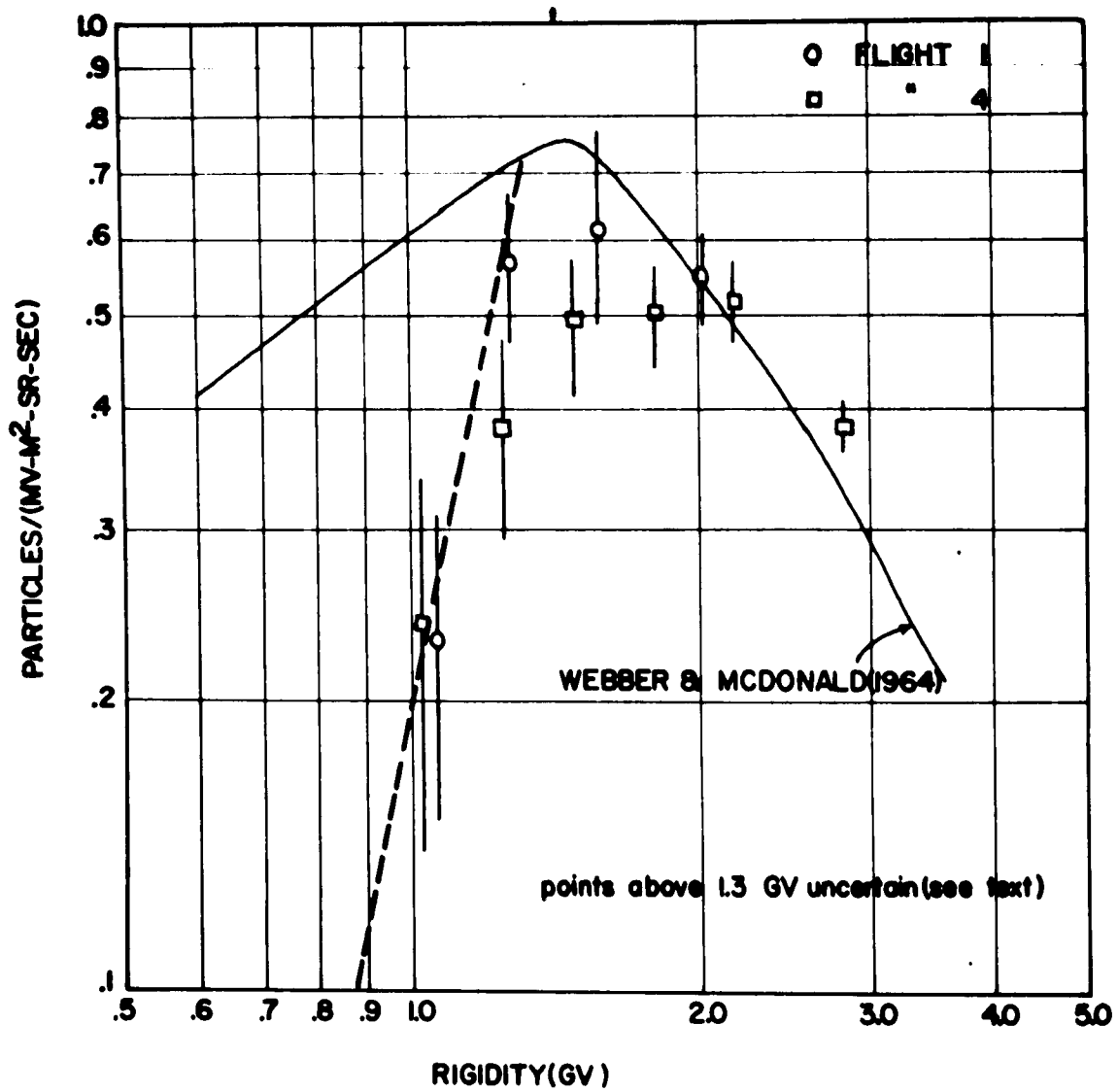


Figure 26 Proton Differential Rigidity Spectra, for Calgary Flights

neutron monitor rates between these two times was noted, but this effect was not evident for neutron monitors at Deep River, Churchill, Climax, or Dallas. However, no ground level monitor is expected to be very sensitive to primary protons of 1 GV rigidity, and the Sulphur Mountain monitor, because of its combined low geomagnetic cut-off (app. 1 GV) and high altitude (7500 feet above sea level) may have just seen the upper edge of this low rigidity variation. No outstanding geophysical phenomena which could be related to this flight 2 decrease was listed in the NBS-CRPL F-Series Bulletins (Part B), April and May, 1965.

8.5.1.2 Calgary Flights

Figure 26 shows the differential proton rigidity spectra for the two Calgary flights. The Webber and McDonald (1964) curve from data obtained near the previous solar minimum is also shown here. At higher rigidities, both show approximate agreement with this curve. Towards lower rigidities, there is a dropping of intensity, a sharp cut-off in the vicinity of 1.0 GV for both flights, as is indicated by the dotted line. This cut-off is assumed to be geomagnetic in origin.

The theoretical cut-off due to the geomagnetic field, from the calculations of Quenby and Webber (1962), ranges between 1.2 and 1.3 GV for the vicinities of these two flights. The proton data of both these flights indicate slightly lower values, between .99 and 1.15 GV for flight 1, and .94 to 1.13 GV for flight 4.

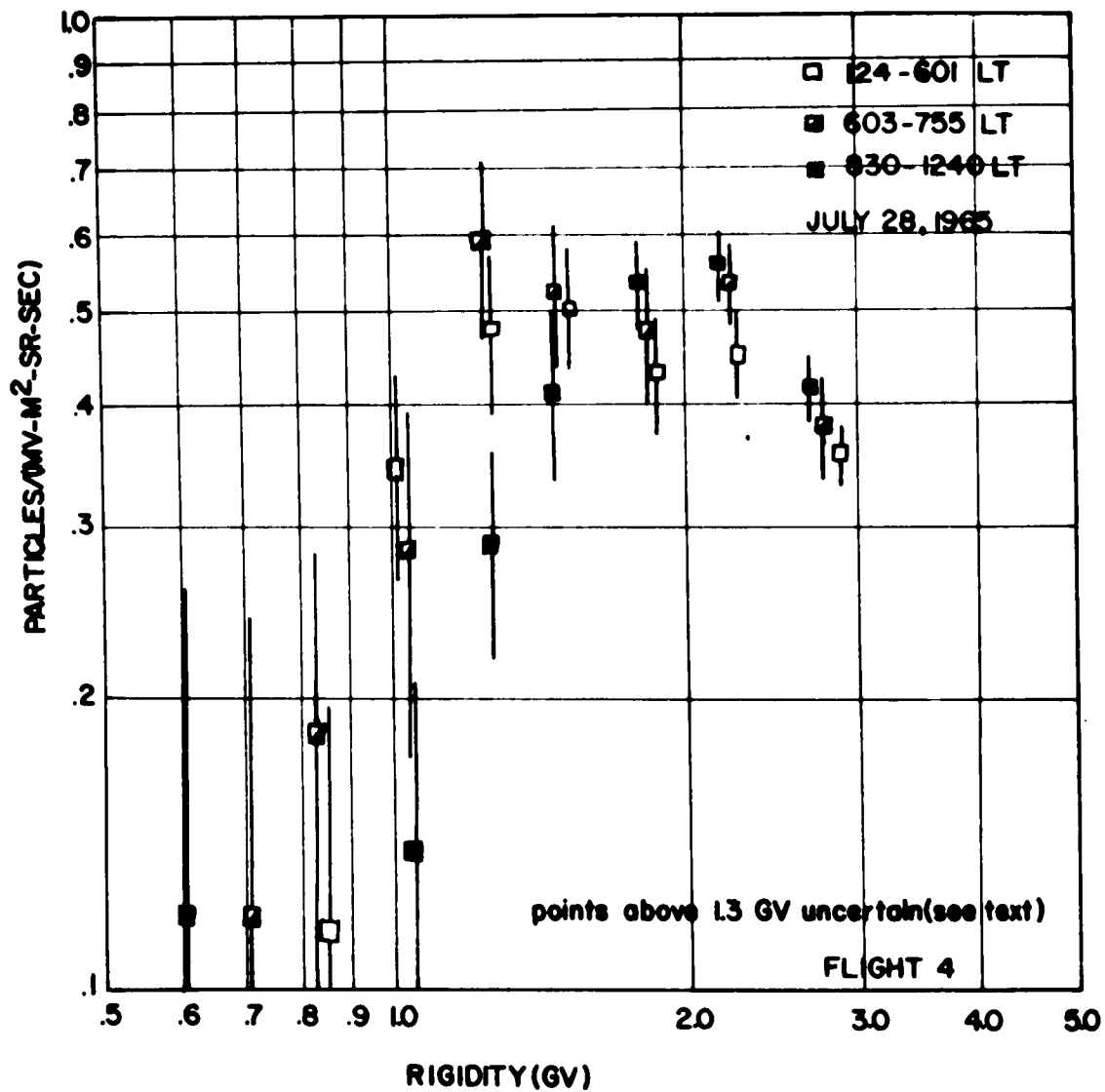


Figure 27 Proton Differential Rigidity Spectra, for Different Times during Flight 4

8.5.1.3 Variation over a Single Flight

The data of flight 4 at altitude was divided into three time intervals, and proton rigidity spectra found for each. The results are shown in Figure 27. The proton spectra for each of the three intervals appear similar, except for the points at 1.25 and 1.03 GV rigidity, where there is a decided decrease between the third time interval and the two previous time intervals. This change can be interpreted as an increase in cut-off rigidity. From Figure 11, it can be seen that the balloon drifted towards lower geomagnetic latitudes (and therefore higher cut-off rigidities) during the flight. The first two time intervals suggest a cut-off between .94 and 1.13 GV, and the third, between 1.13 and 1.38 GV.

8.5.2 Alpha Particles

The alpha particle differential rigidity spectra are shown in Figure 28, for all four flights. They show an increasing intensity with decreasing rigidity, down to a rigidity of 2.5 GV, then a decrease down to 1.8 GV, followed by an increase. The relative magnitude of the decrease and later increase varies from flight to flight.

As was mentioned in Section 8.4.2, it is thought that poorly resolved alpha Cerenkov detector outputs in the region where these particles cease to emit Cerenkov radiation and only a small amount of light from scintillation processes is emitted in the Cerenkov counter, could cause an overcorrection of the background in this region. For lower velocity particles, where

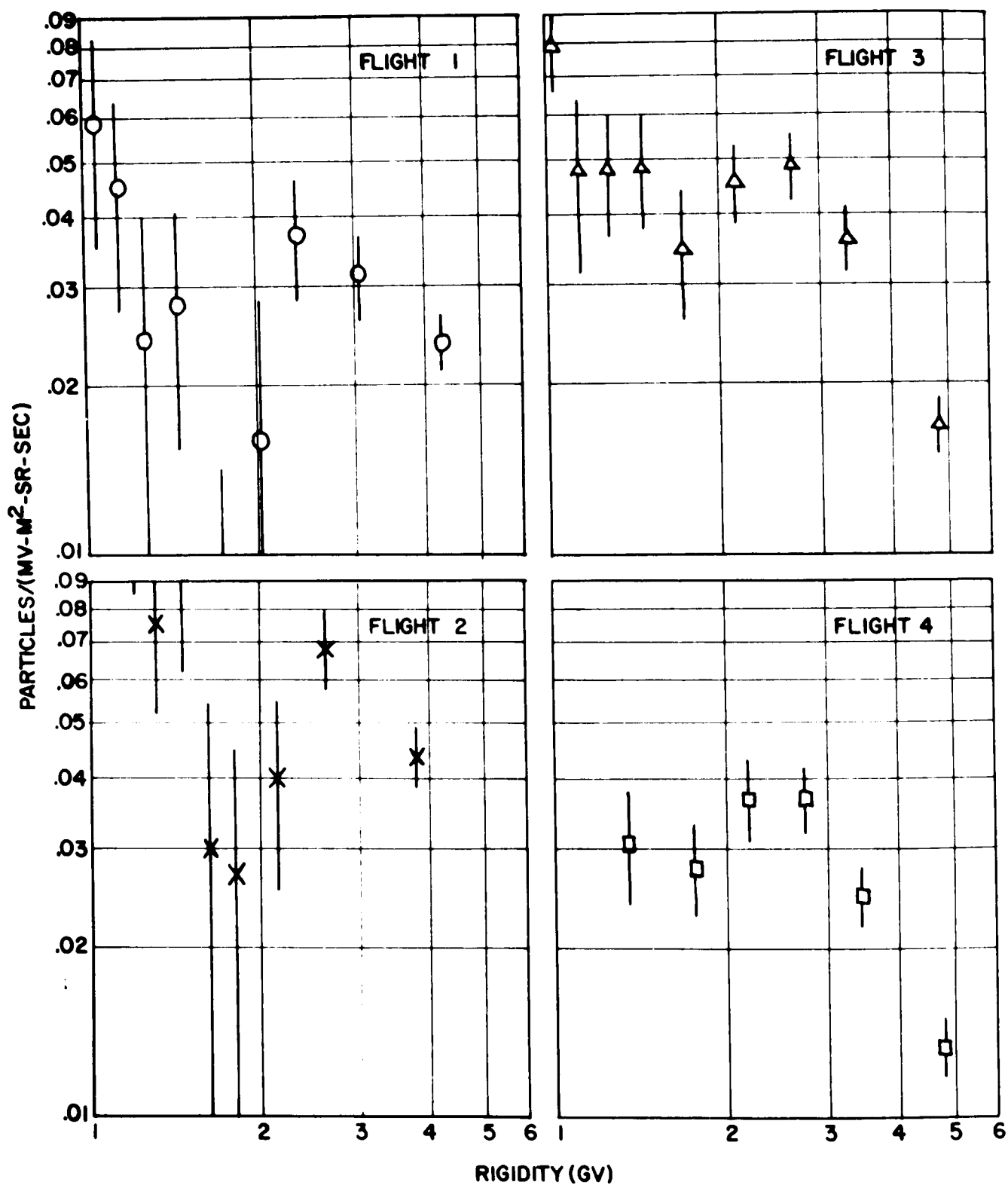


Figure 28 Alpha Particle Differential Rigidity Spectra, for All Flights

this residual scintillation increases, the resolution should improve, and an increase be noted towards lower rigidities. The method of accounting for scintillator output statistics by a convolution transformation (See Section 7.4.3) may make this later increase appear larger than it should be, particularly if there are a large number of particles removed from the higher velocity region where the Cerenkov emission first becomes zero. As the rigidity spread for each of the low rigidity intervals is comparatively small, only a few extra counts are needed for a substantial increase.

The location of the dip in Figure 28, at 1.8 GV, corresponds to the point at which Cerenkov emission becomes zero. Furthermore, the flight with the Cerenkov detector of worst resolution (flight 1) has the largest dip at this point. The Cerenkov detector with the best resolution (flight 4) appears to have the smallest dip. The subsequent increase for flights with small dips (flights 3 and 4) is less than that of flight 2, which has a sharp low rigidity increase and a large dip. Saturation in the scintillation output part of the system may have contributed to this increase, however. Flight 1's increase is less, perhaps suggesting that poor resolution removed particles even down to the lowest rigidities. An examination of Figure 17 agrees with this hypothesis. The smallest subsequent increase is that of flight 4, which had the best Cerenkov detector resolution.

All the points in the last paragraph are consistent with the conclusion that the 1.8 GV dip and low rigidity increase are

caused by poor resolution. The presence of these instrumental effects limits the conclusions one can make about the primary alpha flux at the times of these flights. In June, 1963, a 'rollover point' at 1.9 GV in the differential alpha particle flux was noted by Balasubrahmanyam and McDonald (1964) (See Figure 2.). This point was observed to be at a higher rigidity than that inferred for protons, thus suggesting a difference in the relative rigidity dependences of these two particles, which had not been previously observed. The present flights are incapable of examining this difference, but can give an upper limit to the 'rollover point' for alpha particles, as being that observed in Figure 28, of 2.5 GV.

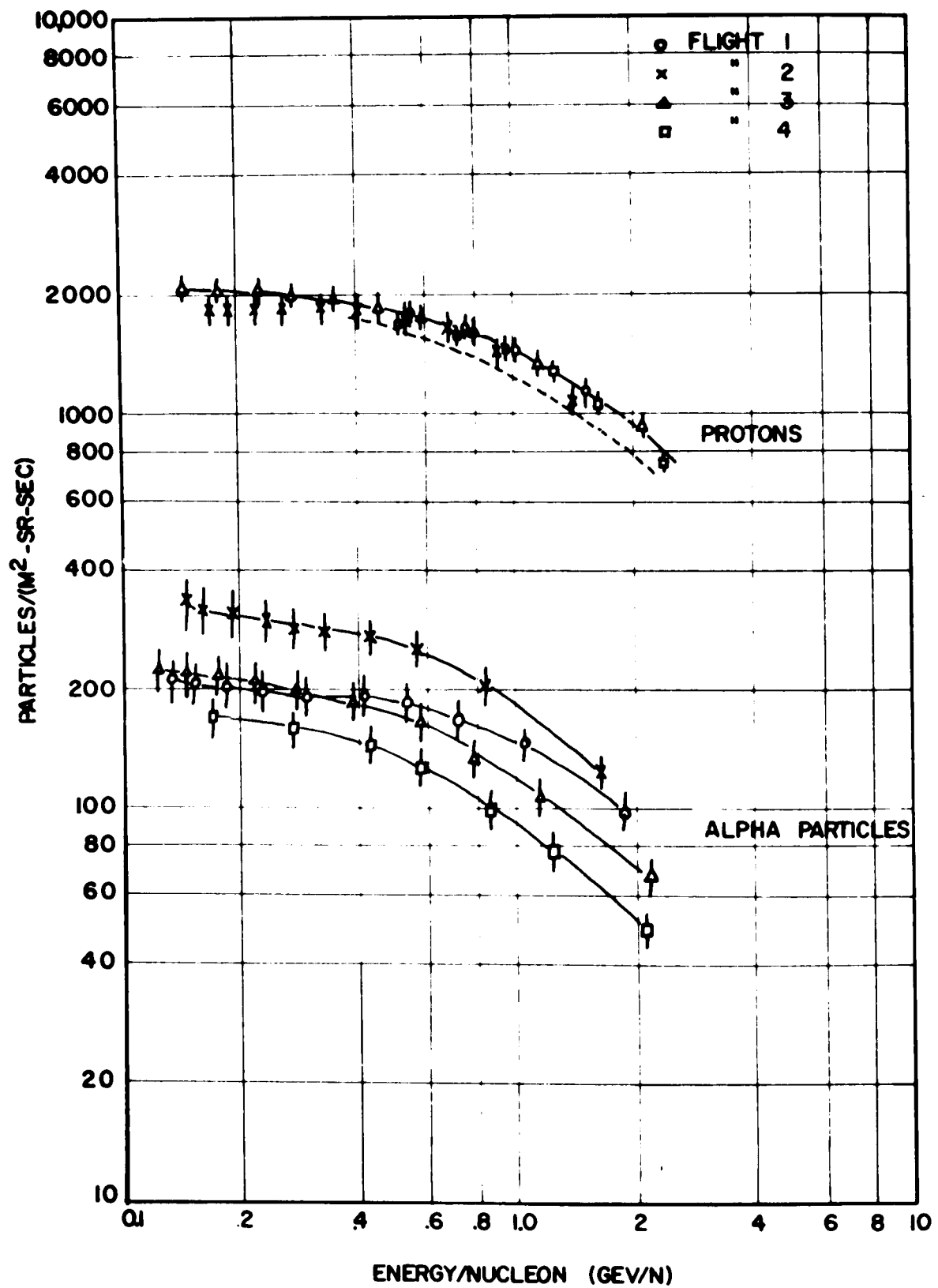


Figure 29 Proton and Alpha Particle Integral Energy Spectra, for All Flights

8.6 Proton and Alpha Fluxes as Functions of Energy per Nucleon

As the combined output of the Cerenkov-scintillation detector is a function of particle charge and velocity only, comparisons of the fluxes of differently charged particles can best be made in terms of some parameter dependent on velocity, but independent of charge. In this way, comparison is possible over the entire measured range of this parameter, as each group of particles will cover this range. Rigidity is not one such parameter, but energy per nucleon is. Also, certain hypothesized mechanisms for the eleven year variation, such as diffusion, depend on particle velocity rather than charge. Recent evidence (Balasubrahmanyam and McDonald, 1964) has suggested that the solar modulation is more than just rigidity dependent during certain phases of the eleven year cycle, thereby allowing the possibility of purely velocity dependent mechanisms being the origin of part, at least, of the eleven year solar modulation of cosmic radiation. For these reasons, energy per nucleon is a reasonable parameter with which to explore the data.

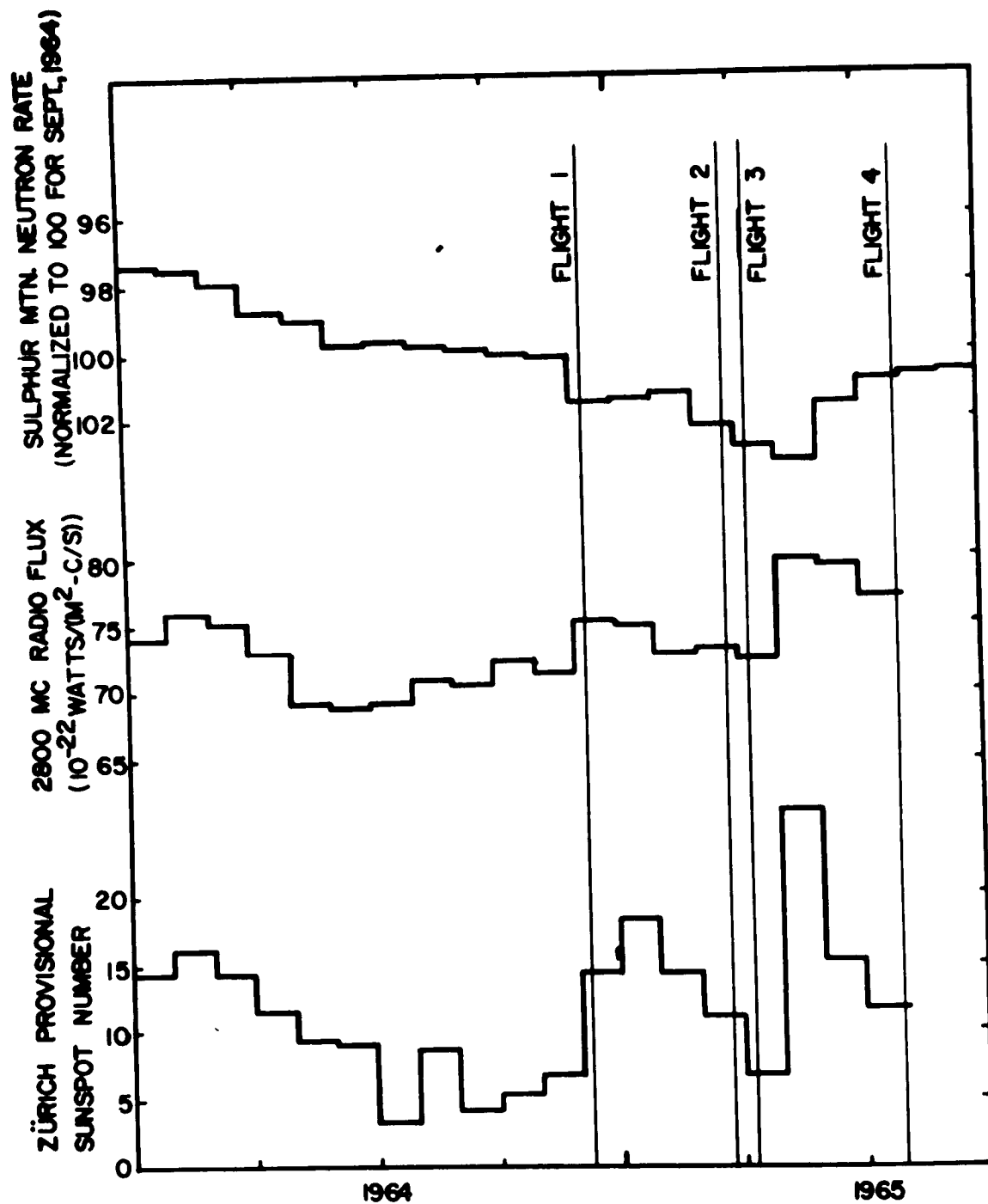
Figure 29 shows the integral proton and alpha particle spectra, as functions of energy per nucleon. A comparison with Figures 23 and 24 shows that the proton and alpha spectra are determined over the same range of the parameter energy per nucleon with a Cerenkov-scintillation detector, but not the same range of rigidity. As the alpha data has been demonstrated to be unreliable at rigidities less than 2.5 GV, and therefore energies less than 640 MeV per nucleon, comparisons between

these two particles cannot be made below this value.

The proton to alpha particle ratio has been determined for the parameter of energy per nucleon for three different ranges. The results are listed below.

| energy per nucleon (E/n) | 0.65-0.80 | 0.80-1.5 | >1.5 GeV/n |
|-----------------------------------|---------------|---------------|----------------|
| ratio ($\Gamma_{p\alpha}(E/n)$) | 7.7 ± 2.3 | 8.5 ± 2.6 | 10.3 ± 3.5 |

All four flights were used. The errors on the three ratios originate mainly in the observed scatter in alpha particle fluxes between flights, and for the highest range, uncertainties due to fast albedo as well. The three values are seen to be in agreement within the errors quoted, although a slight tendency for the ratio to decrease with decreasing energy per nucleon is noted. Thus, these results are not inconsistent with the hypothesis of a purely velocity dependent modulation of the cosmic radiation.



8.7 Associated Solar and Ground Level Cosmic Ray Detector Results

Figure 30 shows data pertinent to the solar activity and cosmic ray level for a period preceding and extending over the four balloon flights. The times of these flights are marked on this figure.

The solar data shown in Figure 30 are the monthly mean Zürich provisional sunspot numbers and monthly mean 2800 mc/s radio flux measured at Ottawa and corrected for the eccentric orbit of the earth. This information was obtained from the NBS-CRPL F-Series Bulletins (Part B), 1964 and 1965. Both these parameters are regarded as reliable indicators of solar activity. In terms of the sunspot number and 2800 mc/s radio noise, the eleven year minimum in activity occurred somewhere about July, 1964.

The mean Sulphur Mountain neutron monitor rates for each month are shown in Figure 30, as an indicator of the cosmic ray level during this period. A maximum occurs for this detector during the month of May, 1965. Comparison with the Dallas and Deep River monitors reveals a similar maximum at this time for these detectors. A delay between the recent eleven year solar minimum in activity and maximum in cosmic ray intensity as measured by ground level neutron monitors, of approximately 10 months, occurred therefore.

From Figure 30, the present balloon flights straddled the time of cosmic ray maximum inferred from the ground level detectors. The neutron monitor data for this period is shown in greater detail in Figure 31. The two Churchill flights, in

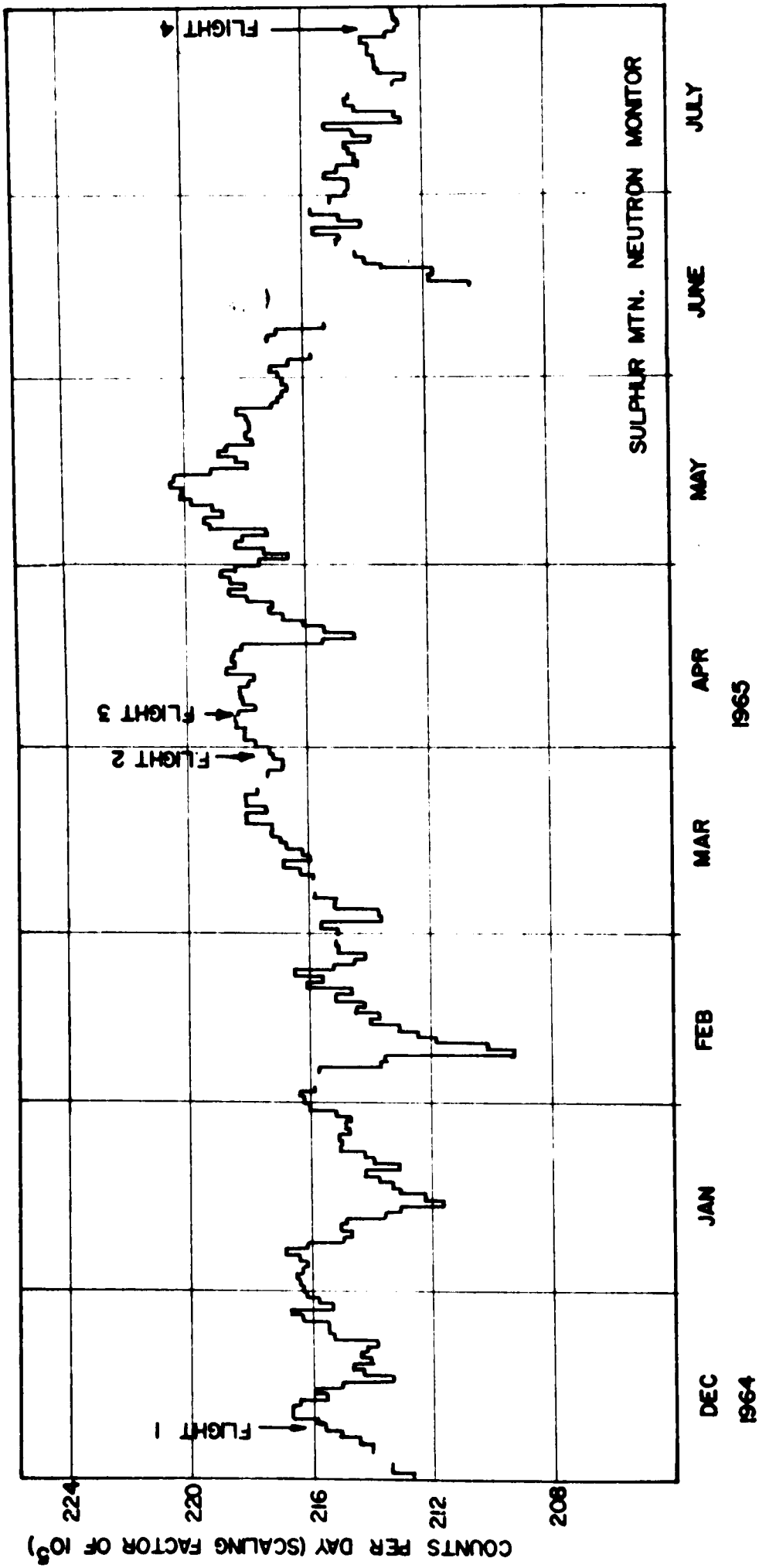


Figure 31 Sulphur Mountain Neutron Monitor Rates over Period of Balloon Flights

particular, were made at a time very close to the eleven year cosmic ray maximum. It should be mentioned that a cosmic ray energy dependence was noted for the delay time of the previous maximum from solar minimum (Forbush, 1958), and may perhaps also exist for the present minimum. It is possible that the Churchill flights may not correspond to a maximum for particles of rigidity lower than those detectable on the ground. The correspondence of balloon flight ionization measurements with ground level nucleon measurements (Forbush, 1958) for the 1954 minimum suggest that this is unlikely, however.

CHAPTER NINE

CONCLUSIONS

The four balloon flights made with the present Cerenkov-scintillation counter system span the recent eleven year maximum in ground level cosmic ray nucleon intensity. The presence of a large number of background events of uncertain origin in these flights severely limits the meaning of the results. Nevertheless, the following conclusions may be made.

1. The proton results of the present experiment are consistent with the hypothesis that the differential rigidity curve obtained by Webber and McDonald (1964) (See Figure 1.) near the previous solar minimum is representative of the spectrum for the present minimum as well, over the range 0.7 to 2.5 GV. The Webber and McDonald curve was originally obtained using proton data in the range 0.5 to 1.0 GV and normalized alpha particle data in the range 1.0 to 4.0 GV rigidity. The present experiment extends the proton measurements to a rigidity of 2.5 GV. Uncertainty in the higher rigidity measurements (1.3 to 2.5 GV) exists, owing to the large statistical fluctuations in the scintillation detector outputs for these particles. However, the results in this range appear consistent between flights and show agreement with the original curve.
2. The alpha particle data could be examined with some certainty in the range 2.5 to 4.5 GV rigidity. An upper limit to the 'rollover point' in the differential rigidity spectrum of these particles of 2.5 GV is obtained for the present flights. The absorption mean free path of fast alpha particles in the atmosphere,

found from the data recorded during ascent of the first three balloon flights, is $51 \pm 3 \text{ g/cm}^2$. A considerable variation between the primary integral alpha particle fluxes determined on different flights was noted. The mean value of the alpha particle flux above 4.5 GV, from all flights, was found to be $99 \pm 26 \text{ particles/(m}^2\text{-sr-sec)}$, which is in agreement with that given by Waddington (1963) for the last solar minimum, $88 \pm 2 \text{ particles/(m}^2\text{-sr-sec)}$, taken from flights made at the cut-off rigidity, of 4.5 GV.


3. The following ratios for protons and alpha particles were found from the combined data of all four flights.

| | | Ratio of protons to alphas |
|----------------------|-----------------|----------------------------|
| (a) (Rigidity) | >2.5 GV | 5.9 ± 2.1 |
| (b) (Energy/nucleon) | .65 - .80 GeV/n | 7.7 ± 2.3 |
| | .80 - 1.5 GeV/n | 8.5 ± 2.6 |
| | >1.5 GeV/n | 10.3 ± 3.5 |

Comparisons at lower rigidities or energies per nucleon were not possible because of uncertainties in the alpha particle intensities for such values. The present results alone are not capable therefore of distinguishing between a purely rigidity dependent or velocity dependent spectral shape for both types of particles.

4. A sharp geomagnetic cut-off for the Calgary vicinity in the range 0.94 to 1.15 GV was inferred from both flights made in this area. For the last flight, an increase in cut-off rigidity was noted as the balloon drifted towards lower geomagnetic latitudes.

5. A removal of protons of rigidity less than 1.0 GV from the primary cosmic radiation was inferred for flight 2, at Churchill. This removal is thought to be real rather than instrumental, although the likelihood of an instrumental origin cannot be ignored. The time of this flight does not correspond to any other outstanding geophysical phenomena, and is not strongly apparent in the ground level neutron monitor records.

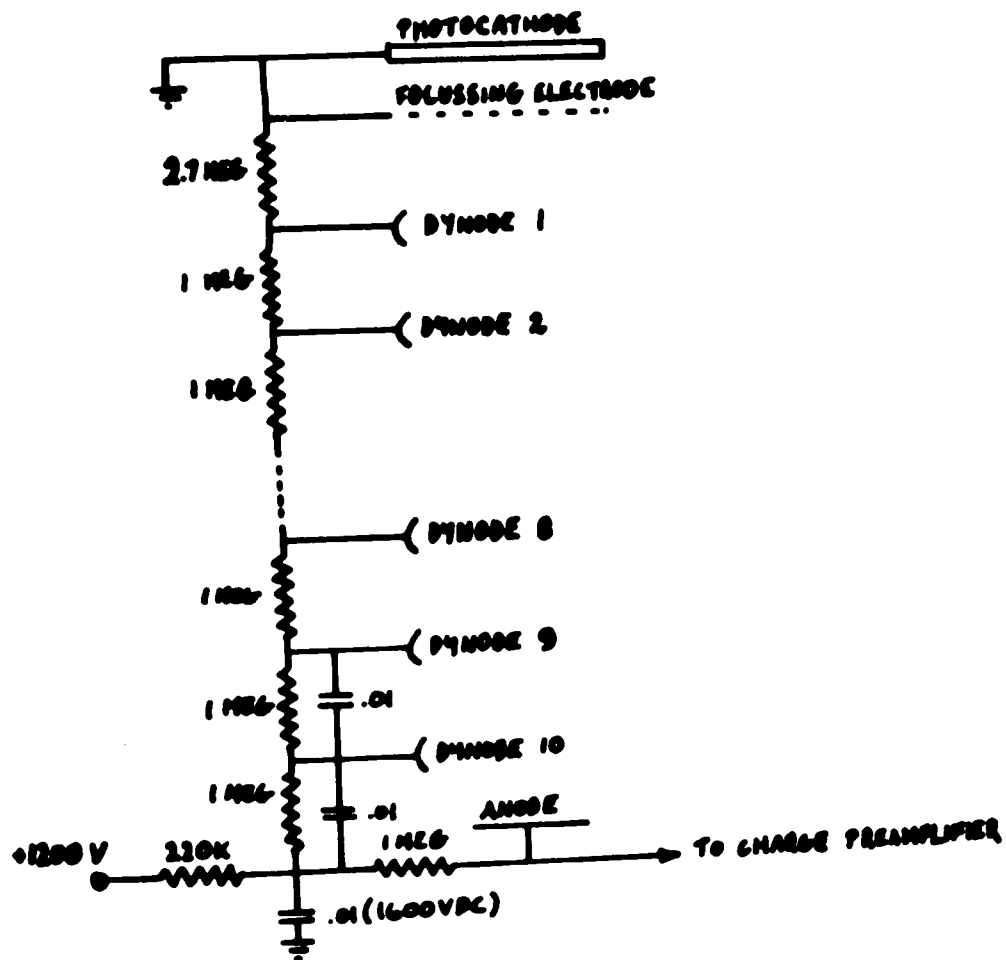


APPENDIX I

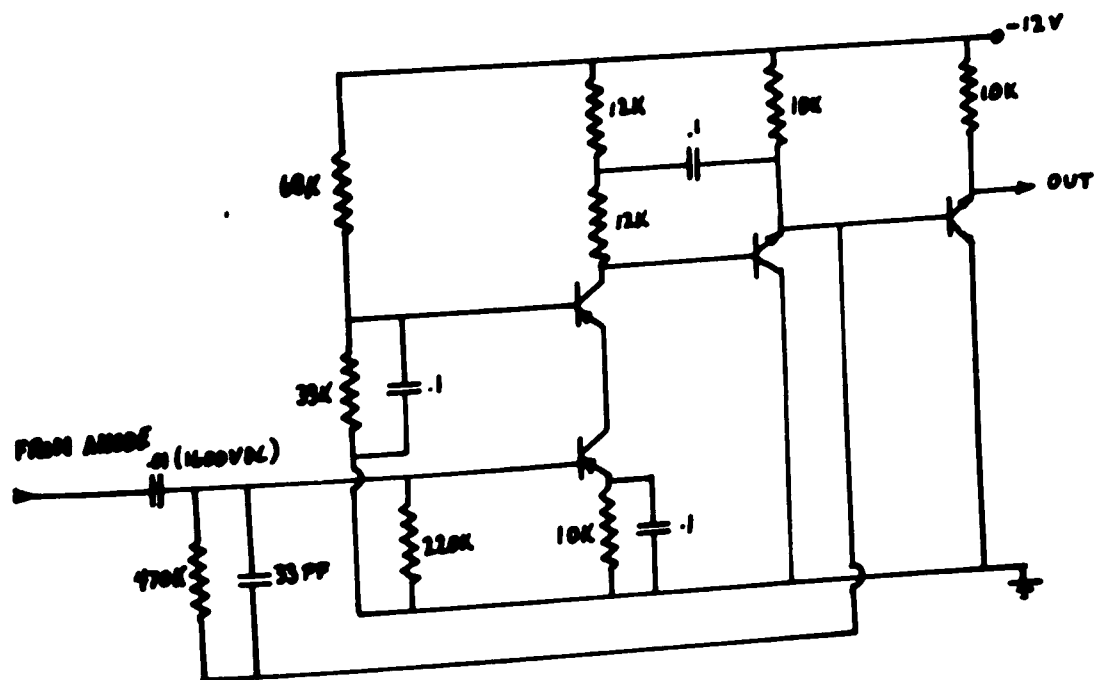
DETAILS OF BALLOON - FLOWN
ELECTRONICS

List of Circuits Appearing in Appendix I

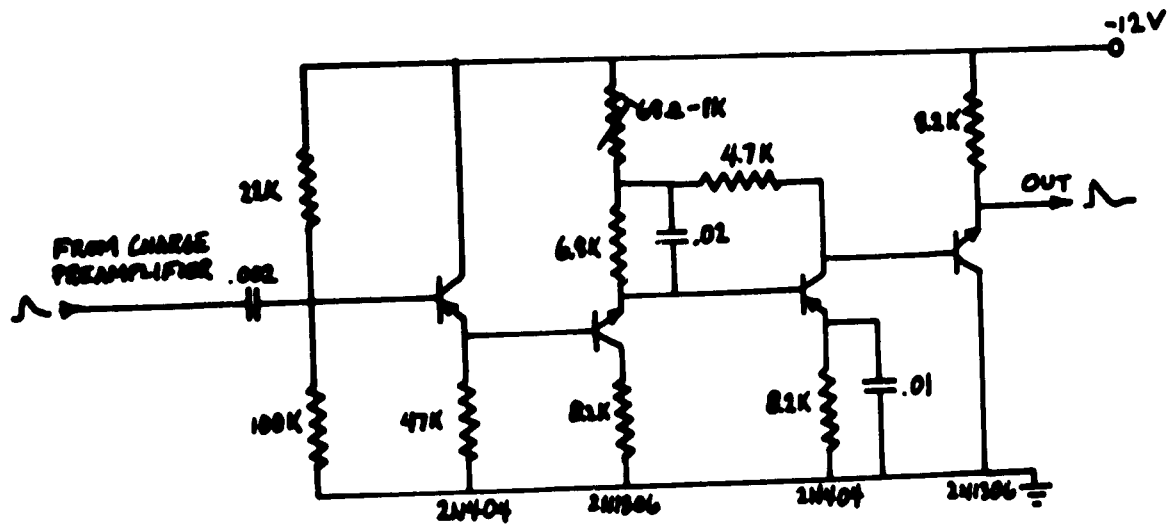
| | Page |
|---|------|
| 1. Photomultiplier tube wiring | 119 |
| 2. Charge preamplifier | 119 |
| 3. Amplifier (adjustable gain) | 120 |
| 4. 1.2 μ s delay and gate | 120 |
| 5. Coincidence circuit | 121 |
| 6. 4 μ s univibrator | 121 |
| 7. 10 ms univibrators and end of pulse selector | 122 |
| 8. Normally open gate | 122 |
| 9. Pulse-stretcher | 123 |
| 10. Amplifier following pulse-stretcher | 123 |
| 11. Schmidt trigger circuit with temperature compensation network | 124 |
| 12. Subcarrier oscillator and gate | 124 |
| 13. Mixer-amplifier | 124 |



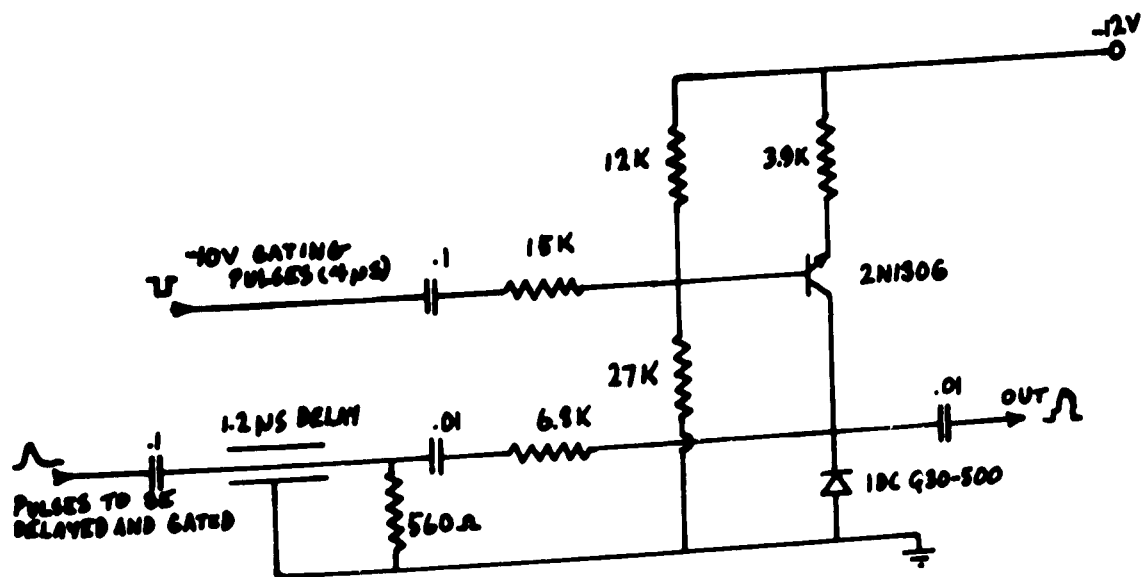
PHOTOMULTIPLIER TUBE WIRING



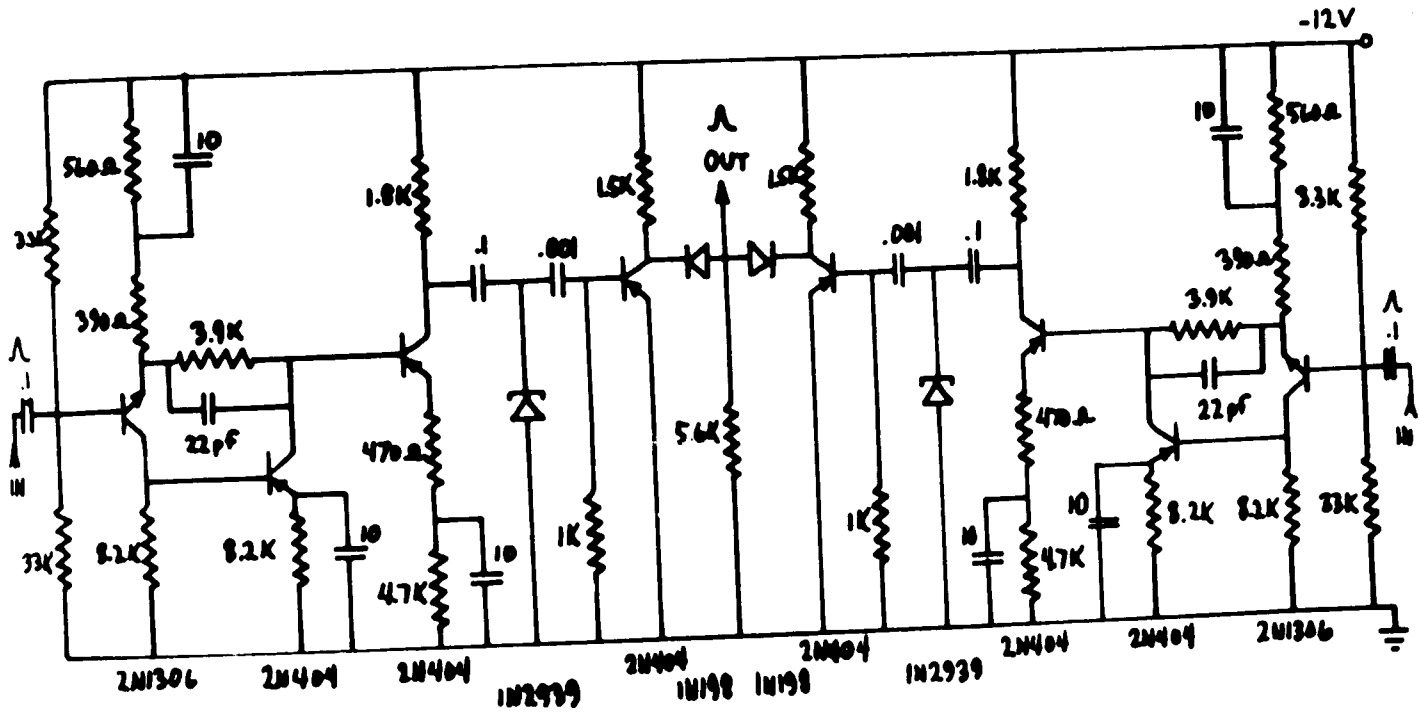
CHARGE PREAMPLIFIER



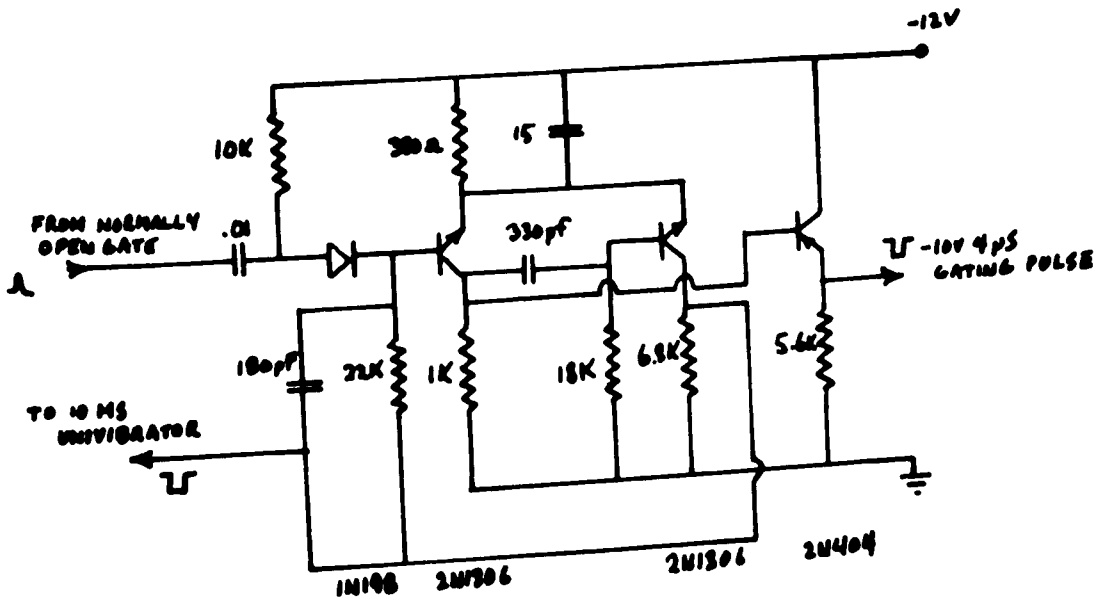
AMPLIFIER (ADJUSTABLE GAIN)



1.2 ns DELAY AND GATE



COINCIDENCE CIRCUIT



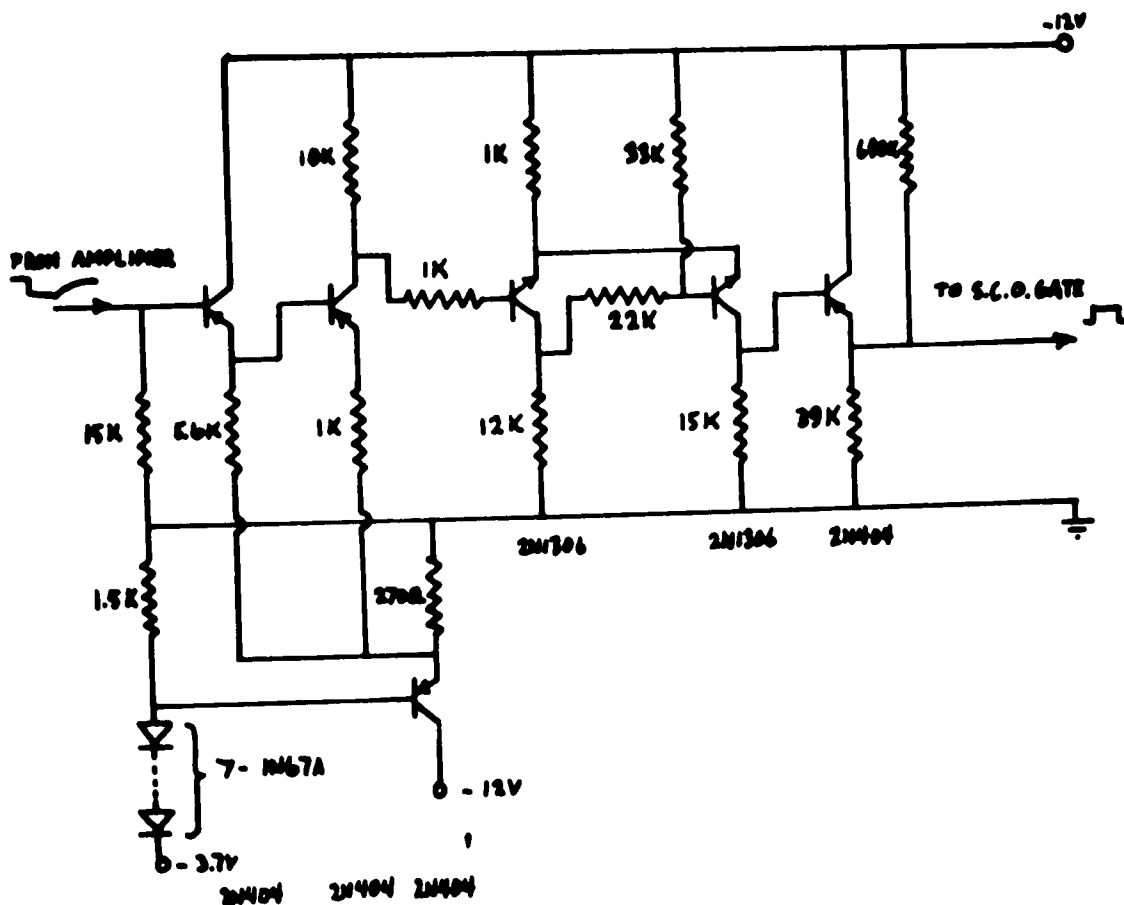
4 μ S UNIVIBRATOR

Hand-drawn schematic diagram of a 4 μ s monostable multivibrator circuit. The circuit is powered by a -12V supply and ground. It features two 1N34A diodes in the input stage, a 2N4004 NPN transistor in the timing network, and a 2N1306 PNP transistor in the output stage. Key components include a 39K resistor, a 6.8K resistor, a 47pF capacitor, a 47K resistor, a 22K resistor, a 2.7K resistor, and a .01F capacitor. The output is labeled "TO 4 μ s UNIVIBRATOR".

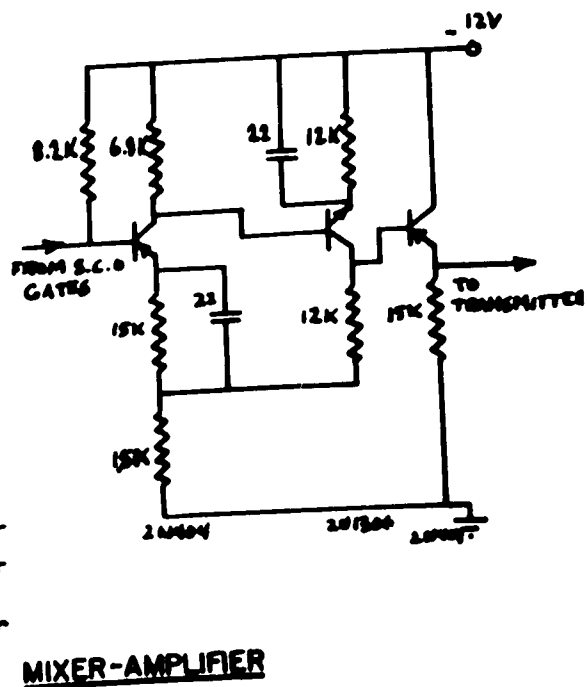
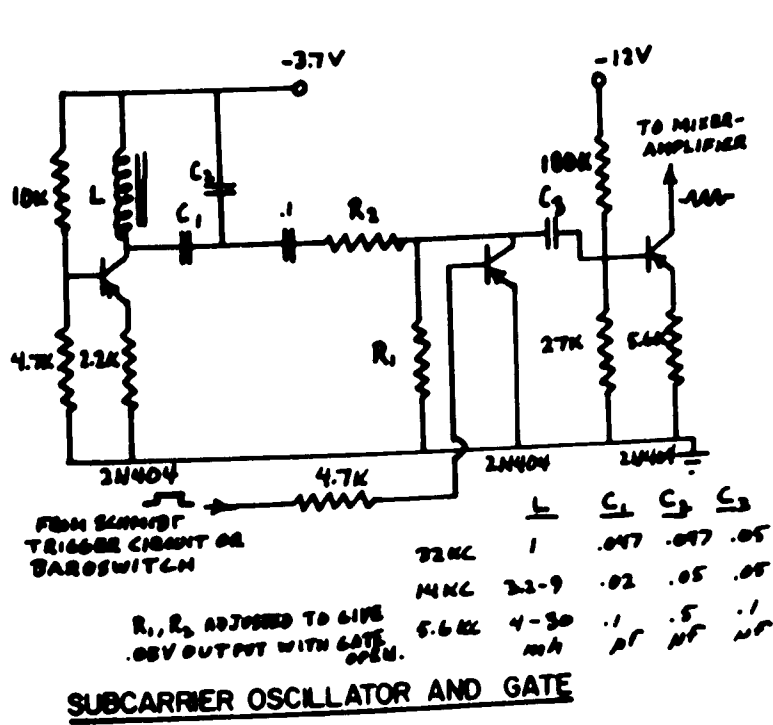
NORMALLY OPEN GATE

The schematic shows a 4-stage CMOS inverter chain. The first three stages are implemented with 2N1306 NPN transistors, and the last two stages use 2N4004 PNP transistors. The circuit is powered by a -12V supply and ground. Various resistors and capacitors are used for biasing and timing. The output is labeled 'OUT'.

AMPLIFIER FOLLOWING PULSE-STRETCHER



SCHMIDT TRIGGER CIRCUIT WITH TEMPERATURE COMPENSATION NETWORK

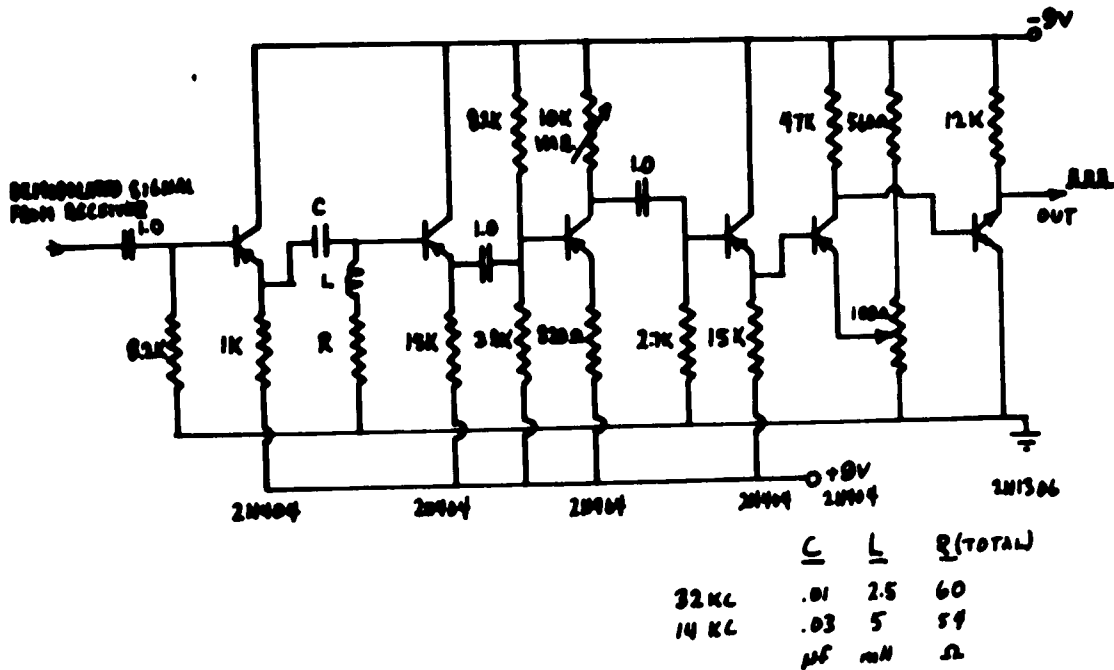


APPENDIX II

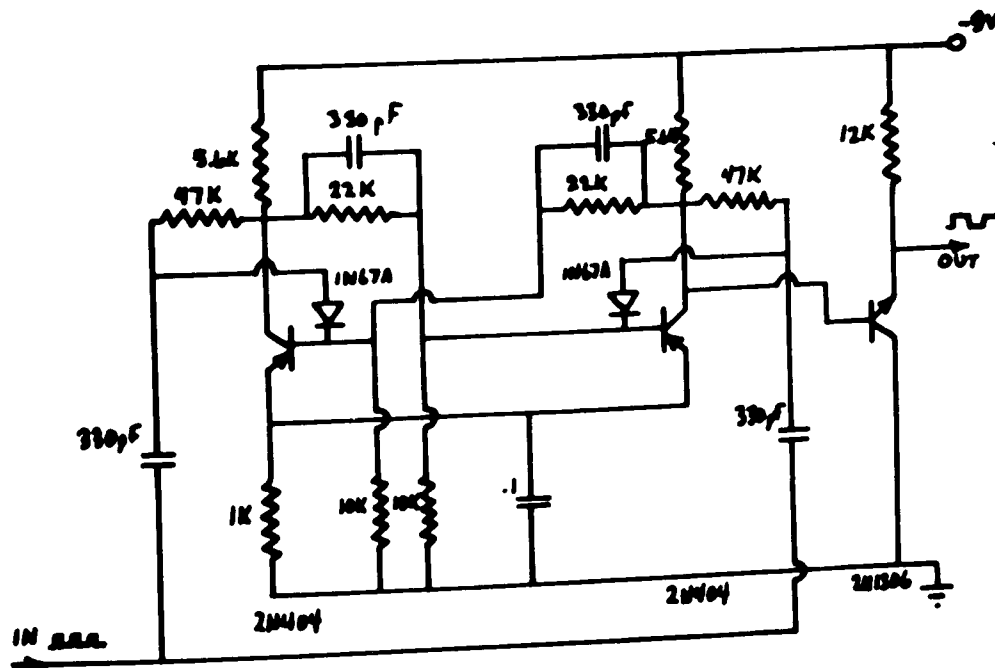
DETAILS OF GROUND-BASED
ELECTRONICS

List of Circuits Appearing in Appendix II

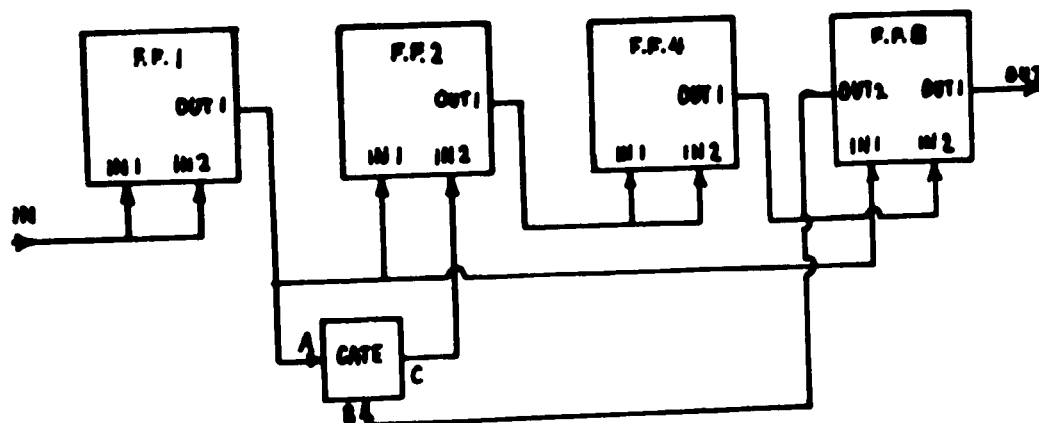
| | Page |
|--|------|
| 1. Tuned circuit and pulse shaper | 125 |
| 2. Scale of two | 125 |
| 3. Decade counter (block diagram) | 126 |
| a. Gate | 126 |
| b. Flipflop | 126 |
| 4. End of signal indicator circuits (block diagram) | 127 |
| a. Normally open gate | 127 |
| b. 6 ms univibrator (A) | 127 |
| c. 6 ms univibrator (B) | 127 |
| d. 100 μ s univibrator | 128 |
| 5. Decade counter reset circuit | 128 |
| 6. Decade to D. C. convertor (block diagram) | 128 |
| a. Convertor | 129 |
| 7. Buffer register transfer system (block diagram) | 129 |
| a. Gate, end of pulse selector, and 100 μ s univibrator | 129 |
| b. End of pulse selector (B) | 129 |
| c. Start of pulse selector | 130 |
| d. Buffer indicator flipflop | 130 |
| e. End of pulse selector (C) | 130 |
| 8. Buffer register input gates | 130 |
| 9. Buffer register output gates | 130 |
| 10. Electronic stepping switch with input gates and 4.5 ms punch drive univibrator (block diagram) | 131 |
| a. Gate A | 131 |
| b. Scalar | 132 |
| c. 4.5 ms univibrator | 132 |
| d. Gates 1, 2, 3, and 4 | 132 |
| 11. 1 minute signal and other punching circuitry (block diagram) | 133 |
| a. Pulse shaper (A) | 133 |
| b. Double gate | 133 |
| c. Pulse shaper (B) | 133 |
| d. End of signal selector | 134 |
| 12. Parity circuitry (block diagram) | 134 |
| a. 'Exclusive or' circuit | 135 |
| b. Pulse shaper | 135 |
| c. Gate | 136 |
| 13. Driver circuit for tape punch | |



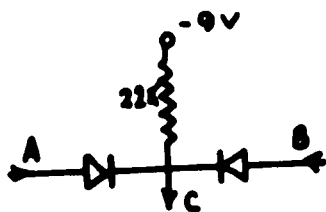
TUNED CIRCUIT AND PULSE SHAPER



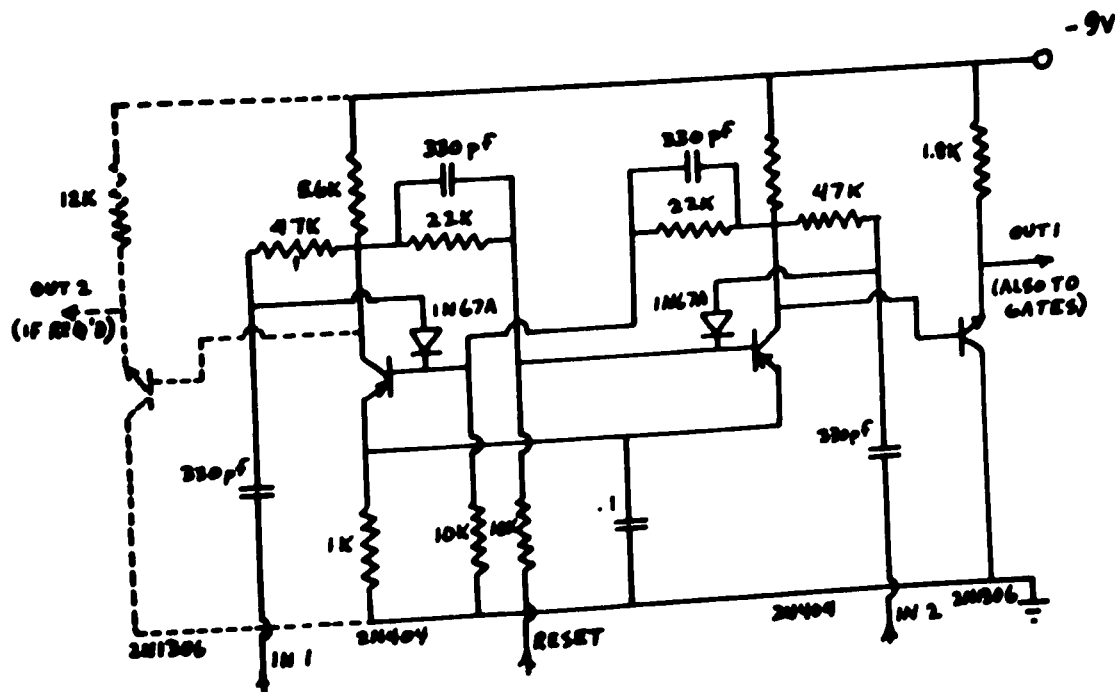
SCALE OF TWO (2 OF THESE IN SERIES FOR SCALE OF FOUR)



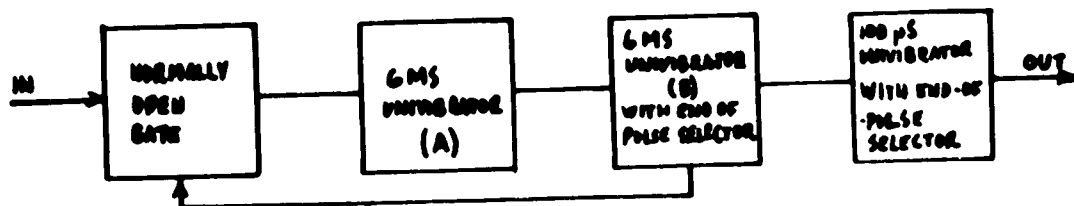
DECADE COUNTER BLOCK DIAGRAM



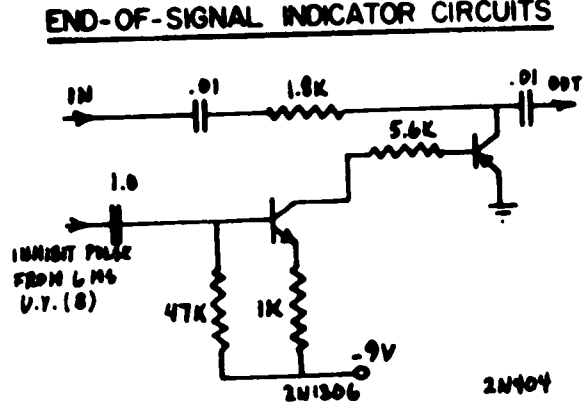
GATE



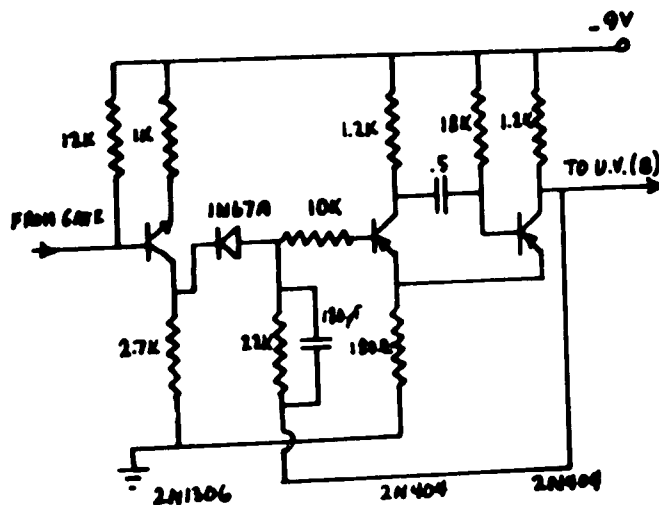
DECADE COUNTER FLIPFLOP



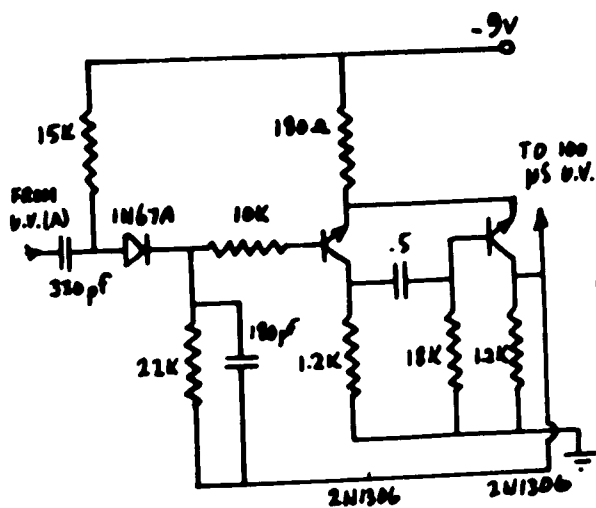
END-OF-SIGNAL INDICATOR CIRCUITS



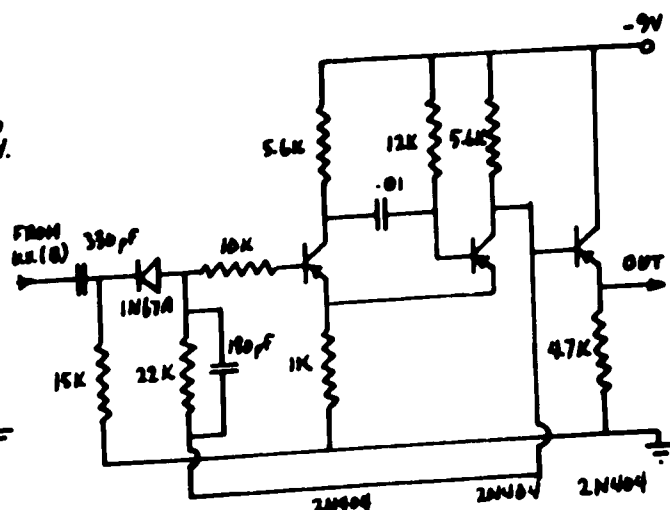
NORMALLY OPEN GATE



6 MS. UNIVIBRATOR (A)



6 MS. UNIVIBRATOR (B)



100 μ S UNIVIBRATOR

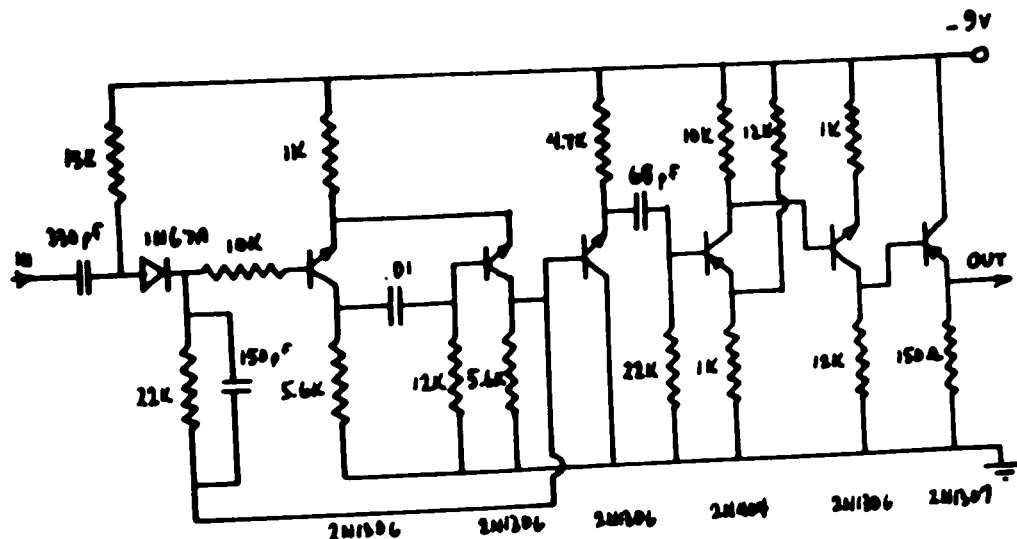


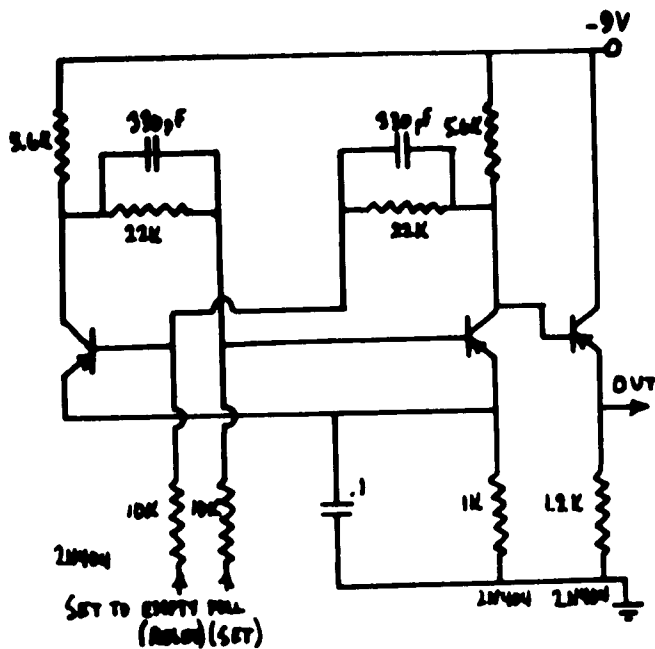
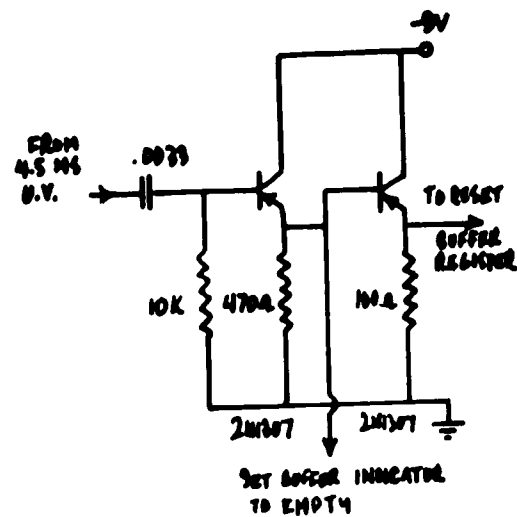
Diagram illustrating an 8-bit digital-to-analog converter (DAC) using comparators. The circuit consists of eight comparators, labeled C1 through C8, each receiving a reference input (F.R. 1 to F.R. 8) and a feedback input (F.F. 1 to F.F. 8). The outputs of the comparators are connected to a common output line, which is then connected to a 100 ohm load resistor and ground. The output is labeled 'OUT'.

| CONVERTOR NO. | R |
|------------------|------|
| 1 | 22K |
| 2 | 10K |
| 4 | 56K |
| 8 | 2.7K |
| 10 | 2.2K |
| 20 | 1K |
| 40 | 560Ω |
| 80 | 270Ω |

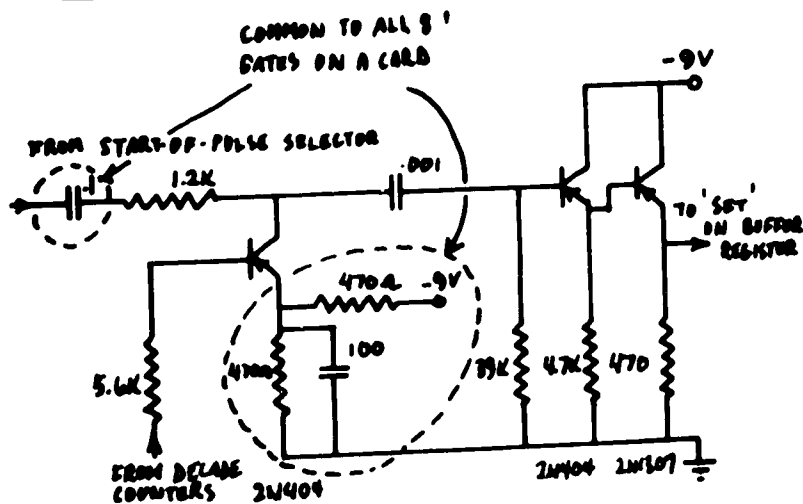
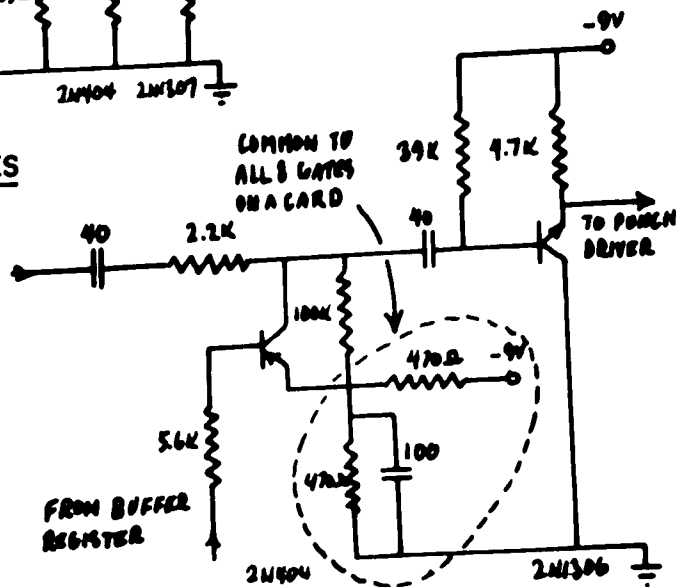
CONVERTOR

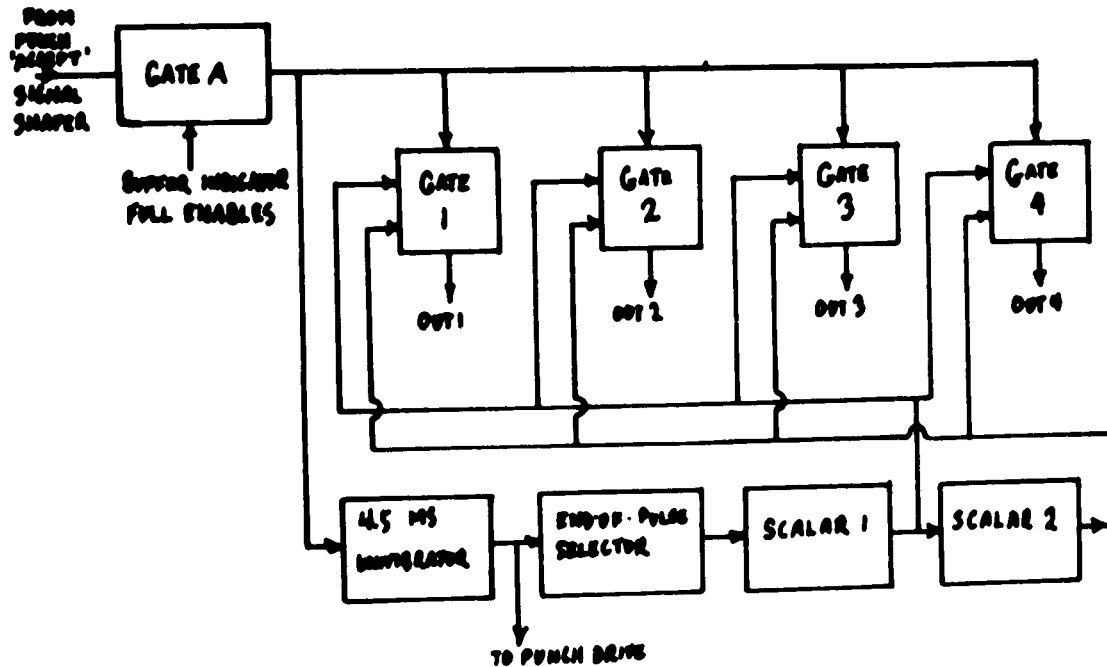
[illegible]

START-OF-PULSE SELECTOR

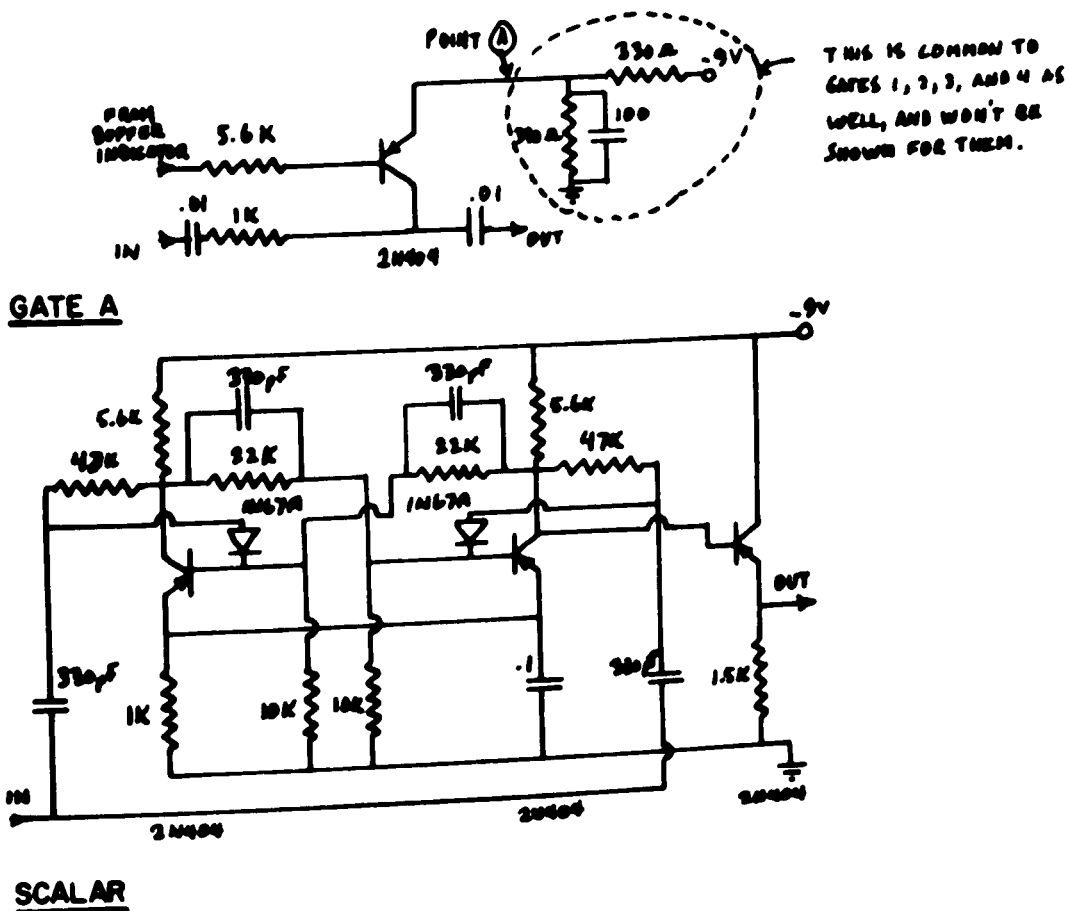
BUFFER INDICATOR FLIPFLOPEND-OF-PULSE SELECTOR(C)

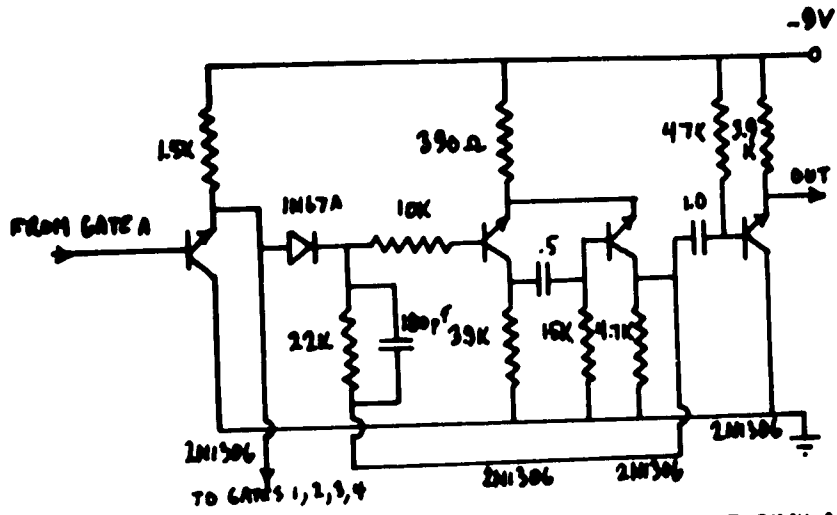
BUFFER REGISTER FLIPFLOPS SAME AS BUFFER INDICATOR FLIPFLOP

BUFFER REGISTER INPUT GATESBUFFER REGISTER OUTPUT GATES

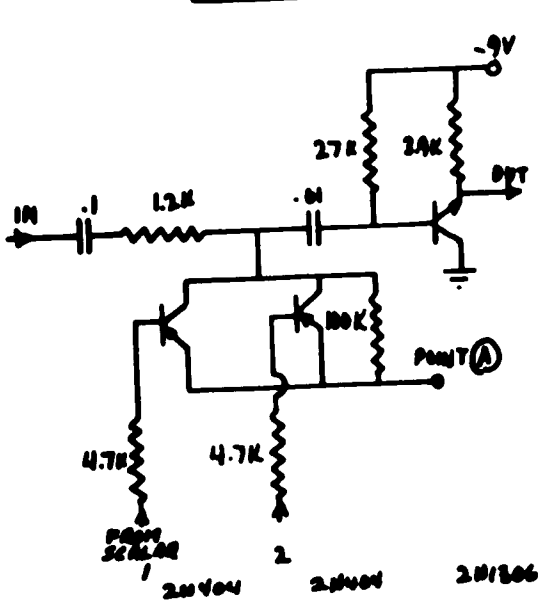


ELECTRONIC STEPPING SWITCH WITH INPUT GATE AND 4.5 MS PUNCH DRIVE U.V.

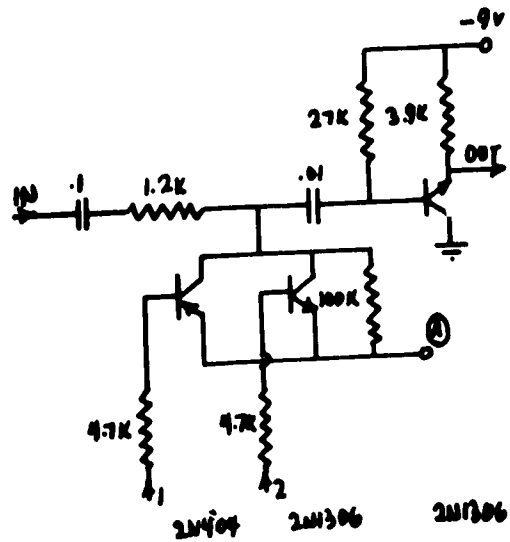




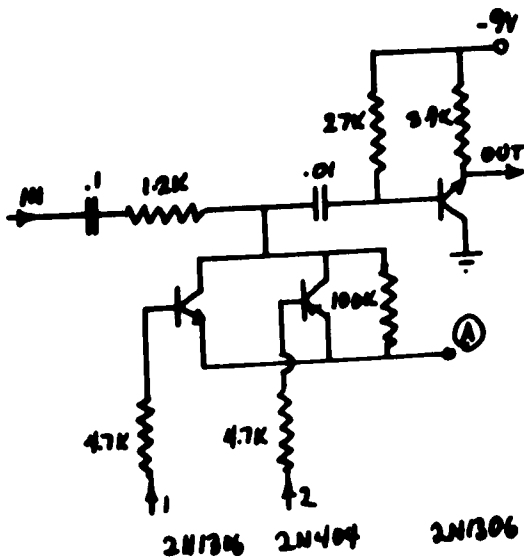
4.5 MS UNIVIBRATOR(OTHER 4.5 MS U.V.'S USED ARE SIMILAR)



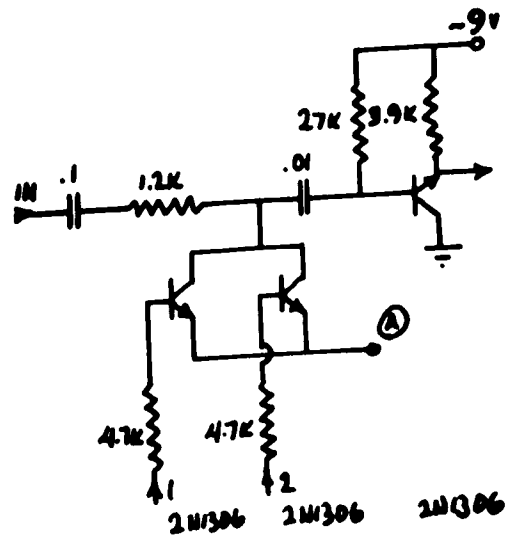
GATE 1



GATE 3

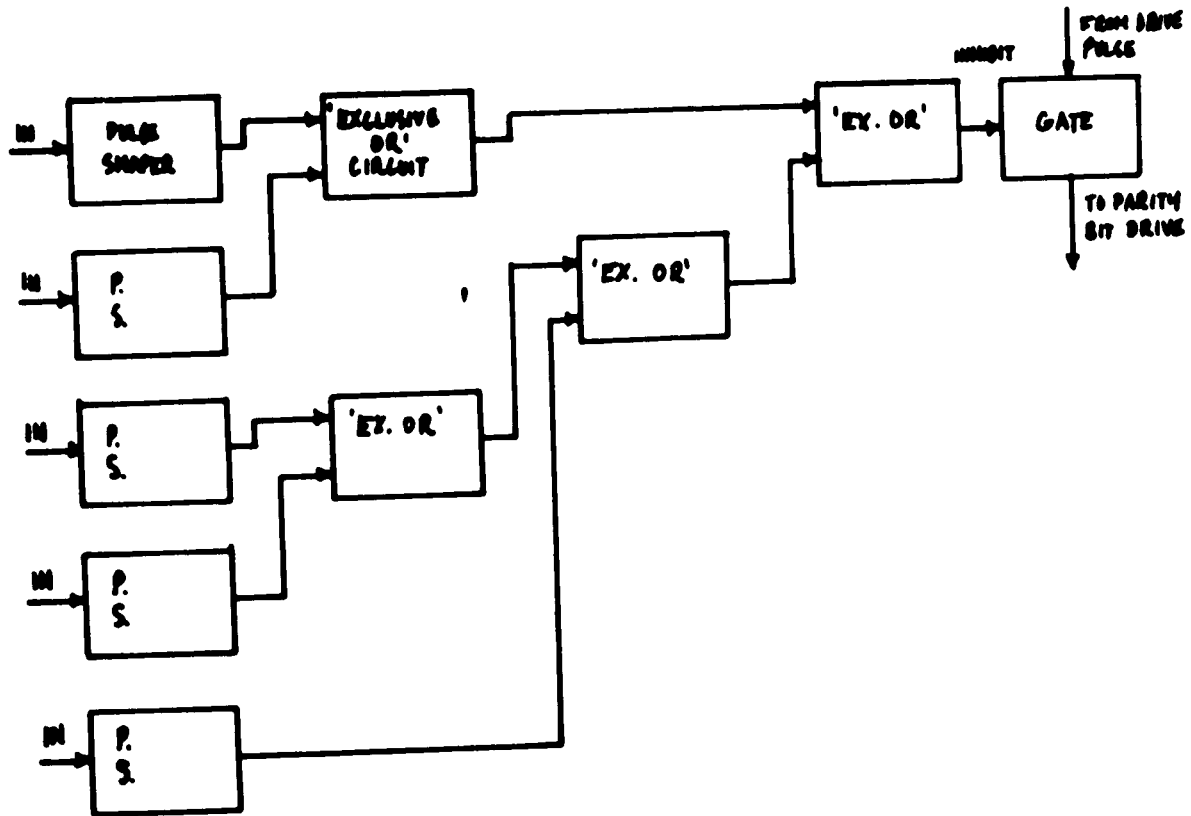


GATE 2

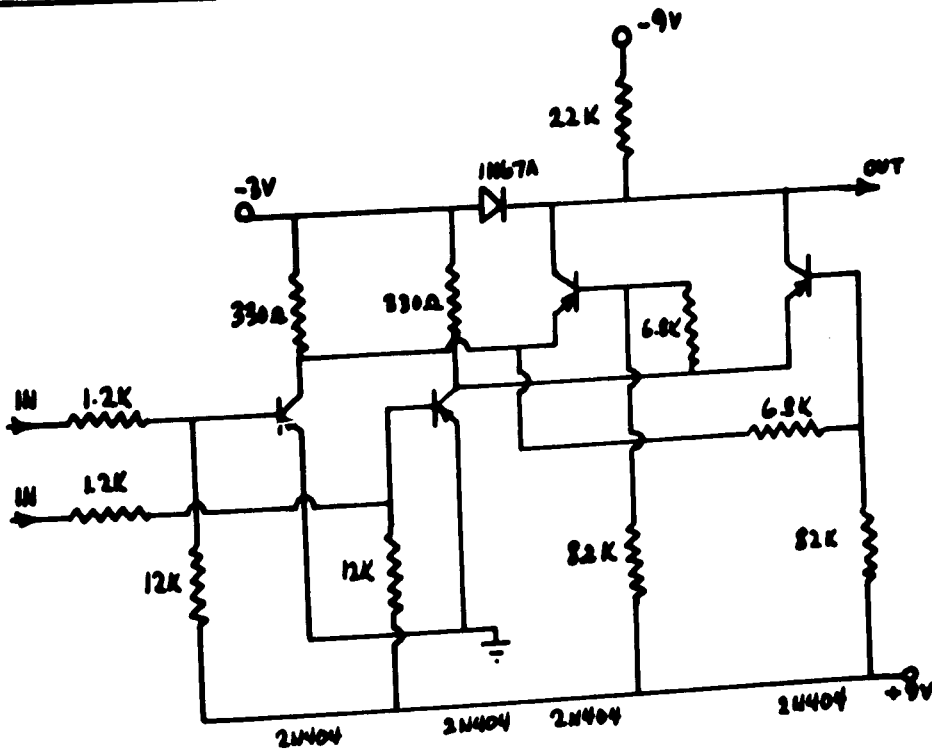


GATE 4

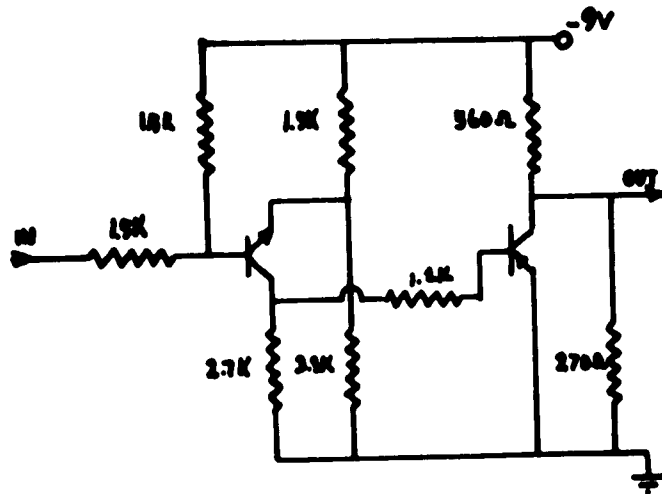
END-OF-SIGNAL SELECTOR



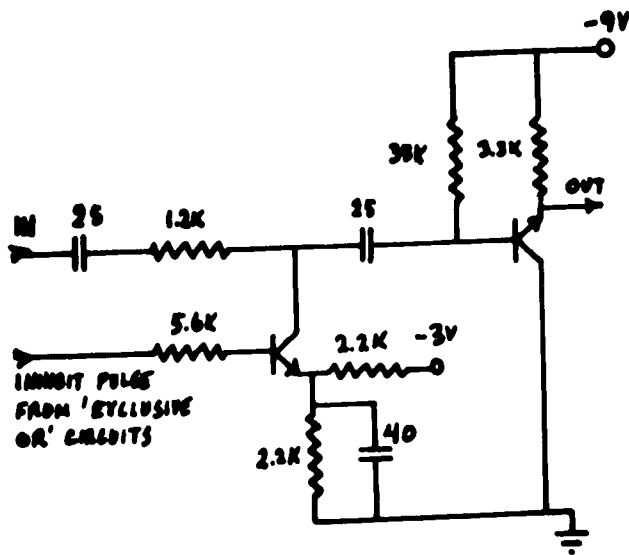
PARITY CIRCUITRY



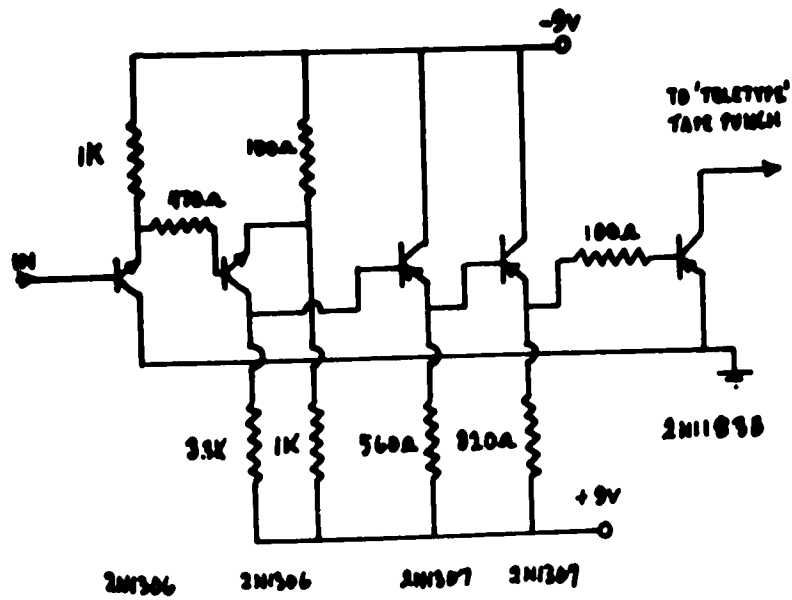
'EXCLUSIVE OR' CIRCUIT



PULSE SHAPER



GATE



DRIVER CIRCUIT FOR TAPE PUNCH

REFERENCES

- Anderson, K. A., Suppl. Nuovo Cimento, 5, 389.
- Bailey, D. K., 1957, J. Geophys. Res., 62, 431.
- Balasubrahmanyam, V. K., and McDonald, F. B., 1964, J. Geophys. Res., 69, 3289.
- Biermann, L., 1951, Zeit. f. Astrophys., 29, 274.
1952, Zeit. f. Naturforsch, 7a, 127.
1957, Observatory, 77, 109.
- Birks, J. B., 1951, Proc. Phys. Soc. (London) A, 64, 874.
- Bryant, D. A., Cline, T. L., Desai, V. D., and McDonald, F. B.,
1962, J. Geophys. Res., 67, 4983.
- Crispin, A., and Hayman, P. J., 1964, Proc. Phys. Soc., 83, 1051.
- Durney, A. C., Elliot, H., Hynds, R. J., and Quenby, J. J., 1964,
Proc. Roy. Soc.. A, 281, 553.
- Fan, C. Y., Meyer, P., and Simpson, J. A., 1960, Phys. Rev.
Letters, 5, 272.
- Fenton, A. G., Fenton, K. B., and Rose, D. C., 1958, Can. J. Phys.,
36, 807.
- Fichtel, C. E., Guss, D. C., Kniffen, D. A., and Neelakantan, K. A.,
1964, J. Geophys. Res., 69, 3293.
- Forbush, S. E., 1954, J. Geophys. Res., 59, 525.
1958, J. Geophys. Res., 63, 651.
- Freier, P. S., and Waddington, C. J., 1964, technical report
CR-70, Dept. of Physics, University of Minnesota.
- Hedgecock, P. H., 1964, Sparmo Bulletin, No. 1, 14.
- Hubbard, E. L., 1962, IRE Trans. Nucl. Sci., NS-9, 357.
- Linsley, J., 1955, Phys. Rev., 97, 1292.
- McDonald, F. B., 1956, Phys. Rev., 104, 1723.
1959, Phys. Rev., 116, 462.
- McDonald, F. B., and Ludwig, G. H., 1964, Phys. Rev. Letters,
13, 783.

- McDonald, F. B., and Webber, W. R., 1959, Phys. Rev., 115, 194.
1962, J. Geophys. Res., 67, 2119.
- Meyer, P., and Simpson, J. A., 1955, Phys. Rev., 99, 1517.
- Meyer, P., and Vogt, R., 1963, Phys. Rev., 129, 2275.
- Morrison, P., 1956, Phys. Rev., 101, 1397.
- Neher, H. V., and Anderson, H., 1958, Phys. Rev., 109, 608.
- Noon, J. H., and Kaplon, M. F., 1955, Phys. Rev., 97, 769.
- Parker, E. N., 1963, 'Interplanetary Dynamical Processes',
Interscience Publishers, New York.
- Peters, B., 1951, 'Progress in Cosmic Ray Physics, Volume 1',
193, edited by J. G. Wilson, North-Holland Publishing
Company, Amsterdam.
- Prescott, J. R., and Rupaal, A. S., 1961, Can. J. Phys., 39,
221.
- Quenby, J. J., and Webber, W. R., 1962, 'Progress in Cosmic
Ray Physics, Volume 6', 82, edited by J. G. Wilson and
S. A. Wouthysen, North-Holland Publishing Company, Amsterdam.
- Ritson, D. M., 1961, 'Techniques of High Energy Physics', edited
by D. M. Ritson, Interscience Publishers, New York.
- Rossi, B., 1956, 'High Energy Particles', Prentice-Hall Inc.,
New York.
- Schiff, L. I., 'Quantum Mechanics', McGraw-Hill Book Company,
Inc., New York.
- Segre, E., 1964, 'Nuclei and Particles' W. A. Benjamin, Inc.,
New York.
- Simpson, J. A., 1951, Phys. Rev., 81, 895.
- Simpson, J. A., Fan, C. Y., and Meyer, P., 1961, J. Phys. Soc.
Japan, 17, suppl. AII, 505.
- Simpson, J. A., Fonger, W., and Treiman, 1953, Phys. Rev.,
90, 934.
- Sternheimer, R. M., 1952, Phys. Rev., 88, 851.
1953, Phys. Rev., 91, 256.
1956, Phys. Rev., 103, 511.

- Symon, K. R., 1948, thesis, Harvard University, unpublished.
- Tongiorgi, V., 1949, Phys. Rev., 76, 517.
- Vallarta, M. S., 1961, 'Handbuch der Physik, Volume 46/1', 88,
edited by S. Flügge, Springer-Verlag, Berlin.
- Vogt, R., 1962, Phys. Rev., 125, 366.
- Waddington, C. J., 1963, 'Course 19: Cosmic Rays, Solar Particles
and Space Research', 135, edited by B. Peters, Academic Press,
New York.
- Webber, W. R., 1956, Il Nuovo Cimento, 4, 1285.
1962a, 'Progress in Cosmic Ray Physics, Volume 6', 206,
edited by J. G. Wilson and S. A. Wouthysen, North-Holland
Publishing Company, Amsterdam.
1962b, *ibid.*, 100.
- Webber, W. R., and McDonald, F. B., 1955, Phys. Rev., 100, 1460.
1964, J. Geophys. Res., 69, 3096.
- White, G. M., 1965, thesis, University of Alberta, Calgary,
unpublished, 9.
- Winckler, J., and Anderson, K., 1954, 1954, Phys. Rev., 93, 596.